Studies on Atmospheric Hydrometeors Retrieval Using Dual Wavelength Cloud Radar

이중파장 구름레이더를 이용한 대기 중 수함량 회수에 관한 연구

Advisor: Prof. Dong-In LEE

by

Hyo-Kyung KIM

A thesis submitted in partial fulfillment of the requirements
for the degree of

Doctor of Philosophy

In the department of Environmental Atmospheric Sciences, Graduate School
Pukyong National University

August 2004

Studies on atmospheric hydrometeors retrieval using dual wavelength cloud radar

A dissertation

by

Hyo-Kyung KIM

Approved by:

(Chairman) Young-Ho HAN

(Member) Dong-In LEE

(Member) Young-Seup KIM

(Member) Byung-Hyuk KWON

(Member) Sung Nam OH

August 2004

이중파장 구름 레이더를 이용한 대기 중 수함량 회수에 관한 연구

김 효 경

부경대학교 환경대기과학과

요 약

미래 기후를 예측하는 일은 그 중요성으로 인해 다양한 기후모델로부터 예측되어 오고 있으나 예측 결과는 모델마다 다른 양상을 보여 주고 있다. 그 주 원인은 지구의 복사 수지에 중요한 영향을 미치는 요인인 구름이 기후모델에서 실제와는 다르게 표현되기 때문이며 이것은 구름의 특성이나 거동에 관한 정보의 부족으로부터 기인한다. 따라서 구름 물리 과정을 더 잘 이해하고 기후 변동에 영향을 미치는 구름 인자의 전지구적 거동에 대한 정보를 얻기 위해서는 각 지역에서의 사례 연구와 전지구적 관측이 시급히 선행되어야 할 것이다.

본 연구는 구름을 관측하는데 있어 탁월한 원격 장비인 mm 파장대의 구름레이더로부터 구름을 구성하고 있는 입자들의 분포 및 정량적 특성을 회수하고자 하며 특히 이중파장의 해석에 초점을 두고 있다. 또한 비강수성 구름 뿐만 아니라 강수를 포함하고 있는 혹은 비가 오는 경우 구름레이더의 이용 가능성 및 입자의 분포 특성의 회수에 관해서도 연구 되었다. 비강수성 구름의 경우 전지구에 걸친 넓은 분포 범위로 인해 지구 복사에 영향을 미치는 하층운 속의 운수량을 회수하는 방법과 장·단파 복사에 대해 알베도가 높은 권운 속 얼음입자로부터 직경 분포 및 그 양을 추정하였다. 따라서 일본 방재과학 기술연구소에 설치된 구름레이더로부터 2001년 6월 21일 관측된 자료로부터 각 입자들의 직경 분포 특성 및 그 양에 대한 연직 프로파일을 구하였다.

파장이 다른 2대의 구름레이더로 상층 얼음입자로 구성된 권운을 관측할 경우 2대의 레이더는 서로 다른 반사도 값을 가지게 된다. 두 반사도의 차이의 크기(Dual Wavelength Ratio, DWR)는 두 대의 레이더 파장에 대해 얼음 입자의 산란 크기의 차이와 전자기파의 감쇄 정도의 차이의 합으로 나타난다. 얼음 입자의 전자기파의 감쇄 정도를 모의한 결과 얼음입자의 전자기파를 거의 흡수하지 않아 파장에 따른 감쇄의 차이는 실제 관측된 반사도의 차이에 기여하지 않는 것으로 조사되었다. 따라서 얼음 입자의 경우 서로 다른 파장에 의해 나타나는 반사도의 차이는 산란 정도의 크기에 의존하며, 산란의 크기는 입자의 크기와 직접 관련이 있으므로 권운 속 얼음 입자의 크기를 측정할 수 있다. 이 방법은 한 대의 레이더를 이용하여 빙수량 (Ice Water Content)를 추정하는 방법에서 발생하는 에러를 극복할 수 있어 더 정확한 빙수량의 연직 프로파일을 구할 수 있다.

35 GHz 와 95 GHz, 두 대의 구름 레이더를 이용하여 여름철 중위도의 높이 7-12 km에 위치한 두께 5 km 정도의 권운을 관측하였다. 구름 레이더와 같이 짧은 파장대의 레이더로 고층에 위치한 권운을 관측할 경우 대기 가스에 의한 레이더 파의 감쇄가 실제 DWR에 상당한 영향을 미치는 것을 알 수 있었으며, 이것은 가스 보정이 반드시 필요함을 의미한다. 감마의 직경 분포(μ=0)를 가정한 이중파장 레이더기법으로부터 관측된 권운 속 얼음 입자의 평균 체적 직경(Median volume diameter, D_O)은 구름의 운저 약 100m를 제외한 부분에서 0.1~0.7 mm의 분포를 가졌으며, IWC은 0.001~0.15 g/m^{3}의 분포를 보였다. 실제 동시에 관측된 실측자료의 부재로 인해 문헌적 자료와 비교될 때, 두 값 모두 구름의 운정에서 운저로 올수록 증가하는 전형적인 권운의 분포와 잘 일치하고 있다. 그러나 구름의 운저 약 100m 정도에서는 운정과 비교할 때 IWC 양은 유사하나 D_O는 현저한 차이를 보이고 있고 Do가 1.5 mm에 달하는 크기로 과대 평가된 것을 알 수 있었다. 운저에서 작은 입자의 증발로 상대적으로 큰 입자의 비율이 증가하는 분포를 가지는 미물리 특성을 감안할 때 감마 분포로 잘 표현되지 않는 입경 분포를 가지는 것으로 유추할 수 있다. 감마 분포를 적용할 시에는 상대적으로 큰 입자의 직경 비율이 높은 분포를 가지는 μ 값을 선택하는 것이 적절한 것이 민감도 테스트를 통해 확인할 수 있었다. 따라서 권운의 운저에서는 그 위쪽 영역과 서로 다른 μ를 사용함으로 전형적인 권운의 입자 분포를 구할 수 있다. 또 한 대의 레이더로 도출된 IWC 양과는 다른 양상을 보이므로 한 대의 레이더를 이용한 power law 관계식의 문제점을 확인할 수 있었으나 그 타당성 여부는 향후 실측 자료로부터 검증될 수 있을 것이다.

층적운은 지상 3 km 이하의 높이에 주로 존재하기 때문에 대부분 100 ㎛ 이하의 작은 액상의 구름입자로 구성 있으며 이런 입자들은 mm 파장대의 구름레이더에 대해서도 대부분 레일리 영역에 포함된다. 따라서 두 대의 레이더로 이런 조건의 층적운을 관측한다면 두 파장에서 관측된 반사도의 차이(DWR)는 오직 구름 속에 존재하는 입자의 흡수에 의해 감쇄된 양에 비례하게 된다. 따라서 운수량(Liquid Water Content, LWC)의 연직분포는 두 층 사이의 DWR 차이에 비례하게 되고 연직적으로 두 파장에 나타나는 DWR은 연직으로 누적된 감쇄로 인해 고도가 높을수록 커질 것이다. 그러나 이런 방법은 미이 영역에 해당되는 큰 입자가 존재할 경우 에러를 유발시키고 LWC 양을 음의 값으로 산출해 낸다. 본 연구의 사례는 전형적인 층적운의 경우가 아니라 10 GHz에서도 감지될 정도의 큰 입자로 구성된 하층운에 대해 10 GHz와 35 GHz의 두 대의 레이더로부터 운수량을 구하고자 하였다. 이 사례에 대해 레이더에 측정된 반사도는 약 -30 ~ 5 dBZ 정도 약한 분포를 보였으며, 10 GHz와 35 GHz에 의한 DWR의 연직 분포는 가정과는 달리 연직으로 일률적으로 증가하는 분포를 보이지 않았다. 이것은 이 파장대의 레이더에 대해 미이 영역에 해당되는 큰 입자가 구름 속에 존재하고 이것이 전체 DWR에 음의 효과로 기여되었음을 의미한다. 따라서 본 연구는 이 영역에 대해서만 연직으로 일률적인 LWC를 가정함으로 전체 DWR에 기여하는 미이 산란 효과의 크기를 알 수 있게 되고 이것으로부터 체적 평균직경, D_O를 구할 수 있게 된다. 이런 방법은 기존의 방법에 비해 Do를 추가적으로 산출해 낼 수 있고 큰 입자가 존재할 경우에는 적용될 수 있다는 점에서 기존의 방법에 비해 개선 효과가 있다. 10 GHz와 35GHz를 이용할 경우 비강수운 속에 0.7 mm 이상에 큰 입자가 있을 경우에는 이 방법 역시 한계점을 가지게 된다.

마지막으로 본 연구는 구름을 관측하기 위해 개발된 mm 파장대의 레이더가 강우를 관측하는데도 이용될 수 있는지를 평가하였다. 구름레이더는 cm 파장대의 레이더에 비해

강우에 의한 감쇄가 심하기 때문에 감쇄 정도가 약한 강한 강우에 대해 강우 입자의 직경 분포 특성 및 강우강도를 추정하였다. 이중 파장의 구름레이더에 관측된 두 레이더의 반사도 차이(DWR)는 강우 입자에 의한 감쇄 효과와 Mie 산란에 의한 효과의 합으로 나타나 두 개를 분리하기 위한 가정을 두었다. 또한 강우 입자의 직경분포를 약한 강수를 대상으로 하므로 Marshall-Palmer (N_0 =8000, μ=0)의 분포에 대해 실시하였다. Marshall-Palmer(M-P)의 분포를 가정한 경우 이 사례에 대한 D_0는 0.7 ~ 1.5 mm 정도의 크기 분포에 존재하였으며, 수함량은 0.2 ~ 0.6 g/m^3의 분포를 보였다. 지표의 disdrometer에서 관측된 Do와 비교되었을 때 좋은 일치를 보였다. 또 본 연구에서 사용된 35 GHz와 95 GHz의 민감도 자료를 바탕으로 두 파장에 대해 M-P를 가정하여 강우 강도에 따라 어느 정도의 감쇄가 일어나는지를 계산하였다. 그 결과 95 GHz 의 레이더는 강우에 의해 심한 감쇄 현상이 일어나 시간당 약 10 mm/hr의 강우에 대해 약 3.5 km 이상의 높이에서는 관측될 수 없으며, 35 GHz의 경우 11km 정도의 높이까지 관측할 수 있고 강우가 강할수록 관측할 수 있는 높이는 지수적으로 감소된다.

실제 강우시 구름레이더의 성능을 평가하기 위해 강우 레이더로부터 추정된 강우 입자의 직경과 이중 파장 구름레이더로부터 구한 직경을 상호 비교하여 보았다. 두 결과 모두 지상의 disdrometer로부터 얻어진 직경과 비교하였을 때 비교적 잘 일치하고 있으나, 이중파장 구름레이더를 이용한 경우는 강우레이더를 이용한 경우에 비해 입자의 크기가 상대적으로 커지는 피크 영역을 잘 표현하는 것으로 나타났다. 이것은 구름레이더의 경우 2대를 이용함으로 인해 상대적으로 한대를 이용한 강우레이더의 경우에 비해 피크 영역에서 더 좋은 결과가 얻어졌다.

위에서 기술한 바와 같이 본 연구는 이중 파장 구름레이더로부터 비강수성 구름 및 강우에 대해 대기 중 입경분포의 연직 특성과 양을 정량적으로 추정하는 방법에 대해 소개하고 실제 구름에 대해 적용시켜 보았다. 본 연구의 결과들은 실제 항공기를 통한 직접 관측을 통해 검증이 선행되어야 할 것이다. 구름 레이더로부터 추정된 고해상도의 정보들은 향후 기후 모델의 검증 및 더 정확한 구름의 표현하기 위한 정보를 제공함으로써, 모델의 미래 기후 예측 능력을 향상시키는데 기여할 수 있을 것으로 판단되며, 약한 강우에 대해서도 활용할 수 있어 강수의 발달 과정에 대한 상세한 정보를 제공할 수 있다.

Acknowledgements

I am greatly indebted to my supervisor **Dong-In LEE** for his spiritual guidance, enthusiasm, patience and generosity for all my years in Pukyung National University. I would like to express all my respects for his energetic research activities and his ability to academically support students. I can't forget his thoughtful consideration, support and words of encouragement for me to the end of my life.

Secondly, I was fortunate to work with senior researcher, **Koyuru IWANAMI** of National Research Institute for Earth Science and Disaster Prevention (NIED) in Japan. Thank you for his providing the all data which have been such a fundamental part of this thesis, and for answering all my many questions on how to interpret it. He has unconditionally shared his deep experience with me. I'd like to thank **Masayuki MAKI** and his wife, **Ikuko** for useful discussions and warm hospitality whenever I visited NIED.

I'd like to thank Professor **Young-Ho HAN, Young-Seup KIM, Byung-Hyuk KWON** and **Sung-Nam OH** for their patient reviewing and editing of this thesis that improved its clarity and readability. I am especially grateful to Professors, **Hi-Ryong BYUN, Hyeong-Bin CHEONG, Jai-Ho OH** and **Gon OK** in department of environmental atmospheric sciences for their thoughtful consideration and guidance.

I am grateful to all the GEAR members for their support; to **Pu-kyung, Min, Gil-Jong, Mi-Young, Suk-Hee, Su-Jeong, Sang-Min, Young-Seup, Yun-Jeong, Min-Ji, Mi-Hye** and **Sung-Hwa** and also wish to express my thank to all the GEAR alumni; **Cheol-Hwan, Min-Soo, Young-Soo, Ji-Yeun, Dong-Soon, Ji-Young, Ha NA** and **Hae-Mee**. I especially thank to **Dong-Cheol** for his challenging questions and discussion and sending me the reference papers from U.S.A.

I wish to thank to all my good friends I've met at the department; **Tae-Kook, Hyun-Hee, Young-Cheol, Mo-Rang, Kyung-Won, Hyo-Soon, Joung-Hee** and **Hyo-**

Bang. They always gave me some relaxation and courage whenever I depressed. I'd like to specially thank **Sam-Yeun, Sung-Hee, Min-Soo, Bong-Gun, Tae-Young, Tae-Hoon, In-Hyunk** and **Gi-Man** who enjoyed coffee-break, tennis and movies over last a few years. And I wish to express to thank all my seniors and juniors of the third floor of Building No.4. My sincere friends, **Yang-Hee, Hyun-Ju, Mi-Jung, Ha-Yong** and **Young-Hwan** gave me unchanged friendship and careful consideration in spite of my careless for doctoral courses. I'd like to very much thank to them and **Kyung-Yeup** who gave me reference papers without any compliant. I wish to express my special love to my soul mate for his trusts and affection.

Most of all I would like to express all my sincere gratitude to **my parents** and **family** for their unfailing love, understanding and support, and specially thank my younger sister, **Hyo-Ok** and her husband, **Sung-Il** whose spiritual assistance enabled me to complete this thesis.

CONTENTS

List of Tables

List of Figures

Chapter 1

INTRODUCTION

There are two motivations in this study. One is to show the importance of data sets of high resolution of vertical cloud properties (cloud boundaries, ice water content, liquid water content and it's drop size distribution) for fulfilling the requirement of climate models from millimeter wavelength cloud radar. The other is to test the feasibility of millimeter wavelength cloud radar for rain measurement.

On average, clouds are covering more than 60% of the Earth's surface and they strongly affect atmospheric radiative fluxes and heating rates. In producing precipitation, clouds form an essential link in the hydrological cycle and the cloud-climate feedback is of great potential importance. For example, clouds are the main controller of global albedo, the fraction of solar radiation which is reflected back into space (Salby, 1996). Cahalan *et al.* (1994) calculated that a 10% decrease in this reflectance could increase the earth's surface temperature by ± 5℃, producing a warming similar to that since the last ice age, or that expected from a doubling of CO_2.

Despite the significance of clouds in the climate system, cloud induced processes are still not well understood. This is partly due to the complexity of inferring accurate and unambiguous information from in-situ and remote-sensed cloud measurements.

As a consequence, the representation of clouds remains one of the greatest sources of uncertainty in present-day General Circulation Models (GCMs) and numerical models. In GCMs, cloud properties have been parameterized. Small modifications in parameterization schemes produce large climate changes in modelled cloud properties

and distribution. NCEP's global model has used a diagnostic cloudiness scheme for many years. This is now being replaced by a prognostic cloud water scheme that was implemented in NCEP's regional model several years ago. A prognostic cloud water scheme adds cloud water/ice to the model's prognostic variables. Such a scheme calculates the local time-rate-of-change of cloud water/ice due to the combined effects of condensation/deposition, evaporation/sublimation, conversion to precipitation, turbulent transport, and large-scale advection.

Cloud heights and vertical distributions of cloud properties, for instance particle sizes, concentrations, ice and liquid water masses, are some of the most difficult quantities to monitor in the atmosphere. Present satellite measurements give only the top-of atmosphere radiation information but do not provide the essential vertical profiles of cloud; as a result the vertical profile of the radiative flux divergence is not known, although different heating profiles have a profound effect on climate simulations. This required vertical cloud structure can only be obtained by millimeter wave cloud radar; accordingly, the past GEWEX meeting (29 June to 2 July 1993) recommended that urgent action should be taken to formalize a development program for a vertical pointing cloud profiling radar and that in parallel there should be an intensification of studies using airborne and ground-based cloud radars, together with in situ observations and supporting work to refine and validate retrieval algorithms for the space-borne radar.

With the recent advance of powerful instruments like cloud radars and multi-channel microwave radiometers and the ongoing development of synergy algorithms to consistently interpret the measurements from different instruments the representation of clouds properties in GCMs and numerical models has improved considerably.

Millimeter wavelength radars have been primarily used as cloud radars (Lhermitte 1987; Miller and Albrecht 1995; Clothiaux et al. 1995; Vali et al. 1998; Kollias and Albrecht 2000) due to their capability to make high temporal and vertical resolution observations of weak targets.

Technological developments in the 1980's resulted in relatively low cost, high quality millimeter wave components and power sources, leading to the development of millimeter wavelength radars operating at 94 GHz (Lhermitte 1981, 1984, 1987). Millimeter wavelength radars have high temporal and spatial resolution, extreme sensitivity and high velocity resolution. Due to their short wavelength, millimeter radars are capable of detecting very small droplets with diameters of tens of microns. This capability of millimeter wave radars has established them as the ultimate observing systems for the study of weak meteorological targets undetectable by centimeter radars. In addition to the advantage of short wavelength, millimeter radars have very narrow beams, resulting in small sampling volumes. As a result, these radars provide excellent resolution in space and time. Parallel with the development of millimeter wavelength radars, retrieval techniques for the estimation of cloud and drizzle drop distributions were developed (Gossard 1988, 1994, 1997; Frisch et al., 1995; Babb et al., 1999).

Although the advantages of millimeter radars over centimeter radars are overwhelming for detecting clouds, the range of millimeter radars in the upward looking mode is limited due to attenuation by precipitation. Attenuation and low power transmitters limit the penetration and strength of the radar signal and these are parts of the hesitation in using the millimeter wavelength radars for precipitation studies. However, if it were correct for attenuation, millimeter cloud radars would be the ideal tool for studying all aspects of precipitation with cloud.

1.1 Overview of general researches about clouds

It is no surprise that clouds are not easily measured until developing the millimeter wavelength cloud profiling radar. Climate researchers still have many questions about clouds and the lists below are showed the main concerns of climate researcher about them.

- How many layers of clouds are there ?
- Are the clouds made of ice or water ?
- At what altitude is the cloud base and cloud top ?
- How much does it rain or snow ?
- How large are the water droplets or ice crystals in the cloud ?
- What fraction of the sky is cloudy ?

The distribution, fraction, type and microphysical properties of clouds play an important roles in regulating our climate. By knowing how much of the Earth is covered with clouds, climatologists can improve their models and watch for signs of climate change. Increases or decreases in the number and type of clouds could indicate that climate feedback loops are at work to the cooling or warming the planet. Counting clouds however is not easily done. From space, satellites are limited to seeing the tops of clouds and many clouds are smaller than the satellite footprint. From the surface, cloud observations have traditionally been made by a human observer, which are often very inaccurate, especially at night.
This problem is being addressed by using powerful remote sensed instruments such as millimeter wavelength cloud radars, lidars and radiometers for studying clouds.

Figure 1.1 shows the cloud radar images observed by ground based cloud radar

(Reading University in UK) according to cloud type. These figures can give the answers to the questions (the number of layer, height, type, cloud base, top, their fraction and so on) presented above and are showed the evidences of useful capabilities of cloud radars. The cloud radar technology is new and a number of mm-wavelength radars are being used for cloud profiling studies around the world or are under development. This research by cloud radars will give the information with the high resolution of cloud properties and be benefit to the cloud physicists and meteorologists for the observation and understanding of physical inside cloud structure in detail.

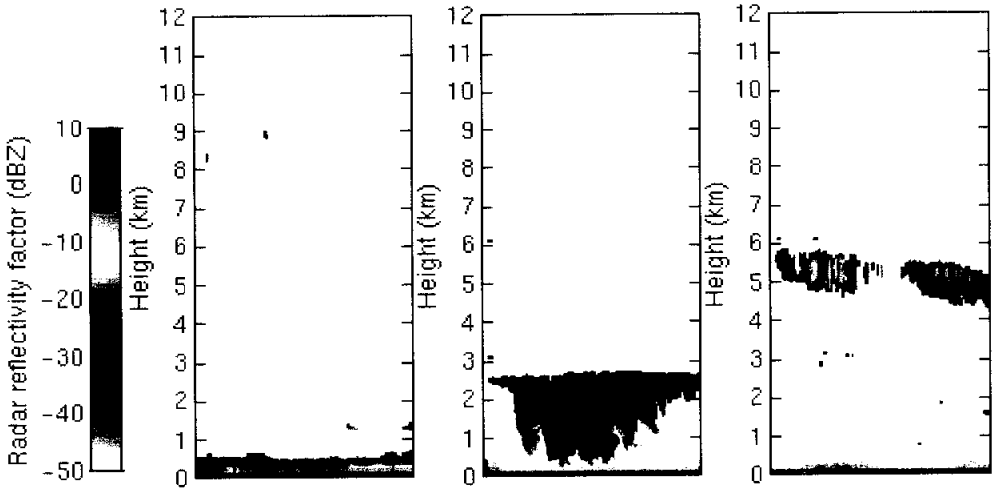

Stratocumulus

This is the most common cloud type in sky and is composed entirely of liquid water droplets. Because the droplets are very small (around 10-20 microns in diameter), they tend to give a fairly low radar signal.

Stratocumulus with drizzle

If stratocumulus is more than a few hundred meters thick, then larger `drizzle' drops (around 100-200 microns in diameter) can grow. These give a larger return to the radar, but usually evaporate before they reach the surface.

Altocumulus

This mid-level cloud occurs below freezing and is typically composed of both ice crystals and super-cooled liquid water droplets. The radar signal is usually dominated by the larger ice crystals, which tend to be several hundred microns across.

Figure 1.1 The cloud radar images observed by ground based cloud radar (this is possessed by Reading University in UK) according to cloud type.

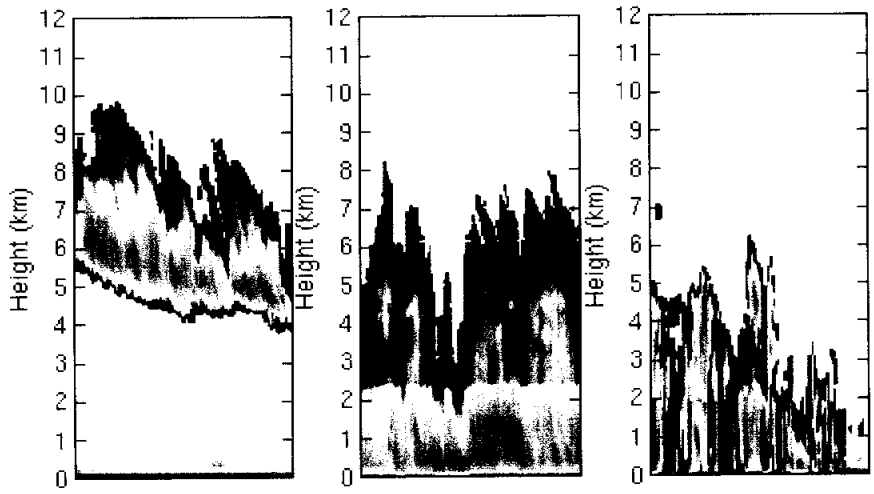

Cirrus

Cirrus clouds are composed purely of ice crystals and in radar images are characterized by their classic ` fall-streak' structure.

Rain

Frontal or `stratiform' rain looks like this. Ice crystals nucleate high in the atmosphere and grow as they fall. At the melting level (2.4 km in this example) the radar reflectivity at increases sharply because the dielectric constant of liquid water is higher than that of ice. The effects of attenuation by rain are also visible as vertical swaths of anomalously cloud-free air above the regions of highest rainfall rate, but this is only really a problem for high-frequency radars such as the 94 GHz Galileo.

Showers

When the rainfall is generated by convection the rainfall rate is much more variable. The melting level is visible at 2 km in this example.

(continue)

1.1.1 Challenging clouds for climate research

At present, the predicted change in global albedo for a future climate greatly varies between different General Circulation Models (GCMs), and even the sign of the change is uncertain (Cess *et al.*, 1996). Uncertainties such as this have motivated research in reliable modeling of clouds and their radiative properties.

Typically clouds are represented as a grid-box average of liquid or ice water content which is either diagnosed every time step as a function of humidity and temperature, or in more advanced schemes is a prognostic variable (Smith 1990, Tiedtke 1993). This is then related to the radiative properties of the cloud via parameterizations for effective radius (r_e), single scatter albedo (w) and asymmetry parameter (g) as a function of the wavelength of the radiation. Liquid droplets are close enough to spherical that Mie theory can be applied and so r_e is the only variable about which there is much doubt, but for ice crystals things are far more complicated, since all three of these parameters are a function of crystal type, orientation, density and size, which are generally unknown. Of course to correctly calculate the radiative effects of a model grid-box containing either liquid or ice phase cloud requires the water content to be known accurately, and another substantial problem is how to parameterize cloud cover and the effects of inhomogeneous cloud fields.

Research on cloud for climate has mainly focused on the most spatially frequent cloud type, stratocumulus, which being low and optically thick, primarily cools the climate by reflecting solar radiation back out to space. In the last few decades (Sassen and Mace, 2001), more attention has been drawn to cirrus, optically thin, high-altitude ice-clouds.

Liquid water content in stratocumulus

The term "low clouds" refers to clouds whose base is less than about 3 km above the ground. Low clouds are usually entirely composed of water droplets, however ice particles may occur when the temperature is below 0℃ and when an appreciable amount of crystal condensation nuclei are present.

Of all low-level clouds, stratus and stratocumulus have the most profound impact on the earth's radiation budget because of their high optical depth and large global coverage and extension to many km in horizontal direction. They usually form over oceans and contribute about 25% to the total cloud coverage of the Earth. Stratocumulus clouds are generally long-lived and can produce rain or snow precipitation. Generally they are situated above the oceans that humid air-masses are lifted in a sheared environment, e.g., in frontal situations and their dynamics are strongly driven by radiative processes.

Stratus and stratocumulus clouds have an overall cooling effect on climate since they reflect most of the incoming solar radiation back into space, yet emit in the long-wave at a similar brightness temperature to the surface (Randall *et al.,* 1984). Their climatic importance was demonstrated by Slingo (1990), who found that a modest 15 ~ 20% increase in the total global coverage of these clouds would offset the increase in mean global temperature caused by a doubling of the amount of carbon dioxide in the atmosphere. The same effect could be achieved by increasing liquid water path by 20 ~ 35% on average, or decreasing the mean droplet radius by 15 ~ 20%. Clearly it is crucial to our understanding of climate change that the behavior of low clouds in response to other changes in the climate system is understood.

Ice water content in cirrus

In the understanding of the climate system, cirrus clouds represent an important but challenging problem (Stephens et al. 1990). Measurements of ice water content (IWC), effective radius (r_e) and optical depth are required to determine their effect on the earth's radiation budget and to validate climate models. Currently such models tend to carry cloud water content as a prognostic variable and relate it to radiative properties by means of an effective radius which is usually fixed. There is a need to test the skill of models to diagnose IWC, and to determine whether a fixed value of r_e is adequate. A global climatology of cirrus would be particularly useful, although this could be only obtained from a satellite-borne radar or lidar.

It is generally accepted that cirrus clouds cause a net warming of the climate system, but exact calculation of their radiative properties is very difficult because of the multitude of crystal habits that are present. This introduces uncertainty into the interpretation of remotely sensed measurements, and to simplify matters it is common to assume, for the purposes of solar, infrared and millimeter-wave radiative transfer calculations, that ice crystals can be adequately represented by spheres or spheroids. Aspect ratio and crystal density remain free parameters and must be prescribed in remote retrieval algorithms if they cannot be measured directly.

1.1.2 Cloud measuring instruments

The process of measuring cloudiness has always been somewhat subjective. Cloud measurements were once made by solely human observation, however new technology enables instruments to view the sky and make the more objective cloud measurements needed by both operational and research meteorologists. Generally,

there are two types of sensor, passive and active, for observing clouds.
Passive sensor means a measuring instrument by means of which information is obtained by reception of radio waves of natural origin such as satellite and radiometer. The other hand, radar and lidar are typical active sensors which obtain information by transmission and reception of radiowaves.

Passive radiometric measurements of the earth from space have been available for a number of decades and have greatly improved our understanding of the energy balance of the earth. Before they were available, estimation of the effects of clouds on surface temperature was based on very limited ground-based observations of albedo and cloud cover, such as those presented by London (1957). The most extensive attempt to measure the global properties of clouds from space was the International Satellite Cloud Climatology Project (Rossow and Schiffer, 1991), in which all the visible and infrared information from the various polar orbiting and geostationary satellites was used to provide cloud amount and cloud top height for each of four basic cloud types.
Satellite measurements have improved considerably in the last few years, with microwave radiometry providing LWP routinely over oceans free from surface (Greenwald *et al.*, 1993), and multi-spectral measurements being used to estimate particle size at the top of stratocumulus (Han *et al.*, 1994) and in cirrus (Baran *et al.*, 1998), although validation is required. However the principal limitations of such passive measurements are the lack of vertical resolution and the poor penetration when multiple cloud layers are present.

A detailed information about the cloud characteristics must be available on large scales. Beyond the cloud structure itself, crucial cloud parameters are the particle

size distribution (liquid or ice), and crystal shape which are known to have a strong influence on the radiative property of clouds. Such information is particularly difficult to obtain at the meso-scale from passive instruments, and remote sensing systems are potential candidates to fill the gap. The greatest advance in measuring the global effect of clouds on climate in the next decade is likely to be from the launch of a space-borne radar and/or lidar. This would enable a global climatology of vertically-resolved cloud properties to be retrieved over a period of several years.

1.1.3 International research activities of cloud radar

Some large scale global monitoring networks using remote sensed instruments are currently operational or are setting up to address the problems of climate change around the world.

Millimeter wavelength cloud profiling radar and satellite play important roles in these field projects. ISCCP (The International Satellite Cloud Climatology Project) and ARM (The Atmospheric Radiation Measurement) project are a kind of world wide and useful for understanding the feedbacks between clouds and climate.

ISCCP has been an outstandingly useful project and is established in 1982 to address climate problems by systematically collecting and condensing satellite data for climate studies before they are consigned to the huge satellite data archives. The resulting datasets and analysis products are being used to improve the understanding and modeling of the role of clouds in climate, with the primary focus being the elucidation of the effects of clouds on the radiation balance. These data can also be used to support many other cloud studies, including the understanding of the hydrological cycle.

The experimental objective of the ARM Program is to characterize empirically the radiative processes in the Earth's atmosphere with improved resolution and accuracy. A key to this characterization is the effective treatment of cloud formation and cloud properties in General Circulation Models. Through this characterization of radiative properties, it will be possible to understand both the forcing and feedback effects. General Circulation Model modelers will be able to better identify the best approaches to improved parameterizations of radiative transfer effects. This is expected to greatly improve the accuracy of long-term, General Circulation Model predictions and the efficacy of those predictions at the important regional scale.

The general and scientific goals of field activities for cloud and climate are shown as follows.

- The creation of a data set on clouds and cloud-radiation interaction
- Validation and calibration of the retrieval algorithms of ground-based and satellite remote sensing instruments
- Validation of cloud and radiative transfer models and parameterizations thereof during the project a new objective was added:
- Sensor synergy: how to combine different instruments to optimize the retrieval of cloud parameters?

A number of mm-wavelength radars are being used for cloud profiling studies around the world. A map showing the locations of the cloud profiling radars as well as a contact for each is available(Figure 1.2) and a preliminary list of these is shown below (Table 1.1).

Figure 1.2 The locations of mm wavelength cloud radar related to field projects.

Table 1 Locations of cloud profiling radars.

Location	Frequency (GHz)	Type
U. Massachusetts	33, 95, 215	Ground
U. Utah	95	Ground
U. Wyoming	95	Airborne
U. Miami	94	Ground
Penn. State U.	94	Ground
JPL	94	Airborne
NOAA/ETL	35	Ground
ARM (6 radars)	35	Ground
U.Washington	35	Airborne
GKSS	95	Ground
U. Hamburg	94	Ground
Laboratoire d'Aerologie	35	Ground
U. Paul Sabatier	35	Ground
U.Reading	94	Ground
Rutherford Appleton Lab	79	Ground
Communications Research Lab	94	Airborne
Nagoya U.	35	Ground

1.2 Outline of this thesis and objectives

The general objective of this study is highly to retrieve resolution of vertical cloud properties (cloud boundaries, ice water content, liquid water content and it's drop size distribution) for fulfilling the requirement of climate models and evaluate the feasibility of millimeter wavelength cloud radar for rain measurement.

- In this chapter 1 the purposes of this study, the research history of cloud profiling radar and international field activities has been discussed.
- In Chapter 2 the information and features of the millimeter wavelength cloud radar used this study will be introduced.
- In Chapter 3 the theoretical basis of millimeter wavelength radar will be discussed and the results of simulation for cloud and precipitation by scattering model will be described.
- In Chapter 4 the retrieval techniques to measure liquid / ice water content in cloud and precipitation will be presented. In addition, the results of real application by introduced techniques will be showed and evaluated.
- Finally, in Chapter 5 the results of this thesis are summarized and concluded.

Chapter 2

DUAL WAVELENGTH CLOUD RADAR SYSTEM

2.1 General characteristics of meteorological radars

Table 2.1 compares typical characteristics of three general types of meteorological radars that cover a wide range of operating frequencies; in order of decreasing wavelength, these include wind profilers, storm-surveillance–precipitation radars, and cloud radars. The millimeter wavelengths used by the cloud radars are about an order of magnitude shorter than those used by storm surveillance radars, such as the 10-cm wavelength (S band) WSR-88D (NEXRAD) operated by the National Weather Service. They are about two orders of magnitude shorter than the 74-cm wavelength (UHF) used by the NOAA Wind Profiler Network. All three types of radars can detect clouds to some degree (*White et al.*, 1996).

Table 2.1 Characteristics for three types of meteorological radars: typical values.

Primary purpose	Wavelengths	Range resolution	Max range coverage	Rain effects
Clear-air wind profiling	6 m–33 cm (VHF / UHF)	60–500 m	5–20 km	Attenuation not a problem
Precipitation surveillance	10–3 cm (S / X band)	150–1000 m	100–450 km	Light-moderate attenuation
Cloud observations	8–3 mm (Ka / W band)	30–90 m	10–30 km	Severe attenuation

The large antennas and powerful transmitters used in most precipitation radars, like the WSR-88D, make it possible for them to detect non-precipitating clouds within a range of several kilometers (Knight and Miller 1993). However, they are generally unable to fully utilize this capability for a number of reasons, including relatively coarse spatial resolution, ground clutter, and operational mission priorities. WSR-88D cloud observations within about 15 km of the antenna are compromised by ground clutter and by the operational scan sequences, which are limited to low elevation angles. On the other hand, clutter does not constrain mm-wave radar from looking as close as 100–200 m because the signal-to-clutter ratio is 43 dB greater for an 8-mm-wavelength radar than for a 10-cm-wavelength radar (Kropfli and Kelly, 1996). This is true even if the beam patterns for the two radars are identical. In addition, the relatively coarse resolution (250–1000 m) of the WSR-88D and the restrictive scanning procedures of its operational storm surveillance mission are not well suited for continuous and detailed profiling of clouds. These radars were designed for a different primary task—the observation of precipitation and severe weather—and they perform this mission well. Their ability to detect some clouds while scanning may be a useful extension of these duties (Miller *et al.*, 1997). However, they are not the best choice if the primary objective is observing the quantitative macro- and microphysical details of nearby non-precipitating clouds.

Even radar wind profilers, operating at much longer wavelengths, possess limited cloud detection capability (White *et al.*, 1996; Orr and Martner, 1996) in addition to good precipitation detection capability (Ralph *et al.*, 1995). A new adaptation of wind profiler technology for profiling precipitation at S band also has demonstrated its potential for observing stronger reflectivity regions of clouds (Ecklund *et al.*, 1995) with moderate temporal and spatial resolution. However, conventional wind profilers are designed primarily to observe advecting atmospheric refractive index

gradients in the clear atmosphere. Their long wavelengths are advantageous for this, but, as a consequence, they generally lack the sensitivity to detect small cloud hydrometeors. Although precipitation and wind-profiling radars provide useful cloud information in some circumstances as an added benefit to their primary functions, it is the mm-wave systems that are specifically designed for fine-scale, quantitative observations of clouds. These radars exploit the inherent short wavelength sensitivity advantage for detecting the small cloud particles and the superior resolution associated with their very narrow beams and short pulses. A typical range resolution for the mm-wave systems is about 50 m (Table 2.1), which is suitable for revealing the intricate structure and motions that are valuable for assessing many basic cloud processes. Beam widths of 0.2° ~ 0.3° yield lateral resolutions of 35–50 m at a height of 10 km for a vertically directed beam.

The mm-wave radars receiving the most emphasis in atmospheric research today are those operating at frequencies in the atmospheric windows near 35 GHz (λ = 8.7 mm, Ka band) and 94 GHz (λ= 3.1 mm, W band). The primary disadvantages of using radars with such short wavelengths are attenuation by rainfall and limited range coverage, compared to precipitation radars. Attenuation by rain at these wavelengths is severe; this restricts the collection of useful data in or through precipitation to situations involving only very light rain, drizzle, or snowfall. The short attenuating paths associated with a vertically pointing system reduce the impact of this problem somewhat. Attenuation by cloud liquid water and by water vapor, although generally not serious, is greater at the shorter of these two wavelengths, thus favoring the use of Ka band, especially for ground-based systems. Ice crystals and snowfall produce minimal attenuation at these wavelengths; thus, even heavy snowstorms cause no significant attenuation problem for mm-wave radar observations. The W-band radars have an important advantage in smaller and lighter hardware

components, which favors their use on airborne and satellite systems.

The use of mm-wave radars to monitor clouds is an updated technology rather than a new discovery. The U.S. Air Force developed 35-GHz radars for use at many air bases in the late 1960s and early 1970s. These AN/TPQ-11 radars were vertically pointing systems and did not have Doppler or dual-polarization capabilities (Paulsen *et al.*, 1970). However, they had good sensitivity and depicted cloud structure overhead fairly well. Unfortunately, they were plagued by recurring hardware maintenance problems including frequent failures of their high-power magnetron transmitters. These problems prompted the air force to decommission the radars in the 1970s. However, there were enough positive results from these fragile instruments to stimulate further developments with mm-wave radar by a few research groups in the 1980s (Pasqualucci *et al.*, 1983; Hobbs *et al.*, 1985; Lhermitte, 1987). Progress intensified in the 1990s in response to an international urgency to better understand the important role that clouds play in climate change. Coincidentally, major radar engineering advances were becoming available at millimeter wavelengths. New or substantially upgraded mm-wave cloud radars were constructed and employed for various cloud studies by several groups (Albrecht *et al.*, 1990; Kropfli *et al.*, 1990; Pazmany *et al.*, 1994; Clothiaux *et al.*, 1995). Work at ETL with 35-GHz radars began in the early 1980s with development of its NOAA/K radar. Through a process of continuing upgrades, this radar is still in active service. NOAA/K is a transportable system with a high-power magnetron transmitter; it possesses Doppler, dual-polarization, and scanning capabilities. In the early 1990s a new high-performance antenna and unique polarization features were added (Kropfli *et al.*, 1990; Kropfli and Kelly, 1996). NOAA/K continues to be used extensively for a variety of cloud studies around the world. Although it can operate unattended for a day or so, NOAA/K is definitely a "research" system that normally requires attention by an engineer and a

scientist during operations. Its ability to reveal the fine-scale structure of most visible nearby clouds, including multiple layer situations (Martner and Kropfli, 1993), was the inspiration for ETL to propose the development of a new, unattended cloud radar for ARM. Aside from using the same wavelength (8.7 mm), however, the new radar's innovative design bears little resemblance to that of NOAA/K. ETL is constructing five of the unattended systems, known as millimeter-wave cloud radars (MMCR) for ARM, and another for the National Science Foundation's Surface Heat Budget of the Arctic (SHEBA) project. NOAA and Radian International LLC have entered into a Cooperative Research and Development Agreement (CRADA) to transfer this technology to industry for the production, refinement, and marketing of future units.

2.2 Frequencies choice of ground based cloud radars

The choice of a wavelength suitable for radar operation is very important thing. The set of frequencies considered as candidates for the envisaged ground-based cloud radar comprises (with free-space wavelengths in parentheses):

- 5.6 GHz (C-band, 5.30 cm)
- 14 GHz (Ku-band, 2.15 cm)
- 24 GHz (K-band, 1.25 cm)
- 35 GHz (Ka-band, 8.60 mm)
- 78 GHz (W-band, 3.85 mm)
- 94 GHz (W-band, 3.19 mm)

These are frequencies assigned for the purpose of radiolocation (some in particular for precipitation and/or cloud observation) in the ITU frequency plan. Moreover, these frequencies have already been used or are envisaged to be used for cloud and precipitation measurement by several research projects around the world. 5.6 GHz is a usual meteorological (weather radar) frequency. For mm-wavelength radar, the choice of a wavelength suitable for radar operation in the earth atmosphere is restricted to spectral regions in which absorption of the radar signal by atmospheric gases, namely oxygen and water vapor, is minimal. The presence of absorption lines at 23 GHz(H_2O), 60 GHz(O_2 absorption band), 118 GHz(O_2) and 183 GHz(H_2O) restricts the wavelength choice to windows centered on 35, 94, 140 GHz and between 200 and 300 GHz(Figure 2.1). The residual atmospheric attenuation in the windows is primarily due to the skirts of water vapor absorption lines and increase systematically with shorter wavelength.

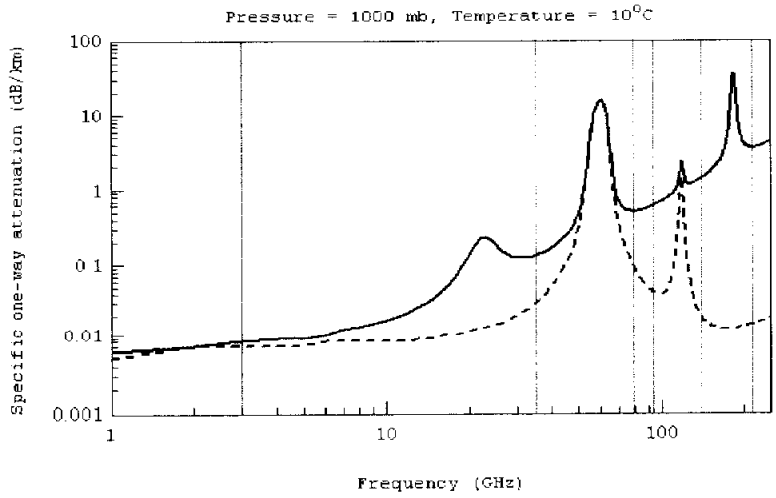

Figure 2.1 One way attenuation due to atmospheric gases a function of frequency, for dry and saturated air at 1000mb and 10℃. Superimposed are vertical solid lines indicating the available frequencies for cloud radar system.

At the highest frequency, 94 GHz, the wavelength is 3.19 mm, still large enough to ensure the validity of the Rayleigh approximation for cloud water droplets (with diameters below 0.1 mm). This approximation yields reflectivity factors being proportional to the sum of the sixth powers of the particle diameters, and specific attenuations being proportional to the sum of the third powers of the particle diameters, or simply the water volume in the cloud. The Rayleigh approximation does not more hold for ice clouds and frequencies above 14 GHz. Ice plates and needles can reach maximum dimension sizes up to a few millimeters, and need already the more complicated Mie theory for scattering and absorption calculations. The same is true for liquid and solid precipitation, with particle sizes up to 10 mm and more, which has to be taken into account when dealing with cloud radar looking up from the ground. In many situations such radar's signals will have to pass the precipitation region below the cloud before reaching the target of interest, i.e. the cloud itself. For types of targets (water droplets and ice clouds, precipitation), backward scattering calculations and results are described in detail in Chapter 3 of this thesis.

A cloud radar looking from the ground up into the atmosphere has to take into account the shadowing by melting layers and precipitation below the clouds, the primary observation target. Fair weather clouds are of course not affected by this type of impairment, but a large fraction of clouds is producing precipitation, whose effects have therefore to be considered in the frequency selection.

The choice of frequency must be done in a way to reveal a maximum of information about the clouds themselves (particle density and size distribution, ice-water distinction);

- Avoid excessive attenuation by structures below the cloud, if present, i.e. the transition region from cloud to precipitation (melting layer, bright band) and the precipitation falling to the ground
- Provide insight into the mechanisms of transition from cloud to precipitation (melting rate, particle aggregation and size distribution formation)
- Allow the acquisition of precipitation vertical profiles (dynamic behavior of particle shape and size distribution, rain enhancement and evaporation) be able to implement the radar in an economical way, i.e. using as far as possible state of-the-art technology and components from the mass market (taking into account the limited budget available).

When aiming at a dual-frequency system, the effect of frequency choice on the ability to extract cloud and precipitation fine structure parameters (particle type and size distribution) is in principle limited to two mechanisms:

- Differential back scattering (reflectivity) due to different scattering regimes, Rayleigh and Mie, if frequencies are spaced far enough. The optimum frequency pair for a dual-frequency cloud radar would of course be that with the farthest spacing, i.e. 14 GHz and 94 GHz when concentrating on the set of frequencies investigated in this study (and in addition assuming that even lower frequencies, e.g. C-band, would also if available in the form of a usual weather radar would be too insensitive for cloud targets with its tiny particle sizes).
- Differential attenuation of the radar signals on their way from the radar to the target and back, partly generated by different scattering mechanisms (Rayleigh vs. Mie).

On the basis of realistic cloud particle spectra and cloud structure scenario in terms of effective or apparent reflectivity, the highest values of differential reflectivity and differential attenuation would be delivered by the frequency pair 35 GHz and 94 GHz in the next Chapter. While these quantities in clouds are rather small, somewhere at the measurement accuracy limit, the additional information gained from differential measurements in the precipitation region can in an indirect way be used to improve cloud type and density retrieval, in a first approximation by simple mass continuity considerations. So, even if the differential back scattering contributions in the clouds themselves are in most cases smaller than the useful limit dictated by dual radar accuracy (and cumulative errors along the radar beam), a dual frequency approach would be of great advantage in the transition and precipitation region below clouds.

One of the main purposes of the ground based cloud radar will be the provision of reference (calibration) information for its space-borne counterpart. At least spot wise, cloud retrievals from space can be compared with the higher accuracy data measured from the ground. Due to the large distance between clouds and the space-borne radar, its range resolution must be compromised with sensitivity. The coarse range resolution (1 km footprint, typically) leads to some averaging between echoes from clouds and the underlying melting and precipitation layers. Even when integrating conventional weather radar observations into the space-borne cloud radar data interpretation, such radar information would not be accurate enough for the proper correction of cloud radar observables.

2.3 Dual wavelength cloud radar system

2.3.1 System overview

National Research Institute for Earth Science and Disaster Prevention (NIED) has investigated rainfall and snowfall clouds, especially that caused disasters, using X-band Doppler and polarimetric radars. But we could not observe non-precipitating clouds and measure simultaneously Doppler velocity and polarimetric parameters. So we have developed a multi-parameter radar system with three frequencies of 9, 35 and 95 GHz on mobile platforms under contract with Mitsubishi Electric Corporation in order to observe cloud and precipitation systems through their whole life cycles. It will be useful for observation researches of not only cloud and precipitation systems but also cloud's affection to the redistribution of energy and water in the climate system.

The developed multi-parameter radar system consists of an X-band radar subsystem for rain and snow observation and a dual-millimeter-wavelength (Ka- and W-band) radar subsystem mainly used for non-precipitation clouds observation. The data receiving facility is also provided for transmission of observation data by satellite communication in NIED.

Figure 2.2 shows the outside appearance of our developed radar system. Each subsystem is mounted on a truck of 4-tons, which we can drive with only normal auto-driving license in Japan, for field experiments. The antenna is mounted on the rear portion of flatbed and the radar control and data acquisition systems are contained in the container on the front portion of flatbed of each truck. The system can be easily transported to observation sites according to the meteorological situation.

Main specifications of developed multi-parameter radar system are listed in Table 2.2. Doppler measurements are available at all frequencies then information of wind field can be collected. The 10 GHz and 95 GHz radars have a function of dual-polarization. It can be derived polarimetric parameters of Z_{hh}, Z_{DR}, ρ_{hv}, Φ_{DP} and K_{DP}. Unfortunately it cannot be measured L_{DR} because the antennas have complex structures and the isolation values between both polarizations are not enough to measure cross-polarization signals. The polarimetric function is expected to be used for discrimination of cloud and precipitation particle type and to improve accuracy of rain rate measurements. The polarimetric function is not used for this study. The RVP7 and IRIS/Open by SIGMET are adopted as the radar signal processor and software for radar control and data analysis of each radar, respectively. Figure 2.3 shows the graphic software for this radar systems.

2.3.2 Features of the 35 / 95 GHz radars

The major remarkable character of our developed 35 GHz and 95 GHz cloud radar sub-system is the adoption of a single Cassegrain antenna with 2.1 m diameter to make collocated measurements at both 35 GHz and 95 GHz (Iwanami *et al.*, 2000). This enables a measurement of liquid water contents in clouds by dual-wavelength method (Wakayama *et al.*, 2000). 95 GHz transmitter and receivers are mounted behind the main mirror, and a part of receiver for 35 GHz near the antenna pedestal in order to minimize signal loss by wave-guide and derive better sensitivities. There are horn antennas at the center of main mirror and 95 GHz circular horn is put between 35 GHz horn array from the top and bottom. Doppler measurements are available at both frequencies. 35 GHz radar using a magnetron for the transmitter tube realizes Doppler velocity range of about ± 8.5 m/s within the limitation of duty cycle of 0.05 % by the adoption of the double pulse operation. Figure 2.4 shows the

block diagram of the subsystem. The left-hand side shows a single antenna for common use, and upper part shows the 35 GHz and lower part shows 95 GHz radar in right-hand side. There are two receivers for vertical and horizontal polarization signals and polarimetric measurement is available at 95 GHz.

Table 2.2 Specifications of dual frequency cloud radar system.

	35 GHz (Ka band)	95 GHz (W band)
Frequency	35.35 GHz	95.13 GHz
Antenna Type	Cassegrain, 2.1 mϕ	
Scan Range (Scan Rate): AZ	Full Circle (≤ 24 deg/s)	
EL	−2 to +182 deg (≤ 12 deg/s)	
Antenna Gain	54.0 dB	58.7 dB
Beam Width	0.3 deg	0.1 deg
Transmitter Tube	Magnetron	Klystron (EIA)
Peak Power	100 kW	2.2 kW
Pulse Length	0.5 μs	0.25 to 2.0 μs
Pulse Repetition Frequency	400/4,000 Hz	≤ 20 kHz
Polarization	H	H or V
Doppler Processing	PPP	PPP, FFT
Noise Figure	3.5 dB	7.5 dB
Observation Range	30 km	30 km
Outputs	Z, V, W	Z, V, W, Z_{DR}, ρ_{hv}, Φ_{DP}, K_{DP}

Figure 2.2 The photos of vertical pointing radar in NIED.

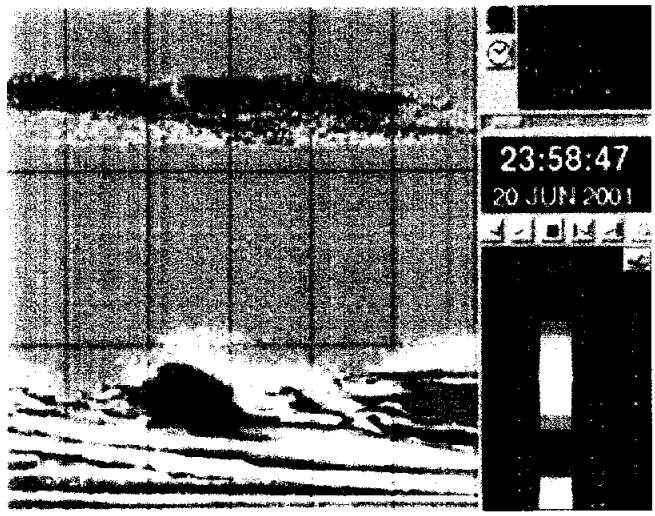

Figure 2.3 Time-height cross section of reflectivity observed by 35 GHz radar. Time duration is 330 seconds.

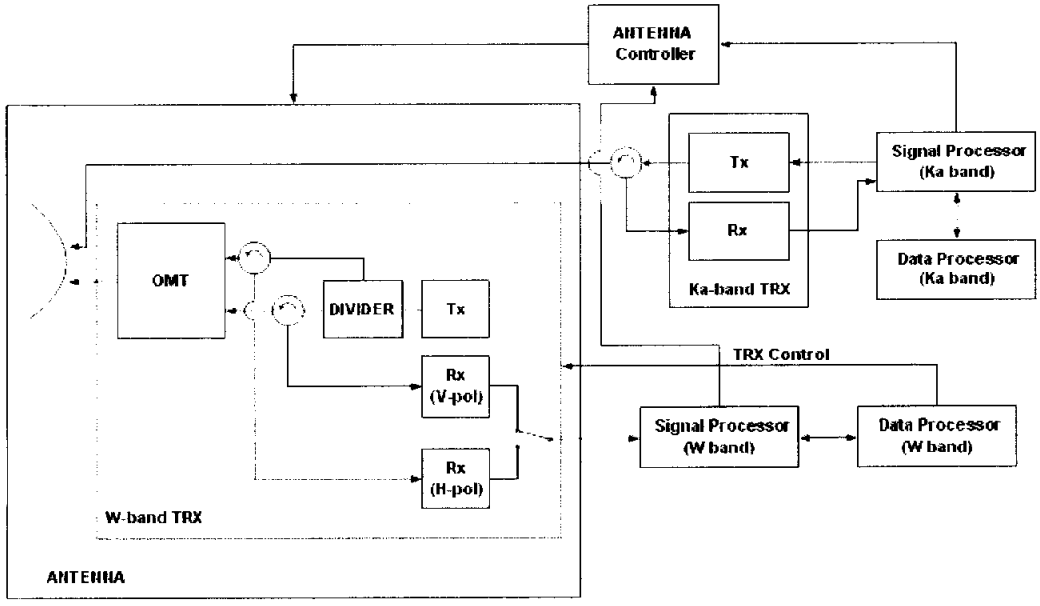

Figure 2.4 Block diagram of the developed cloud radar subsystem.

2.3.3 Sensitivity and calibration

An important way to improve the sensitivity of the radar is to subtract an estimate of the noise N from the measured average power P, where `noise' is taken to be the sum of receiver noise and thermal emission by the atmosphere, as they are generally indistinguishable. This enables the minimum detectable signal to be reduced by at least an order of magnitude below the noise level. Often rain radars simply reject the data that fall below a particular threshold, which is far too crude a procedure if quantitative use is to be made of observations at low reflectivity. The noise component manifests itself as a constant power with range, so in practice P in the cloud-free stratosphere provides an accurate measure of N. In this section we determine the effect of noise subtraction on the accuracy of the final Z measurement, as a function of signal-to-noise ratio SNR = S/N.

Figure 2.5 shows the relationships between minimum detectable reflectivity dBZ and range km for 3 dB signal-to-noise ratio, given a 0.5 and 1.0 μs transmit pulse for 35 GHz and 95 GHz. With one-second integration, 35 and 95 GHz minimum reflectivity is less than –29 dBZ and less than –27 dBZ at the range of 10 km. The numbers of pulse integration are 450 for 35 GHz and 10-thousand for 95 GHz. Figure 2.6 indicates an example of time-height cross sections by vertically pointing measurement at 35 GHz and 95 GHz radar.

Calibration is frequently a problem for meteorological radars, but the solution in this case has been to use range-height scans (RHIs) through low cloud (taken on 1 August 1996) with the co-located 3 GHz antenna in operation. The 3 GHz radar has itself been calibrated to an accuracy of better than 0.5 dB from the consistency of differential reflectivity and differential phase measurements in moderate rain

(Goddard et al. 1994b), but at vertical incidence it is of little use because of severe ground clutter. After matching 35 and 3 GHz reflectivities, the 35 GHz noise at 1 km was found to be was and oxygen becomes important at millimeter wavelengths. After matching 35 and 3GHz reflectivities, the 35GHz noise at 1km was found to be –34dBZ. It is reasonable to assume that this would be approximately the same at vertical incidence, so the radar was calibrated on other occasions simple by averaging the reflectivity so that the mean value of N was –34dBZ.

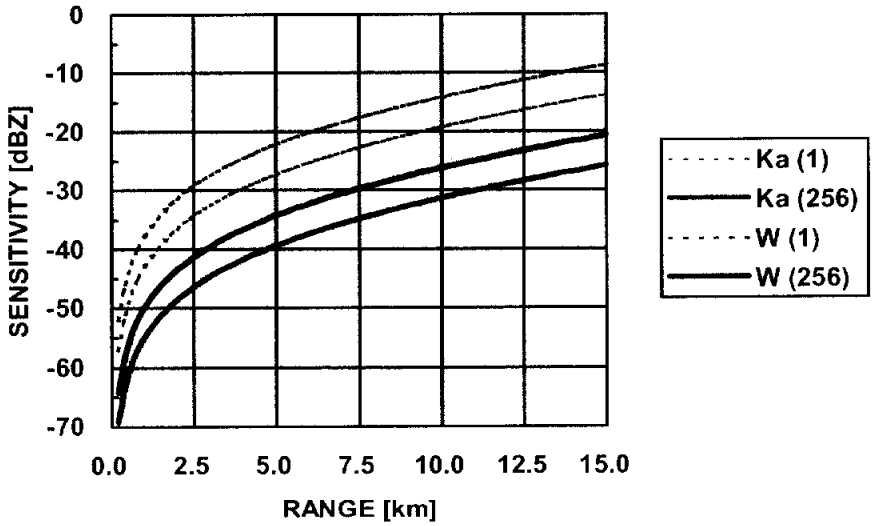

Figure 2.5 Sensitivity of the developed cloud radar subsystem for 3 dB signal-to-noise ratio, given a 0.5 and 1.0 μs transmit pulse for 35 and 95 GHz. Thin and thick dashed lines show sensitivities at 35 and 95 GHz with single pulse. Thin and thick solid curves show sensitivities at 35 and 95 GHz with one-second integration, respectively.

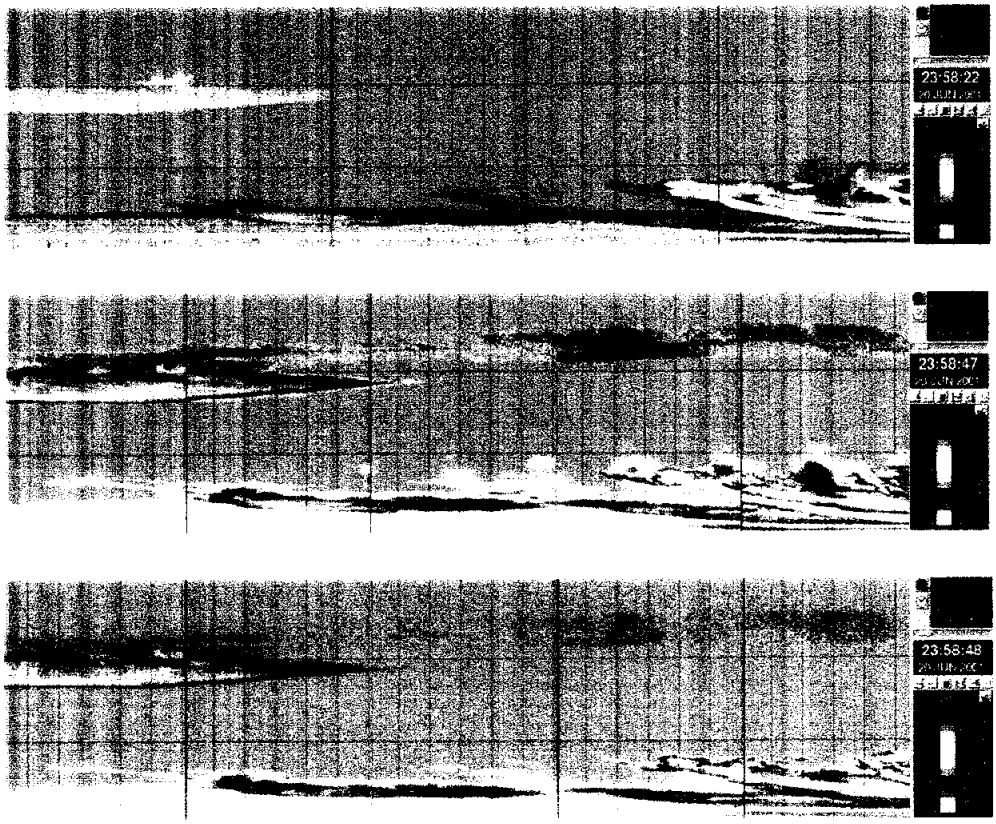

Figure 2.6 Time-height cross section of reflectivity observed by 10 GHz (upper), 35 GHz (middle) and 95 GHz (lower) radar at SNR = 3dB . 10 GHz radar can't clearly detect low level cloud: otherwise, reflectivities of 35 and 95 GHz radar show fine structure of cloud in low level. Sensitivity of 35 GHz radar is higher than that of 95 GHz. This results from low transmit power and attenuation in 95 GHz radar.

Chapter 3

BASIC THEORIES FOR MM WAVELENGTH RADAR

This chapter will describe the application of scattering theory which is central to the quantitative use of radar measurement, and provide relationships between the signal power detected by the instrument and the meteorological parameters of interest. In section 3.1 the focus will be the scattering properties of hydrometeors, Mie theory is regarded as adequate for this thesis.

For mm-wave radar, the first task is to implement Mie function programs for the computation of scattering and attenuation for water and ice type as a function of particle diameter. This is done at the 35 GHz and 95 GHz radar frequency. The scattering coefficients of each type and size of hydrometeor is calculated using transition Matrix theory (T-Matrix) of Barber and Yeh (1975) and Bringi *et. al* (1991) and dielectric properties of ice and water(these will be dealt with next section in detail) are taken from Ray (1972). The attenuation and reflectivity are then calculated using the Mueller-matrix method of Vivekandandan *et al.* (1991).

3.1 Scattering theory

The intensity of the return pulse is a function of the *backscatter* of the hydrometeors encountered and the intervening attenuation or *extinction* which may be due to atmospheric gases (such as water vapor) or any intervening hydrometeors

themselves. Backscatter is defined as the scatter at 180° with respect to incident radiation (i.e. returning to the instrument). Extinction describes the reduction in intensity due to absorption and scattering out of the path of the beam and is defined in terms of the extinction cross section

$$\sigma_e = \sigma_s + \sigma_a \tag{3.1}$$

where σ_s is the scattering cross section and σ_a is the absorption cross section. At short wavelengths the extinction is solely due to scattering (σ_a is negligible) but has a major impact whereas at the longer radar wavelengths the extinction is dominated by absorption and is relatively minor, although noticeable in certain situations.

3.1.1 Rayleigh / Mie scattering

The apparent backscattering cross section is defined as the cross section that would return the same power if it was assumed that the particle was an isotropic scatterer (Battan, 1973). This is quite distinct from the the physical cross section of a particle which need not (and often does not) scatter isotropically. For a spherical water droplet with a diameter small compared to the wavelength, the Rayleigh scattering approximation can be used and the backscattering cross-section is given by

$$\sigma_b = \frac{\pi^5}{\lambda^4} D^6 |K|^2 \tag{3.2}$$

where D is the droplet diameter and λ is the wavelength. $|K|^2$ is the dielectric factor which will be carefully discussed in section 3.2.

From (3.2) it can be seen that $\sigma \propto \lambda^{-4}$ which indicates that shorter microwave wavelengths are increasingly sensitive. However, the diameters for which the Rayleigh scattering approximation is valid decrease with shorter wavelengths. It can be defined an electrical size, a, to normalize with respect to wavelength

$$a = \frac{\pi D}{\lambda} \tag{3.3}$$

where D is the droplet diameter and λ is the wavelength.

Table 3.1 Maximum diameters for which the Rayleigh scattering approximation is assumed valid (a= 0. 5) for a selection of typical radar wavelengths (frequency is in GHz).

Frequency	Band	Wavelength	Maximum diameter	Application
95	W	3.2 mm	0.5 mm	Cloud radar
35	Ka	8.6 mm	1.4 mm	Cloud radar
10	X	3 cm	4.7 mm	Weather radar
5	C	5 cm	10 mm	Weather radar
3	S	10 cm	16 mm	Weather radar
1.3	L	24 cm	38 mm	Wind profiler

Table 3.1 displays the maximum values of D for which the Rayleigh approximation holds at a number of typical radar wavelengths assuming that $a \leq 0.5$. Since raindrop diameters usually range from 1–6 mm it can be seen that although the millimeter wavelength radars have the advantage of greatly increased sensitivity the

Rayleigh approximation will not always hold in rain and is only valid for droplets having smaller diameters such as cloud and drizzle droplets, hence the generic term of cloud radars.

The advantages of shorter wavelengths also include a reduction in clutter and a smaller antenna or lower transmit power required for the same sensitivity. These need to be weighed against the technological maturity of longer wavelength systems, the increase in attenuation at shorter wavelengths and the intended application.

The Rayleigh approximation is valid at centimeter wavelengths when dealing with raindrops but hailstones and graupel can be an order of magnitude larger than raindrops and, if wet, have a similar backscattering cross-section to water spheres of the same size (Battan, 1973). Thus, as instruments move towards shorter wavelengths, it may be necessary to use the complete solution for the backscattering cross-section of spheres (Mie, 1908)

$$\sigma_b = \frac{\pi D^2}{4a^2} \sum_{n=1}^{\infty} (n-1)^n (2n+1)(a_n - b_n)^2 \tag{3.4}$$

where a_n and b_n are coefficients of the scattering field involving Bessel and Hankel functions which relate the scattering angle, electrical size and complex refractive index (following Burgess and Ray, 1986). Although more accurate, this is no longer a simple analytical expression and usually requires numerical evaluation. If it is defined a normalized (with respect to cross-sectional area) backscattering cross–section or scattering efficiency such that then figure 3.1 and 3.2 show the scattering efficiencies calculated as a function of a spherical water and ice droplet at 0℃ for Mie scattering and Rayleigh scattering. The Rayleigh approximation is generally appropriate for diameters $D \leq \lambda/16$ *or* $a \leq \pi/16$ and appears sufficient for diameters as

large as $a \leq 0.5$ as used in table 3.1. However, there is a resonance region (van de Hulst, 1957) at higher temperatures near $a \approx 0.5$ where Mie scattering can exceed Rayleigh scattering. Figure 3.3 shows the ratio of Rayleigh to Mie scattering for water and ice drop, respectively.

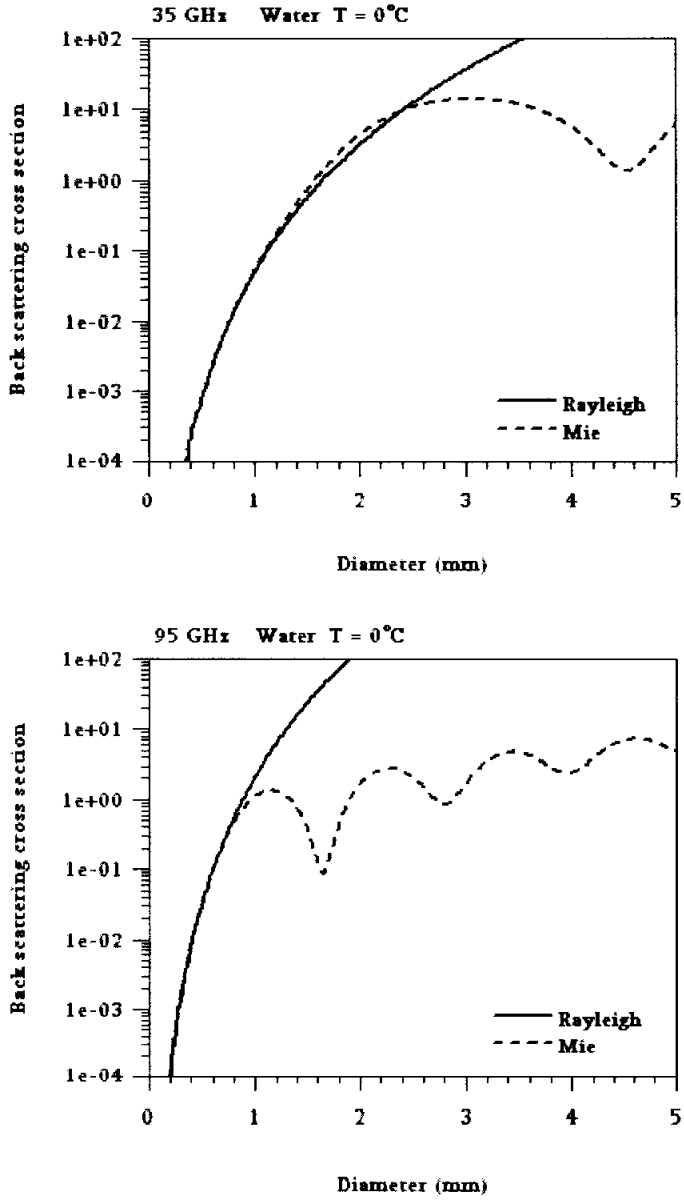

Figure 3.1 Radar backscattering cross section of spherical water as a function of their diameter at a) 35 GHz and b) 95GHz at 0 ℃. The solid lines indicate the Rayleigh scattering approximation.

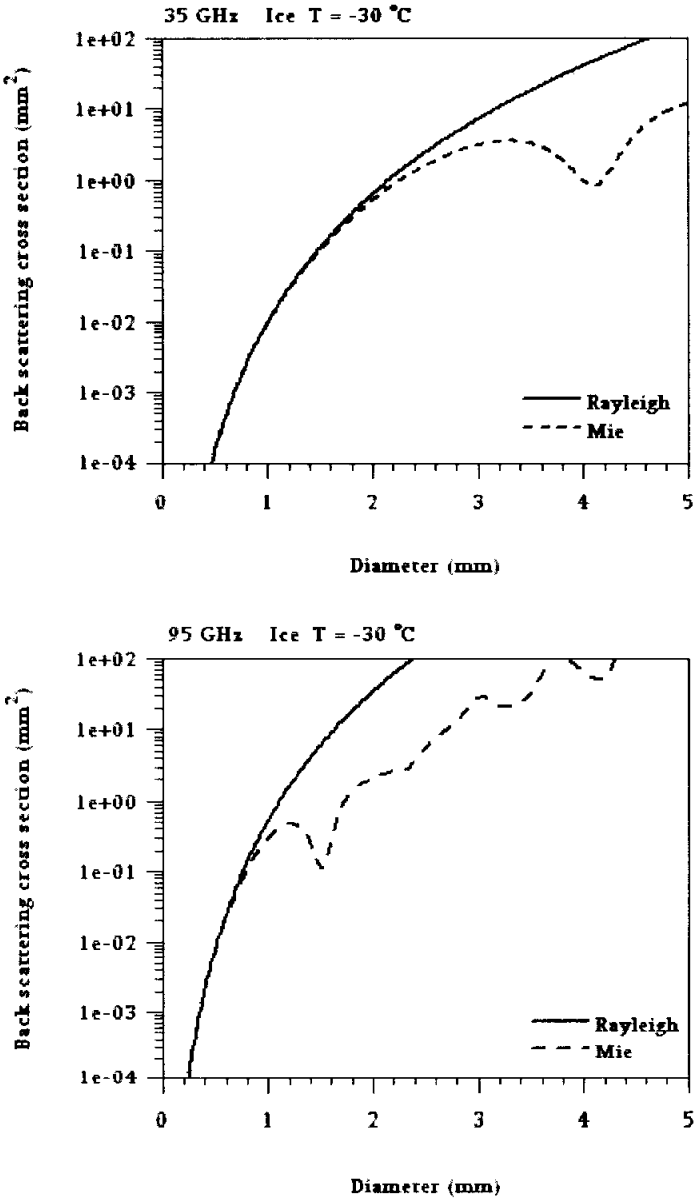

Figure 3.2 Same as figure 3.1, but for ice.

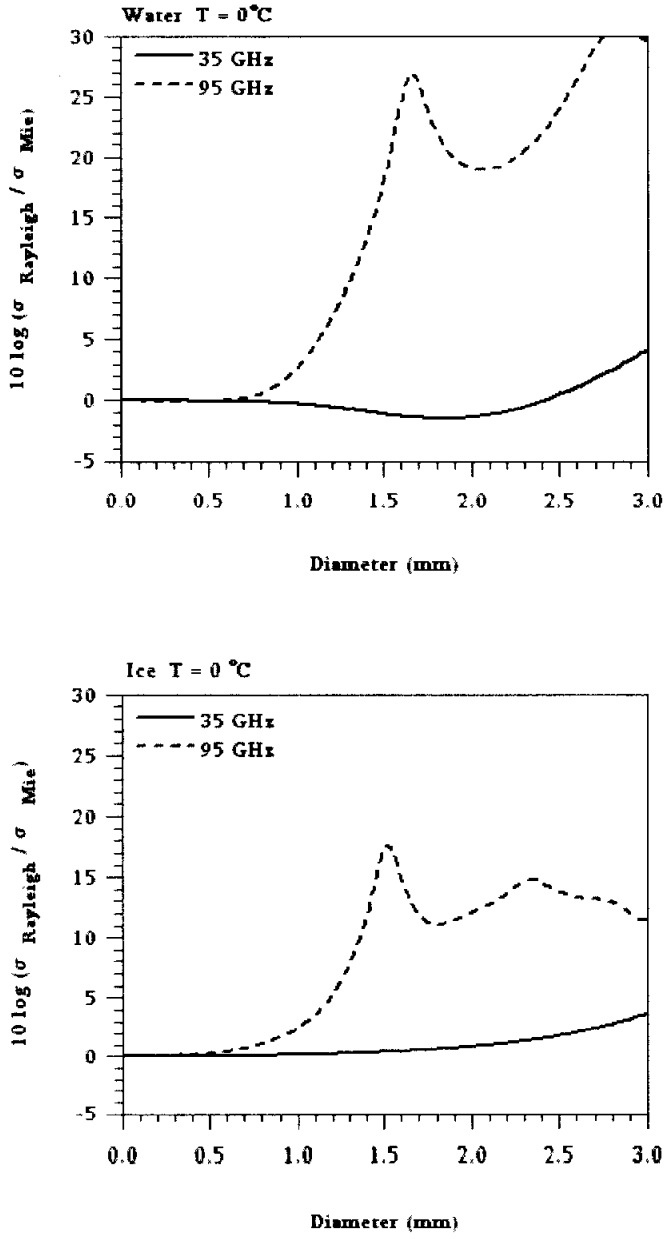

Figure 3.3 Ratio (in dB) of Rayleigh to Mie backscattering cross section of (a) water and (b) ice at the indicated radar frequency as a function of raindrop diameter.

3.1.2 Radar reflectivity

If it is assumed that all droplets are spherical water droplets and are small enough to be in the Rayleigh scattering regime and that the droplets are randomly dispersed throughout the pulse volume, the reflectivity η (Doviak and Zrni´c, 1993)

$$\eta = \frac{1}{\Delta V}\sum_{i=1}^{n}\sigma_i \tag{3.5}$$

is the sum per unit volume of the contributions from the individual scatterers within the pulse volume, ΔV. From (3.2), σ is proportional to the sixth power of diameter and it is referred to the backscattered signal in terms of the radar reflectivity factor, Z,

$$Z = \frac{1}{\Delta V}\sum_{i=1}^{n} D_i^6 \tag{3.6}$$

For a mono-disperse distribution of droplets $Z = ND^6$, and for a range of droplet diameters

$$Z = \int_0^\infty n(D)D^6 dD \tag{3.7}$$

where $n(D)\,dD$ is the number concentration of water droplets per unit volume with diameters between D and $D+dD$. Radar meteorologists measure Z in mm^6/m^3 but because Z varies over many orders of magnitude it is usually preferable to use the logarithmic units dBZ where

$$Z[dBZ] = 10\log_{10}(Z\,[mm^6 m^{-3}]) \tag{3.8}$$

Millimeter-wavelength radars will encounter droplets with diameters that extend into the Mie scattering regime and a factor that describes the departure from Rayleigh scattering is introduced so that in general the radar reflectivity factor for spherical liquid water droplets at frequency f, is defined as

$$\begin{aligned} Z_f &= \frac{\pi^5 \left|K_{f,T}\right|^2}{\lambda^4 \left|K_{f,0}\right|^2} \int_0^\infty n(D) D^6 \sigma(D)\, dD \\ &= \frac{\pi^5 \left|K_{f,T}\right|^2}{\lambda^4 \left|K_{f,0}\right|^2} \int_0^\infty n(D) D^6 \gamma_f(D)\, dD \end{aligned} \tag{3.9}$$

where $\left|K_{f,T}\right|^2$ is the dielectric factor of liquid water at temp $\left|K_{f,0}\right|^2$ is the dielectric factor of liquid water at 0 ℃ is the Mie/Rayleigh backscatter ratio. The ratio of dielectric factors ensures that radars of different wavelengths will all measure the same Z for a 0 ℃ cloud containing Rayleigh scattering liquid water droplets. The dielectric constant varies with temperature at 94 GHz and can be calculated using the empirical formula given in Liebe *et al.* (1989) which will be present in section 3.2.

3.1.3 Attenuation at radar wavelengths

The radar beam can be attenuated by liquid water, water vapor and other atmospheric constituents such as oxygen. In this thesis it have used the *mwps* package provided by Robin Hogan which uses the line–by–line model of Liebe (1985) to calculate the attenuation due to oxygen and water vapor. The inputs are the frequency of the radar, temperature, pressure and relative humidity.

Figure 3.4 displays one-way attenuation coefficient by atmospheric gases as a function of frequency and figure 3.5 plots one-way attenuation coefficient by atmospheric gases as a function of temperature at 10 GHz, 35 GHz and 95 GHz, which were simulated by Liebe model.

At millimeter wavelengths gaseous attenuation is not negligible even when the radar is at zenith and can easily reach 2 dB/km (two–way) in a humid boundary layer. At 94 GHz the one–way gaseous attenuation is 1.32 dB/km at 20 ℃, 1013 hPa and a relative humidity of 100%. At 35 GHz the attenuation is less severe, 0.243 dB/km one–way, in similar conditions.

An estimate of the temperature profile and atmospheric water vapor content can be obtained from radiosonde ascents or from a numerical model. The extinction due to liquid water is the sum of absorption and scattering (3.1) and for Rayleigh scatterers, the absorption is given by (Doviak and Zrni´c, 1993)

$$\sigma_a = \frac{\pi^2 \,\mathrm{Im}(-K)}{\lambda} \sum_{n=1}^{N} D_n^3 \tag{3.10}$$

where Im(-*K*) is the imaginary part of the dielectric factor for liquid water. The scattering term is (Battan, 1973)

$$\sigma_s = \frac{2\sigma_b}{3} \tag{3.11}$$

where σ_b is the backscatter as defined in section 3.1.

Absorption dominates scattering and is proportional to the liquid water content so that at 94 GHz the one–way attenuation of 1 g/m^3 of liquid water is 3.88 dB/km at 20 ℃. At 35 GHz this falls to 0.637 dBkm^{-1}/gm^{-3} at 20 ℃. Characterizing the

attenuation due to liquid water is problematic due to its high variability.

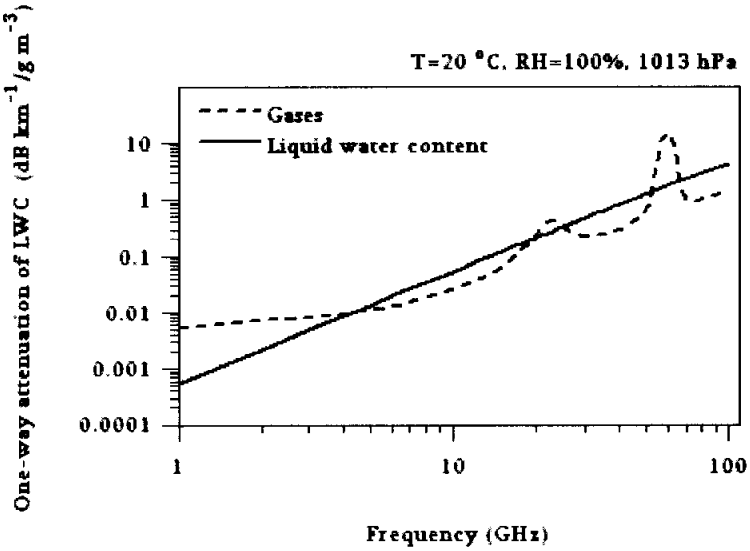

Figure 3.4 One-way attenuation coefficient by atmospheric gases as a function of frequency.

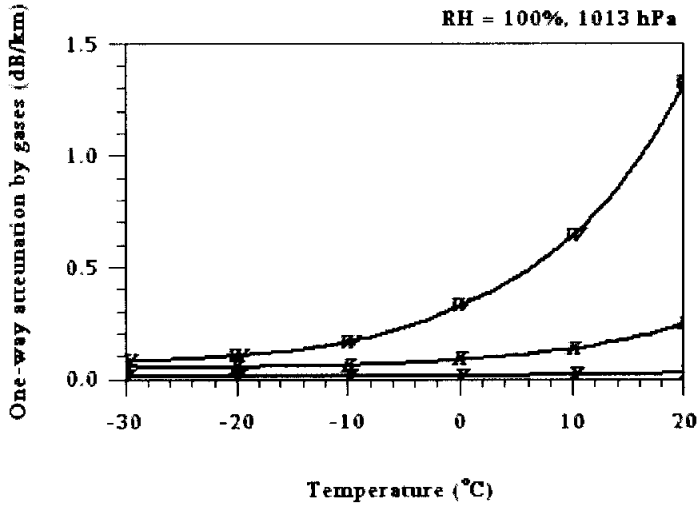

Figure 3.5 One-way attenuation coefficient by atmospheric gases as a function of temperature at 10 GHz, 35GHz and 95 GHz.

3.2 Dielectric factor $|K|^2$ for water and ice

The dimensionless quantity K is given as

$$K = \frac{m^2 - 1}{m^2 + 1} \tag{3.12}$$

where m is the complex index of refraction. For any given substance, the complex index of refraction, m, is a function of λ and temperature and can be written

$$m = n - ik \tag{3.13}$$

where n is the ordinary refractive index and k is the absorption coefficient of the material involved.

Scattering and attenuation by homogeneous spheres are strongly influenced by m. This dependence is expressed in equations for spheres of small dimensions by the terms $|K|^2$ and Im(-K). The scattering and absorption cross sections are proportional to these terms, respectively. For a given substance, m is a function of the wavelength and the temperature of the sphere. The values of n, k, $|K|^2$ and Im(-K) calculated by Ray *et al.* (1972) are given in figures from (3.6) to (3.8).

For a dielectric without loss, $\sigma_a = 0$ and $\sigma_t = \sigma_s$. For a dielectric with high loss such as water and for spheres of small size, $\sigma_s << \sigma_a$ and so $\sigma_t \fallingdotseq \sigma_a$. In the intermediate case of ice, σ_a and σ_s are comparable, and the two terms must be taken into account to obtain σ_t. For water, $|K|^2$ is practically constant at the temperatures found in the atmosphere and wavelengths in the centimeter range, currently used in radar; it is approximately 0.93 for liquid water.

For ice, n and k are independent of wavelength and k is small as shown in Figure 3.6. For ice with normal density (ρ = 0.92 g/cm^3), $|K|^2$ =0.176 regardless of the temperature. For ρ = 0.92 g/cm^3, we have $|K|^2$ =0.208. Therefore, due to the value difference of $|K|^2$, the backscattering cross section σ_b for spherical and homogeneous hydrometeors of the same diameter is about 5.3 times weaker for ice than for water; that is, 7.3 dB. The diameter of the ice hydrometeors has to be superior to that of the water hydrometeors by only 32% to compensate for this difference.

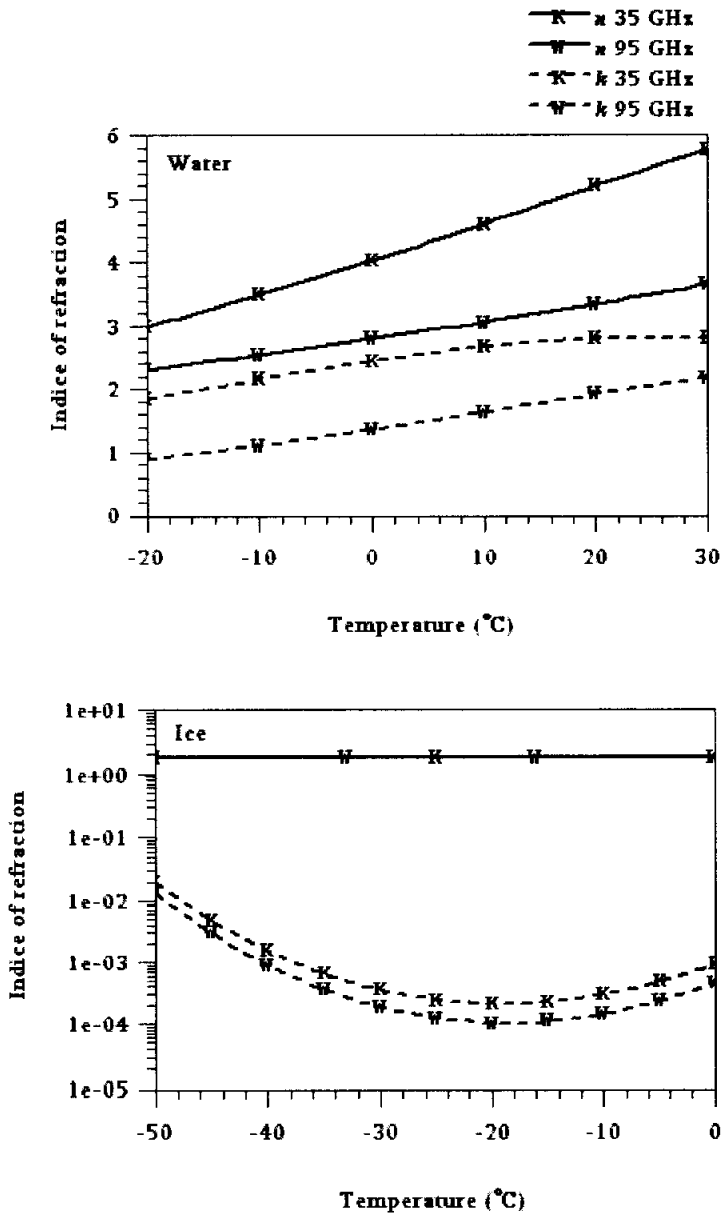

Figure 3.6 Reflective index n and k for water and ice as a function of temperature at 35 GHz and 95 GHz.

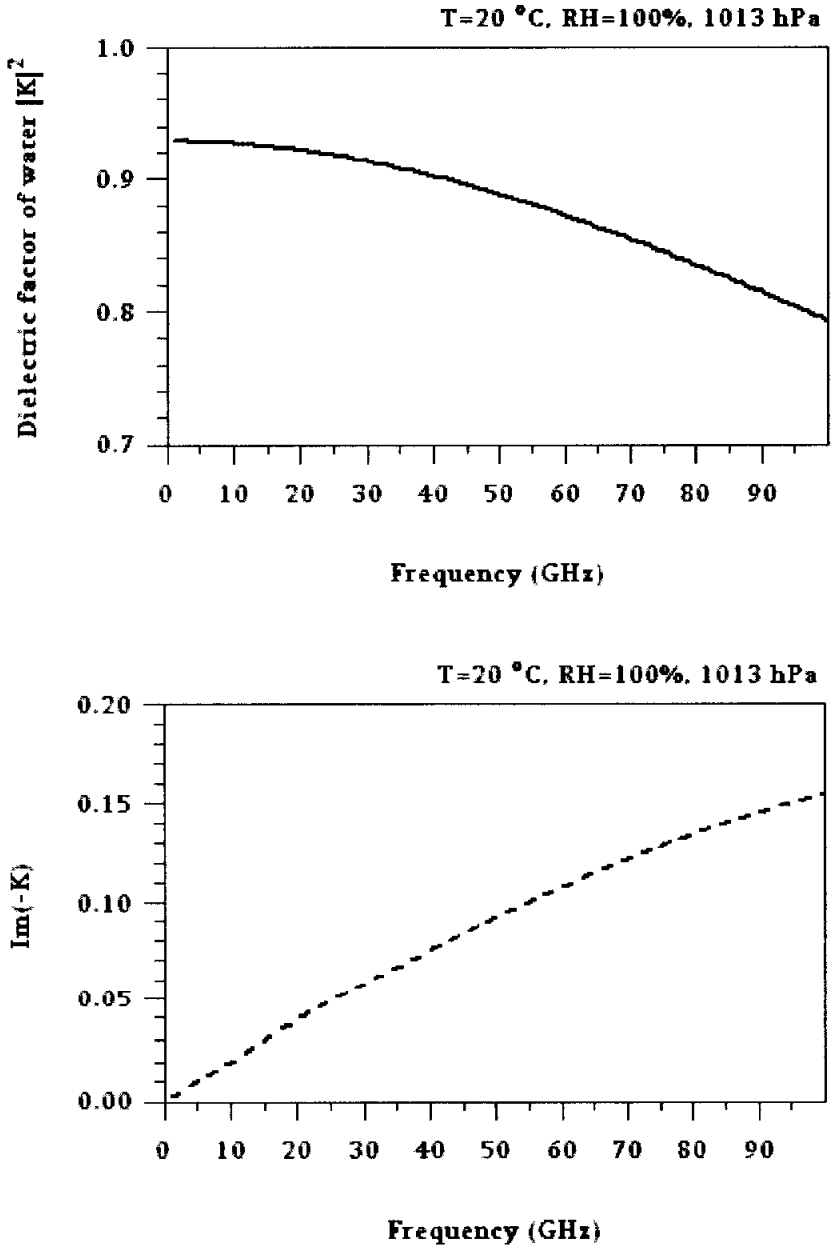

Figure 3.7 The variation of dielectric factor of water $|K|^2$ and $Im(-K)$ as a function of frequency.

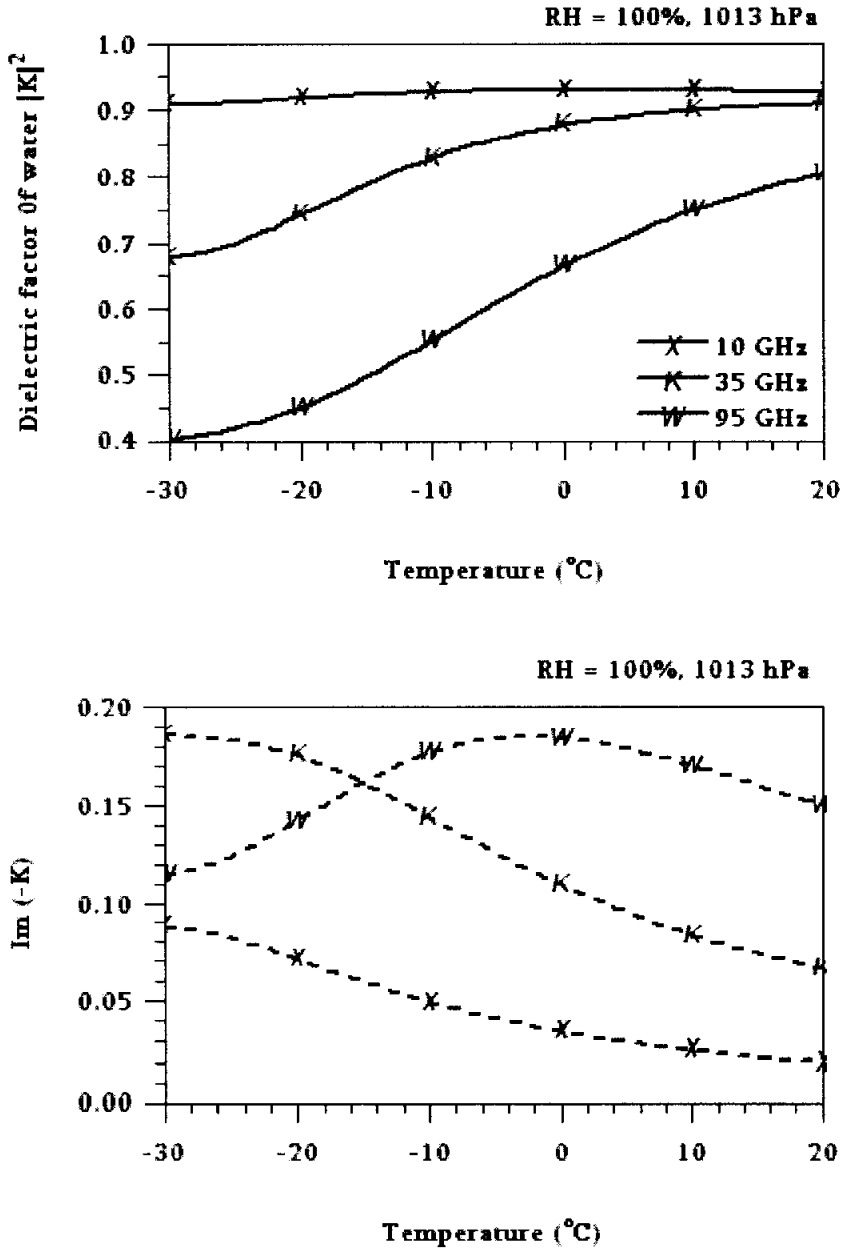

Figure 3.8 The variation of dielectric factor of water $|K|^2$ and $Im(-K)$ as a function of temperature at 10 GHZ, 35 GHz and 95 GHz.

3.3 Drop size distribution

In the presence of non-Rayleigh scatterers, that is in the Mied scattering region, a measured reflectivity Z_m at distance r can be written in equation (3.14) at mm-wave radars for any atmospheric profile.

$$10 \log Z_m = 10 \log Z_e + 2 \int_0^r A(s)\,ds \qquad (3.14)$$

where each term means the equivalent reflectivity factor Z_e and attenuation term $A(s)$, and can be rewritten equation (3.15)

$$10 \log Z_m = \frac{\pi^5 \left|K_{f,T}\right|^2}{\lambda^4 \left|K_{f,0}\right|^2} 10 \log\left[\int_0^\infty n(D) D^6 \gamma_f(D)\, dD\right] + 2 \int_0^r A(s)\, ds \quad (3.15)$$

where $n(D)$ is drop size distribution. In this study, it is assumed that the size spectral of droplets $n(D)$ can be represented by an analytical function which has three parameter such as the gamma distribution (Ulbrich, 1989) .

$$n(D) = N_0 D^{\mu} \exp\left[-(3.67+\mu) D / D_0\right] \qquad (3.16)$$

where N_0 is a intercept parameter and D_0 is the median volume diameter. μ is the dimensionless order of the distribution that determines its shape and as μ increases the distribution becomes narrower. Figure 3.9 shows the drop size distribution due to the variation of three parameters (N_0, D_0 and μ).

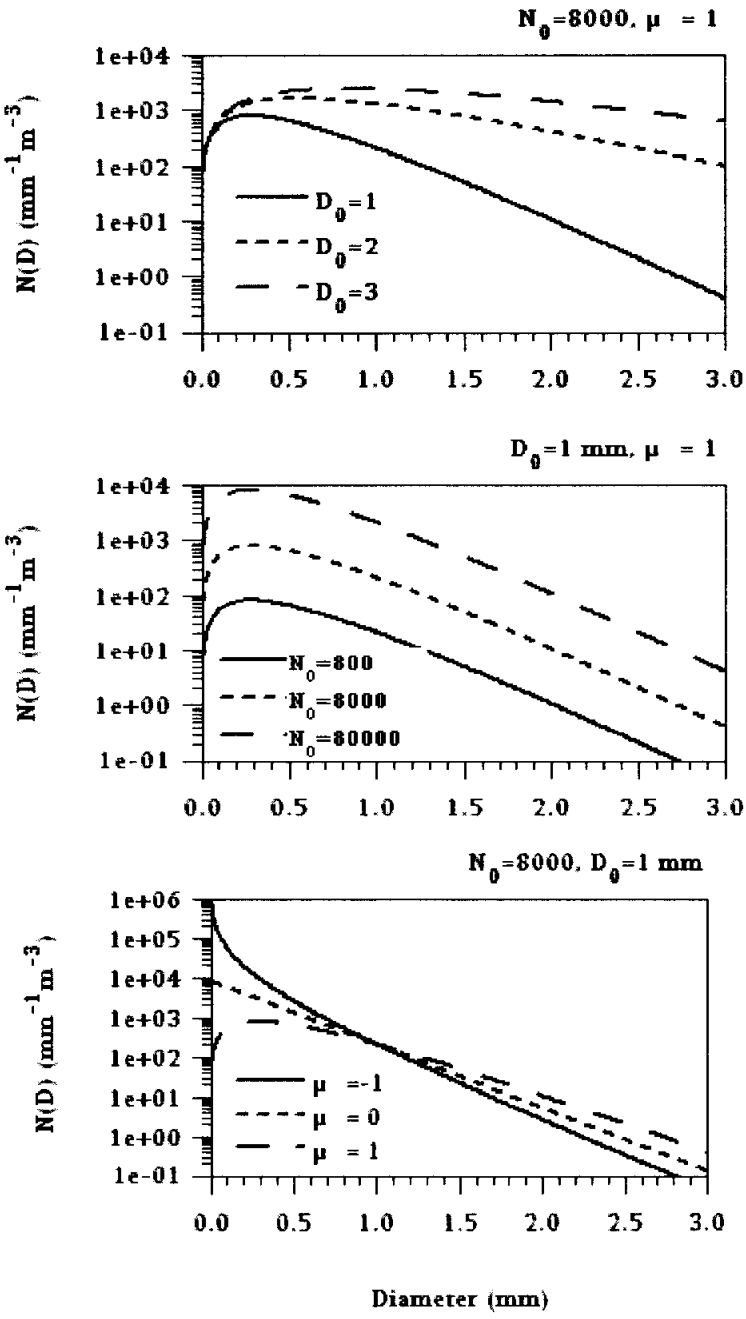

Figure 3.9 The variation characteristics of three parameter N_0, D_0 and μ.

Using this relationship, (3.9) and (3.16) can be given

$$Z_e = \frac{\pi^5 \left|K_{f,T}\right|^2}{\lambda^4 \left|K_{f,0}\right|^2} N_0 \times 10\log\left[\int_0^\infty D^{\mu+6} \exp\left[-(3.67+\mu)D/D_0\right]\gamma_f(D)\, dD\right] \quad (3.17)$$

Equivalent reflectivity factor depends on the drop size distribution parameter *n(D)*. *n(D)* varies with DSD parameters N_0, D_0 and μ and figures from (3.10) to (3.13) the variation of DSD parameter.

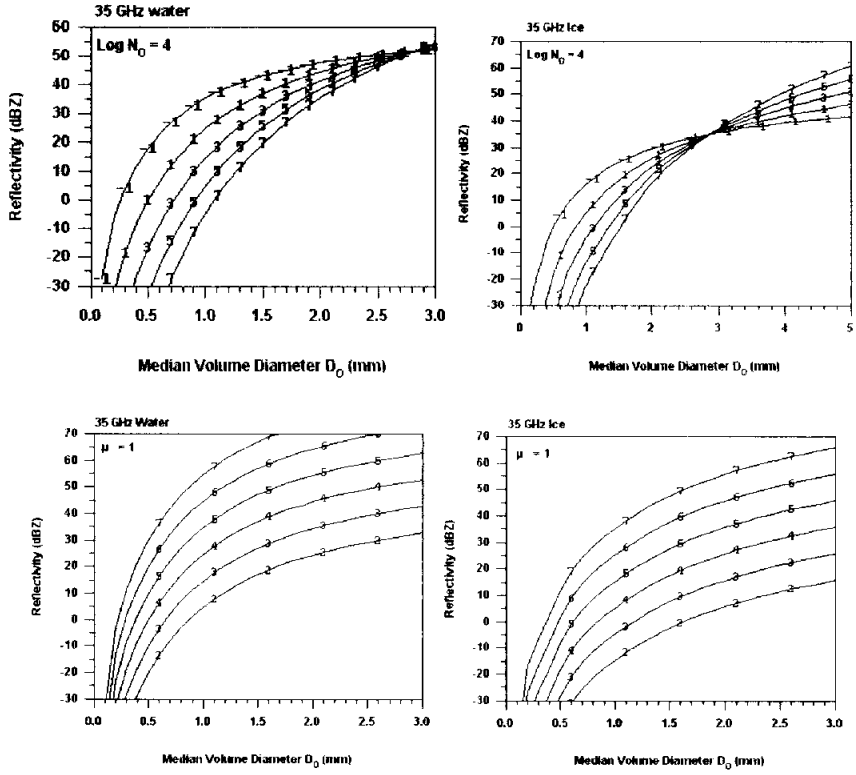

Figure 3.10 The variation of reflectivity factor in Mie region as a function of median volume diameter D_0 (mm) for (a) water (b) ice scatterer at 35 GHz frequency. Log N_0 is fixed with 4 and the number of solid line means μ value, which ranges from -1 to 7. Same as a) and b), but for μ value is fixed with 1 and the number of solid line means Log N_0, which ranges from 2 to 7.

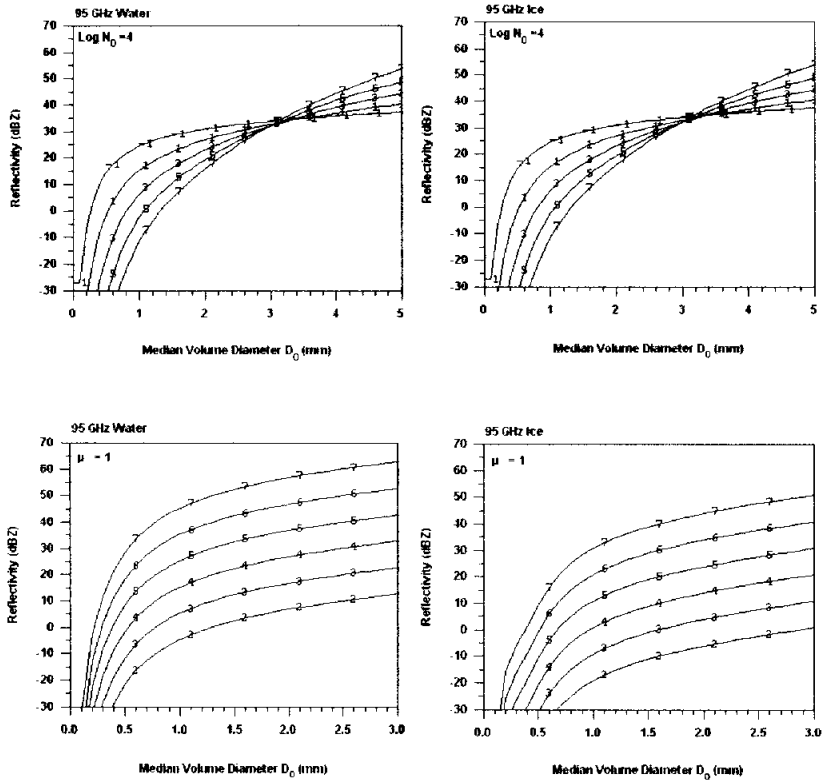

Figure 3.11 Same as figure 3.10, but for 95 GHz frequency.

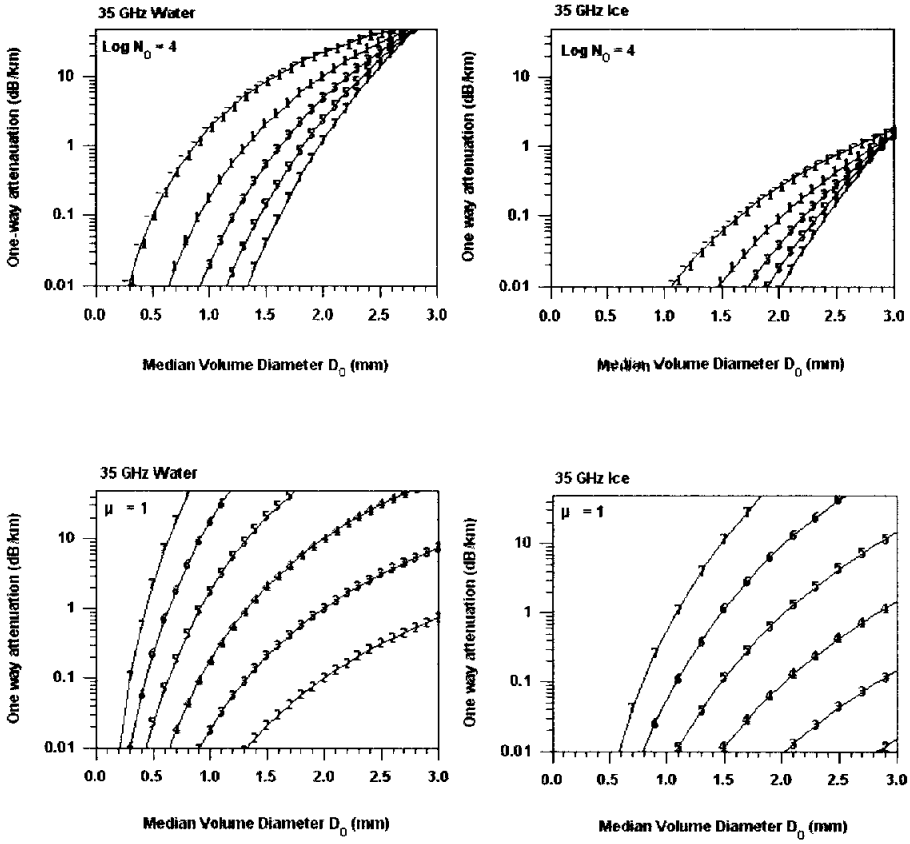

Figure 3.12 The variation of attenuation in Mie region as a function of median volume diameter D_0 (mm) for (a) water (b) ice scatterer at 35 GHz frequency. Log N_0 is fixed with 4 and the number of solid line means μ value, which ranges from -1 to 7. Same as a) and b), but for μ value is fixed with 1 and the number of solid line means Log N_0, which ranges from 2 to 7.

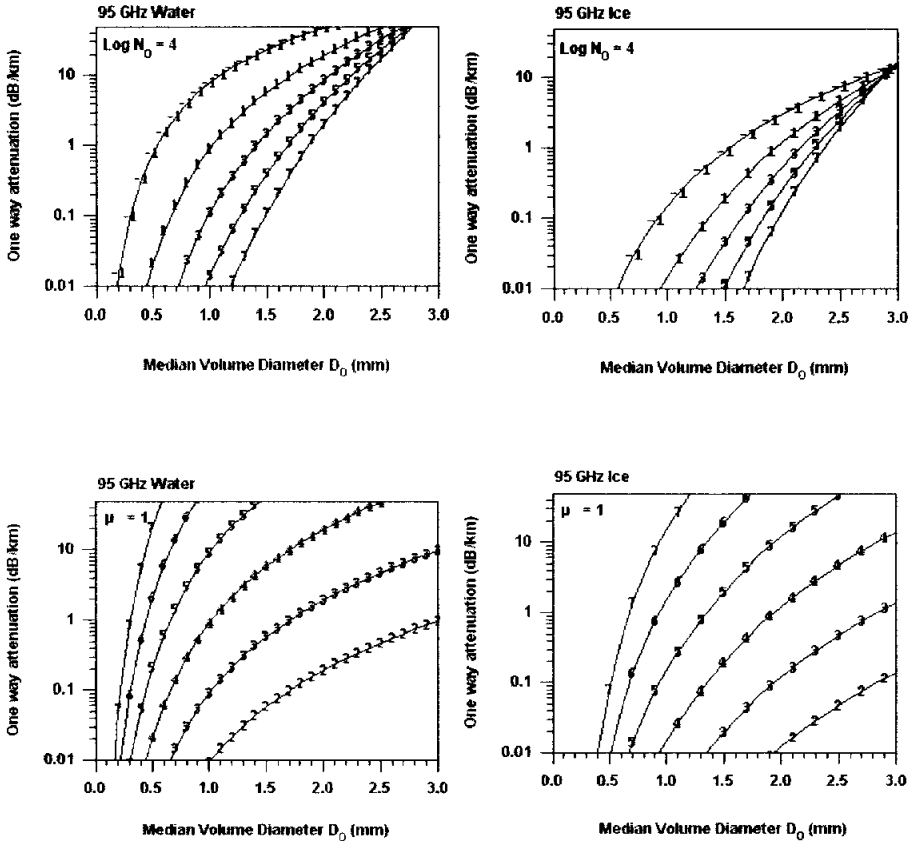

Figure 3.13 Same as figure 3.12, but for 95 GHz frequency.

Chapter 4

HYDROMETEORS RETRIEVAL METHOD USING DUAL WAVELENGTH RADAR

4.1 Introduction

The importance of clouds in the global radiation budget has been widely recognized. Clouds influence both incoming solar radiation and outgoing thermal terrestrial radiation. Their radiative properties are determined by the microphysics (particle size distribution, their shape and phase) and macrophysics (thickness, horizontal extent, cloud height). Knowledge of cloud properties and their variabilities are still insufficient to estimate the cloud radiative impact on the earth climate system. Combination with the additional observational platforms such as satellites, aircrafts, balloons, and ground measurements is necessary to improve our current understanding of cloud formation mechanisms, their microphysics, and their radiative feedbacks in the climate system (Hobbs, 1993).

Remote sensing methods have been extensively used in cloud microphysical researches during the last few decades, and more techniques have been developed. One of the most important advantages of the remote sensing approaches over direct aircraft or balloon-based cloud sampling techniques is that they can be used for the larger scale researches. It can lead us to acquire the representative statistics about cloud properties, which are important for better understanding the role of clouds in the earth climate. However, the accuracy of the remote sensing measurements and

its dependence on the initial assumptions should be clear.

Active remote sensors such as lidar and radar provide vertically resolved information of cloud structure. Low atmospheric attenuation of radar signals makes radar as the promising method for the cloud studies. These results in recent developments of several millimeter-wavelength radar systems dedicated primarily to the cloud research (Kropfli et al. 1995; Mead et al. 1994; Clothiaux et al. 1995). Comparing to the conventional centimeter wavelength weather radars, the millimeter wavelength radars are inherently more sensitive to small cloud particles, providing better spatial resolution, and have the better signal-to-clutter ratio (Kropfli and Kelly 1996). These features make radars very useful tools for studies of non-precipitating clouds.

Current remote sensing developments utilize more advanced instruments. They are often based on the use of the several different remote sensors or the multi-wavelength approaches. The Multi-sensor or multi-wavelength approaches help to prevent some potential retrieval ambiguities, which may exist in a single remote sensoris used. These ambiguities are almost inevitable for the single remote sensor approach, since generally there is no direct correspondence between a given cloud microphysical parameter and a single measurement taken by any remote sensor at a wavelength.

Two radars using different wavelength channels have the capability to estimate hydrometeor size. As diameter increases, the shorter wavelength scatters in the Mie rather than the Rayleigh regime and its reflectivity falls below the longer wavelength. This principle was first proposed by Atlas and Ludlam (1961) in detecting hail. They used both of the Rayleigh-scattering S-band radar and the X-band radar

that Mie-scatters only in the presence of large hail. These schemes have always had to contend with differences in reflectivity due to the attenuation by rain at the shorter wavelength (Tuttle and Rinehart 1983), and it was found that even with well matched beams of very similar beam width, differences in the side lobe level were able to cause the large reflectivity differences in the vicinity of strongly reflective cores where a significant fraction of the signal is returned from the side-lobes (Rinehart and Tuttle 1982). However, the ambiguity is caused by the very different scattering properties of the wet and dry hail that made this technique unworkable.

The dual-wavelength ratio, defined simply as

$$\mathrm{DWR} = 10\log_{10}\left(\frac{Z_{m,35}}{Z_{m,95}}\right)\mathrm{dB} \qquad (4.1)$$

is directly related to some measurement of average crystal size, where Zm,35 and Zm,95 are the reflectivity factors (in mm^6/m^3) measured at 35 and 95 GHz respectively. The use of dual-wavelength radar for the sizing in cirrus was first proposed by Matrosov (1993) who carried out scattering calculations for a first-order gamma distribution of solid-ice spheroids with a variety of the different wavelength combinations and the aspect ratios. In each case DWR was calculated as a function of D_0, the median diameter of the volume-weighted size distribution. Recently, Sekelsky et al. (1999) used three co-located radars at 2.8, 33 and 95 GHz to estimate the crystal size in the precipitating and non-precipitating ice clouds. Crystal size was derived from the measurements using a neural network trained with the results of theoretical scattering calculations also using a first-order gamma distribution of crystals.

4.2 Data and observation

Multi-parameter cloud radar observations of the microphysical phenomena in cloud and precipitation in BAIU season were carried out from June 12 to July 8, 2001 at the National Research Institute for Earth Science and Disaster Prevention (36°07′20″N, 140°05′35″E), Japan (Figure 4.1). The operation of mm-wave cloud radar was carried out with scan mode of vertically pointing PPI. Specification of radar used for the present study is introduced in detail in Chapter 2. To get the information of the liquid water and rain droplets, operations of the disdrometer (DI STROMET LTD., RD-69) and the microwave radiometer (Radiometrics Co., WVR1100) were also carried out to the field for the calibrations and comparisons wit h the radar data (Figure 4.2).

Figure 4.1 The observation site(red circle) and upper air observation by air-sonde for this study.

The Rd-69 Distromet disdrometer (also known as Joss-Waldvogel disdrometer) was leased from Distromet ltd. and was operated next to the NOAA Aeronomy Laboratory profilers. This disdrometer is used as the calibration reference of the profiler observations. The Distromet software was operated and collected the number of drops in the 20 different diameter bins with 60 seconds intervals. New software developed by the Aeronomy Laboratory in order to resolve the full 127 diameter resolution of the Rd-69 Distromet disdrometer. This one was operated in parallel with the original Distromet software. Neither quality control nor error correction of the original observations was not conducted. There also can be data missing due to the computer disruptions or the power failures (Figure 4.2).

The Microwave Radiometer (MWR) provides time-series measurements of column-integrated amounts of water vapor and liquid water. The instrument itself is essentially a sensitive microwave receiver. That is, it is tuned to measure the microwave emissions of the vapor and liquid water molecules in the atmosphere at specific frequencies. The MWR receives microwave radiation from the sky at 23.8 GHz and 31.4 GHz. These two frequencies allow the simultaneous determination of the water vapor and liquid water burdens along the selected path. Cloud liquid in the atmosphere emits in a continuum that increases with frequency, dominating the 31.4 GHz observation, whereas water vapor dominates the 23.8-GHz channel. The water vapor and the liquid water signals can, therefore, be separated by observing at these two frequencies(Figure 4.3).

Figure 4.2 The photo of Joss-Waldvogel type disdrometer in NIED.

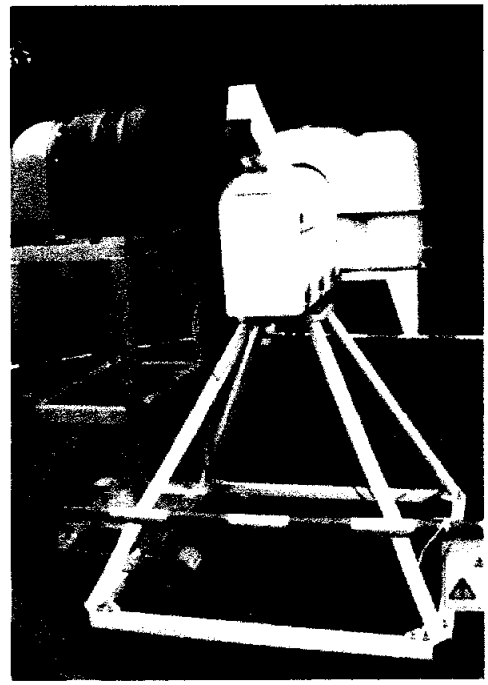

Figure 4.3 The photo of microwave radiometer.

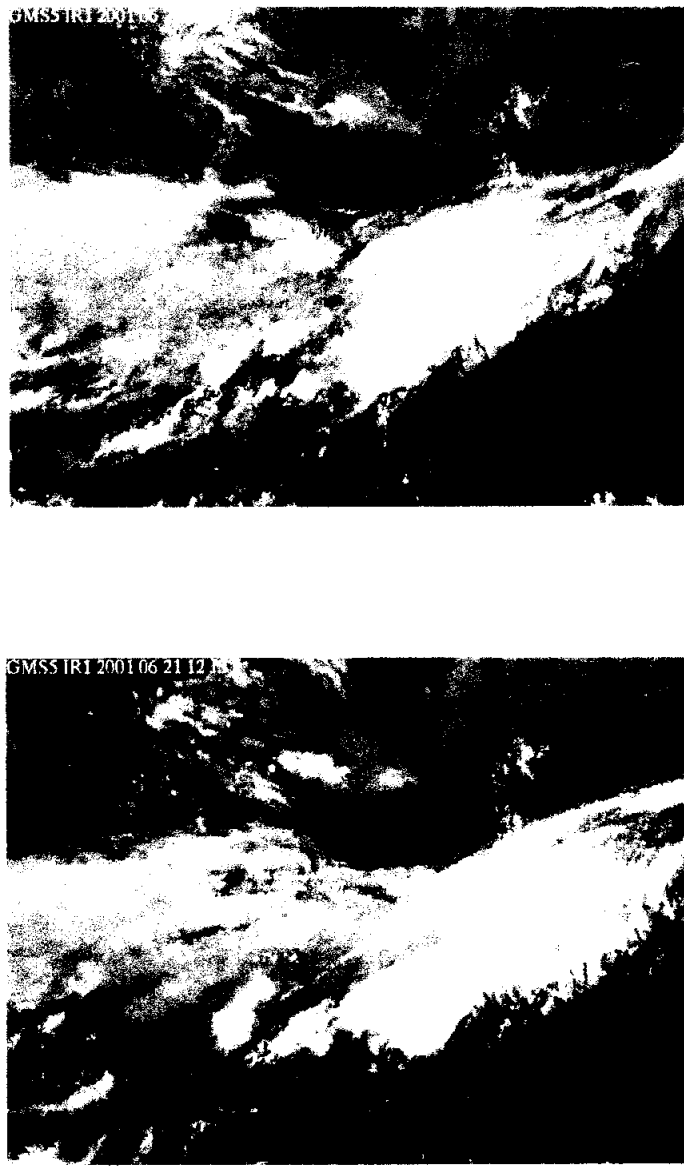

Figure 4.4 GMS-5 IR images (a) 06 LST and (b) 12 LST 21 June 2001.

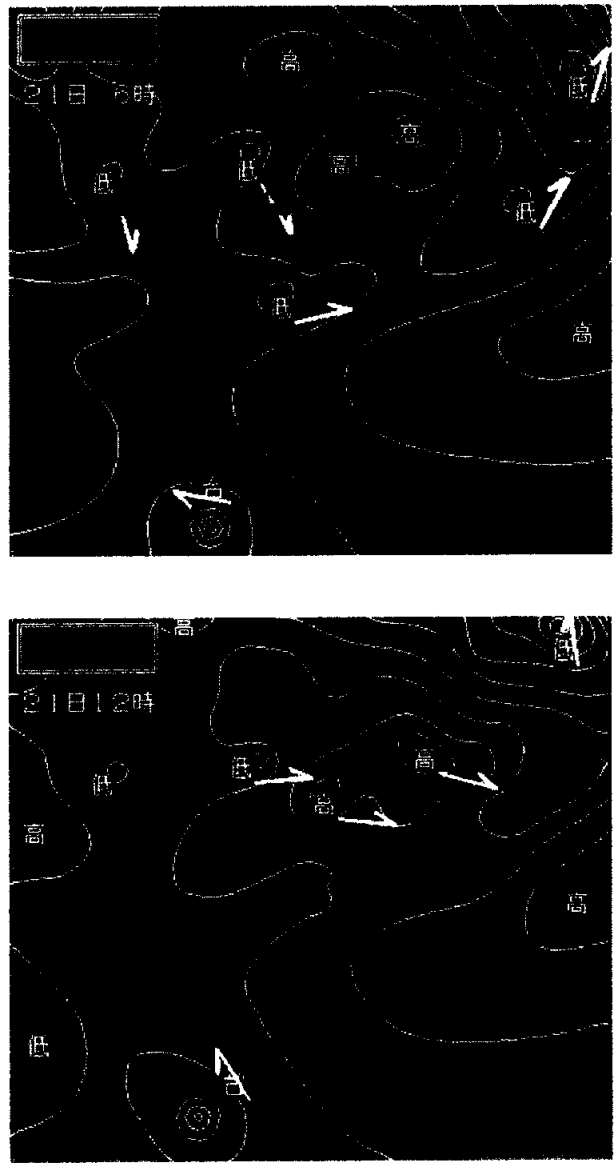

Figure 4.5 Sea level weather charts of (a) 06 LST and (b) 12 LST 21 June 2001.

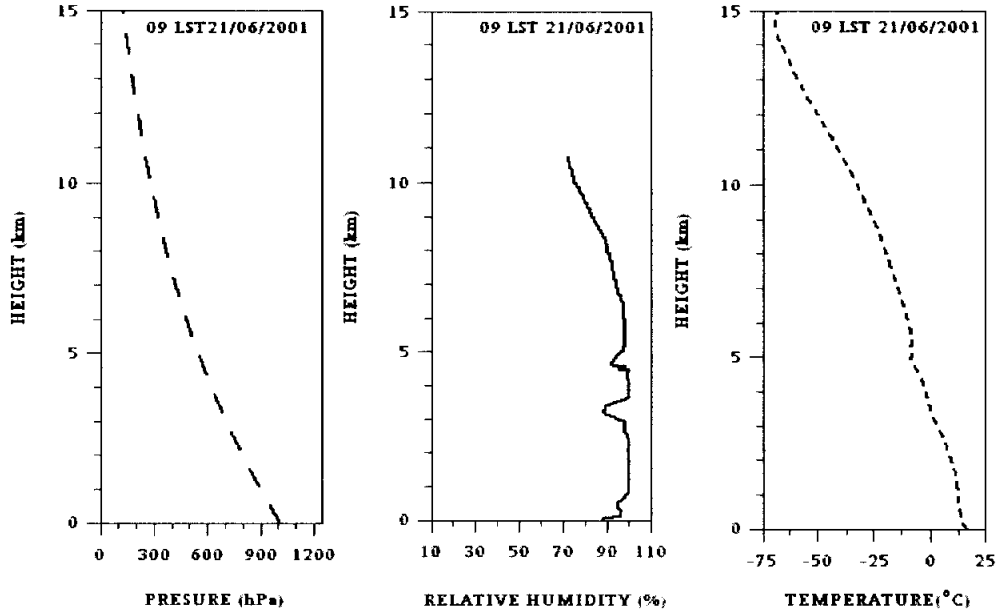

Figure 4. 6 Environmental sounding taken at 09 LST 21 June 2001 at Tateno, Japan. (a) pressure (hPa) (b) relative humidity (c)and vertical temperature(℃).

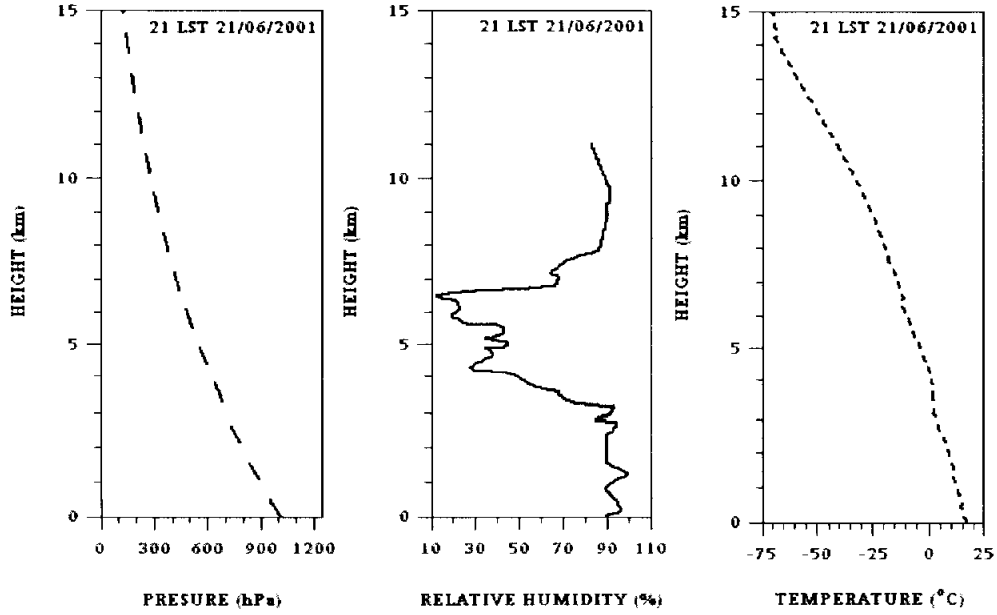

Figure 4. 7 Same as figure 4.2 but for 21 LST 21 June 2001.

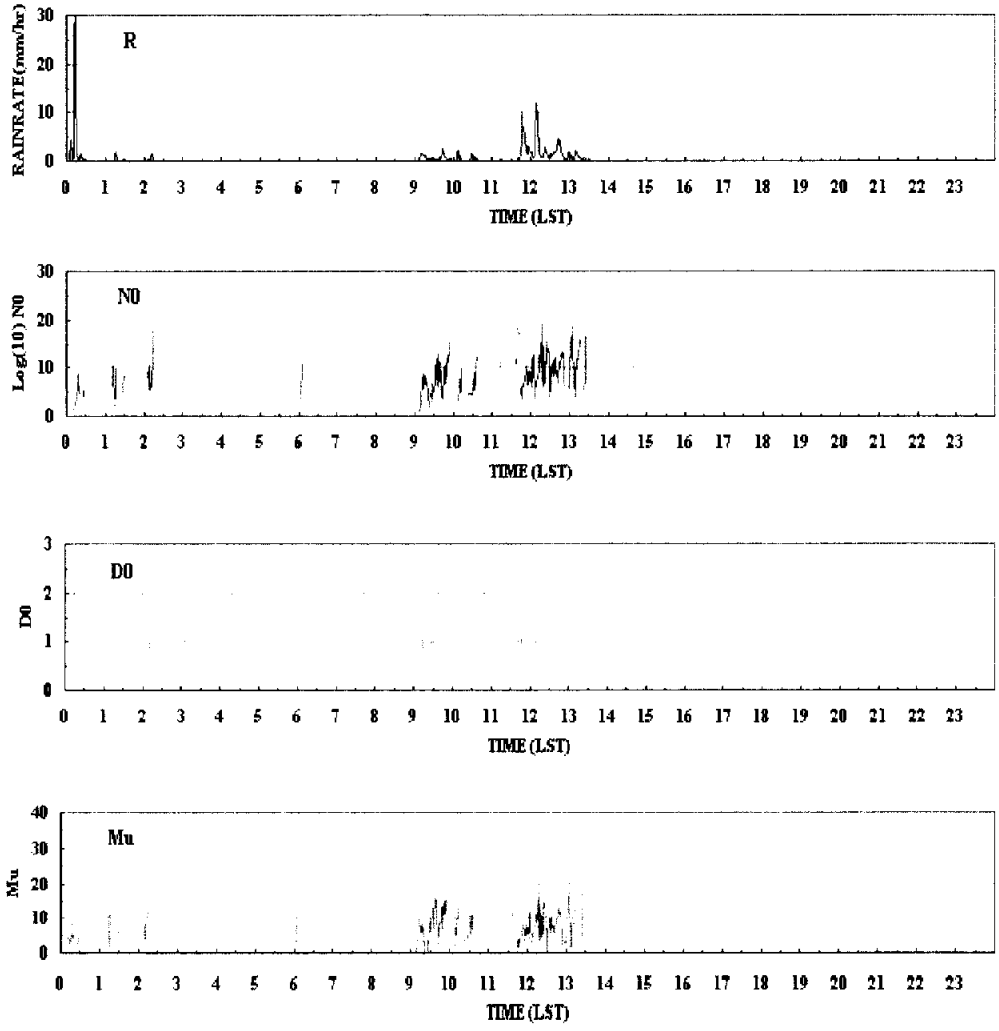

Figure 4.8 Time series of (a) rainrate (mm/hr), (b) log N_0, (c) median volume diameter D_0 (mm) and (d) μ retrieved by disdrometer on 21 June 2001

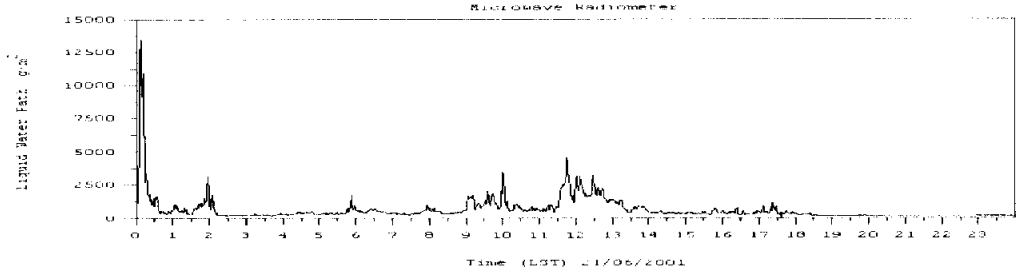

Figure 4.9 Time series of liquid water path by microwave radiometer on 21 June 2001

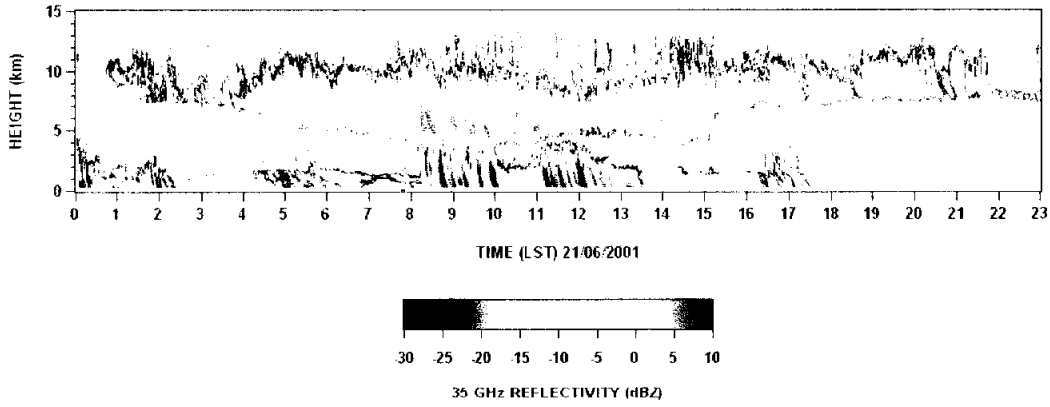

Figure 4.10 Time series of the measured reflectivity at 35 GHz radar on 21 June 2001 at NIED.

4.3 Measuring ice crystal size and ice water content in cirrus

Recent advances in the millimeter-wavelength radar applications for the non-precipitating ice clouds induced a wide interest in developing the empirical relationships between cloud microphysical parameters and the radar reflectivities based on the regression analysis. However, retrievals which based on multi-sensor observations are more robust than those based on these relationships that usually are sought in the form of power-law regressions:

$$IWC = a Z^{b} \tag{4.2}$$

where a and b are the regression coefficients. When the multi-sensor approach is not available for some reasons and only radar reflectivity data is used, such regressions could be helpful. One, however, should realize that the regression approach is limited due to the variability of the relationships between microphysical parameters and reflectivity from cloud to cloud (Atlas *et al.*, 1995).

Recently, most attention has been given to developing the empirical power-law regressions between IWC and the radar reflectivity, Z. Such regressions are deduced from the measured particle spectra, when both IWC and Z are calculated from these spectra. Particle samples are usually taken from the research aircrafts or on the ground. Some recent publications on this subject include Brown *et al.* (1995), Liao and Sassen (1994), Sassen and Liao (1996).

Brown et al. (1995) analyzed the aircraft cloud probe data taken during the two field projects of the European Cloud Radiation Experiment(EUCREX) and the Central

Equatorial Pacific Experiment(CEPEX) . They determine how accurately a single 94 GHz radar could measure ice water content (IWC). They found that it should be possible to measure IWC with a standard error of +85% and -45% for IWC greater than 0.01 g/m^3 from radar reflectivity factor alone. However, the error would be reduced to +50% and -35%, if the median size of the ice crystal distribution could be derived using other instruments on board the satellite. For IWC =0.001 g/m^3, these errors increase to between +140% and -60% when the size is unknown, and +80% and -45% when the size is known. The remaining error the known size is due entirely to deviations of the crystal size distribution from exponential. They concluded that if no size information was available, the data from the radar would still provide a useful constraint for climate models.

A similar study was carried out by Atlas et al. (1995), using aircraft data from the First ISCCP Regional Experiment (FIRE). Although from broadly comparable results, they concluded that any estimate of IWC would be too inaccurate to be of any use for models without size available, and also that a significant fraction of the radiatively important clouds would be missed with a minimum sensitivity of -30 dBZ.

Intrieri et al. (1993) demonstrated the use of combined radar and infrared-lidar measurements to infer size. However, the lidars are subject to significant attenuation in moderately thick cirrus, and furthermore a large fraction of mid-latitude cirrus occurs in conjunction with liquid-phase clouds at lower level which can completely extinguish the signal from a ground-based instrument.

Multi-frequency particle sizing works when the higher frequency experiences non-Rayleigh or Mie scattering. For the cloud particle sizing, the higher frequency must exhibit the non-Rayleigh scattering from the small hydrometeors. For ice

crystals this occurs at millimeter wavelengths where radar systems typically operate in one of several atmospheric transmissions windows centered near 35, 95, 140 and 215 GHz. Because there is an intrinsic lower limit to the size that can be measured by this method, the use of higher frequencies such as 140 or 215 GHz would enable the smaller sizes to be measured. Hogan and Illingworth (1999) investigated the potential of a space-borne dual wavelength radar to make global measurements of crystal size in cirrus, and showed that the most promising frequency combination was 79 (or 94) and 215 GHz, which in general more accurate than the combination of 35 and 94 GHz. However, attenuation by liquid water and water vapor in the lower troposphere is that, the use of frequencies much higher than 94 GHz to monitor cirrus clouds is unfortunately not feasible from the ground.

In this paper, the 35 and 95 GHz radars were considered and the dual-wavelength observations of cirrus, at these frequencies, suffer none of the following problems; (1) attenuation by ice is generally small enough to neglect, (2) attenuation by atmospheric gases is a minor correction, and (3) reflectivity gradients comparable in magnitude to those at the edge of the cores of the convective storms are never observed. Attenuation by the super-cooled liquid water in the mixed-phase clouds can cause the technique to theoretically produce erroneous results. Therefore, the cirrus observed in the present case study had a temperature in the range between -50 and -20℃, and the previous observations of liquid water clouds at temperatures below -10℃ have all shown that they have water contents of less than 0.13g/m^3 (e.g. Herman and Curry 1984; Sassen 1991; Heymsfield et al. 1991). At 20℃, this corresponds to a differential attenuation of only 0.4 dB/km, so the effect is typically much smaller than the differences in reflectivity due to the Mie scattering.

4.3.1 Theory

In the presence of non-Rayleigh scatterers, DWR is thus a function of the attenuation and of Do. Using the equations (3.17) and (4.1), DWR can be written as below

$$DWR = 10\log_{10}\left(\frac{Z_{m35}}{Z_{m95}}\right)$$

$$= \left[\frac{\lambda_{35}^4 \int_0^\infty \xi_b D^{\mu+2} \exp\left[-(3.67+\mu)D/D_0\right] dD}{\lambda_{95}^4 \int_0^\infty \xi_b D^{\mu+2} \exp\left[-(3.67+\mu)D/D_0\right] dD}\right] + 20\log\frac{|K_{95}|}{|K_{35}|} + 2\int_0^r (A_{95} - A_{35})du$$

$$= F_{35,95}(D_0) + R_{35,95} + A_d$$

(4.3)

$$F_{35,95}(D_0) = \left[\frac{\lambda_{35}^4 \int_0^\infty \xi_b D^{\mu+2} \exp[-(3.67+\mu)D/D_0]dD}{\lambda_{95}^4 \int_0^\infty \xi_b D^{\mu+2} \exp[-(3.67+\mu)D/D_0]dD}\right]$$

$$R_{35,95} = 20\log\frac{|K_{95}|}{|K_{35}|}$$

$$A_d = 2\int_0^r (A_{95} - A_{35})\, du$$

where $F_{35,95}(D_0)$ is non-Rayleigh term and A_d is the differential attenuation.

Here, Z_e is a function of several variables, including No. Aside from the selected wavelength pair , DWR depends upon D_0(mm), μ and ρ (g/cm^3). If reasonable

assumptions are made for $\rho(D)$ and μ, D_0 is obtained from DWR and N_0 can also be determined from Z_e.

Panel a) and b) in figure 4.11 show the results of the scattering simulations on the condition $\mu=0$ and $\rho=0.07D^{-1.1}$ (Brown and Francis,1995), that have been carried out to determine the Mie scattering term ($F_{35,95}$) and attenuation term as a function of D_0 at 35 and 95 GHz, respectively. As shown in the panel b in figure 4.11, the third term on the right hand sied, attenuation by ice is generally small enough to be neglected and attenuation by atmospheric gases can be corrected by air-sonde data. The dielectric parameter $|K|^2$ is calculated as a function of density using the expressions of Maxwell-Garnet(1904) and Liebe et al.(1989) based on the air sonde data, and is almost identical at 35 and 95 GHz such as shown figure 3.6. It should be noted that $|K|^2$ are virtually independent of temperature and implies that $R_{35,95} = 20\log\frac{|K_{95}|}{|K_{35}|}$ is close to near 0. DWR for cirrus cloud means only depends on the first term, $F_{35,95}(D_0)$ which is independent on No. Equation (4.3) can be rewritten

$$DWR = F_{35,95}(D_0) \tag{4.4}$$

Ice water content (IWC) in cirrus clouds can be given by

$$\begin{aligned} IWC &= \frac{\pi}{6}\int_0^\infty \rho(D)\, D^3\, N(D)\, dD \\ &= \frac{\pi}{6} N_0 \int_0^\infty \rho(D)\, D^{3+\mu}\, \exp(-3.67 + \mu D / D_0)\, dD \end{aligned} \tag{4.5}$$

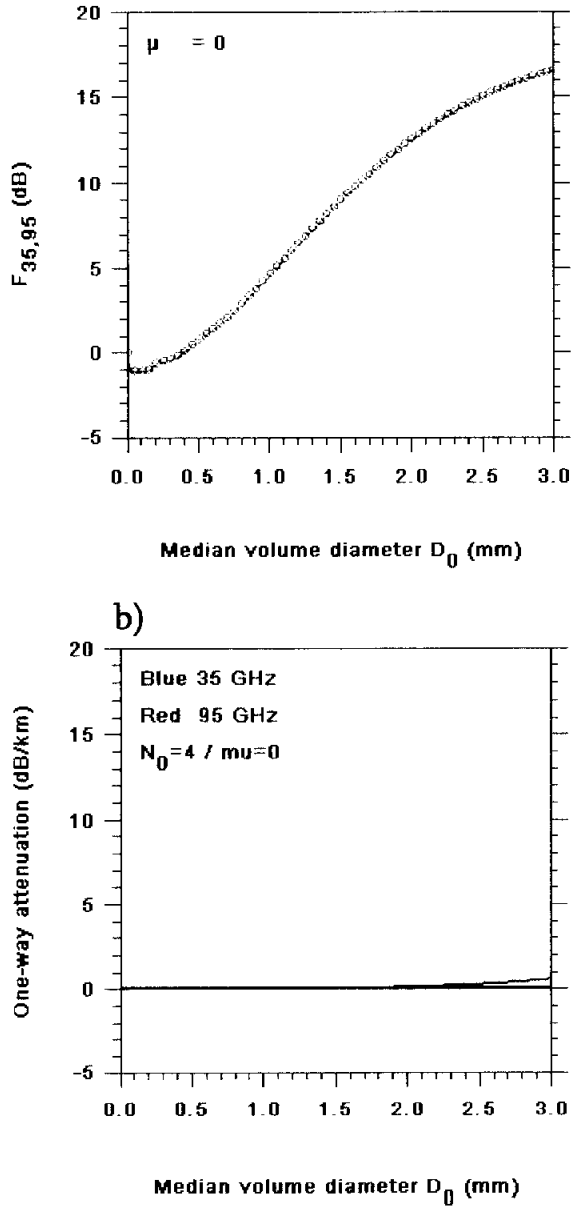

Figure 4.11 Variation of a) the Mie scattering term $F_{35,95}$ for ice and b) the attenuation term A_d for ice as a function of the median volume diameter D_0. Wavelengths of radar are 35 GHz and 95 GHz.

From equation (4.5) and (4.7), the parameter R_f can be simply expressed as the reflectivity factor at the frequency f divided by IWC.

$$R_f(D_0) = \frac{Z_e}{IWC} = \frac{\dfrac{10^{12}\lambda^4}{4\pi^4 |K_w|^2} N_0 \times \int_0^\infty \xi_b D^{\mu+2} \exp[-(3.67+\mu)D/D_0]\, dD}{\dfrac{\pi}{6} N_0 \int_0^\infty \rho(D)\, D^{3+\mu} \exp(-3.67+\mu D/D_0)\, dD} \quad (4.6)$$

The number concentration parameter No has been cancelled from (4.6) and $R_f(D_0)$ is normalized by IWC such as DWR. Hence, an estimate of R_{35} from DWR can be used to obtain IWC simply from $IWC=Z_{35}/R_{35}$, which is not normalized and IWC depends on No. Thus, Median volume diameter Do and IWC can be derived from DWR between 35 GHz and 95 GHz (figure 4.11 and 4.12).

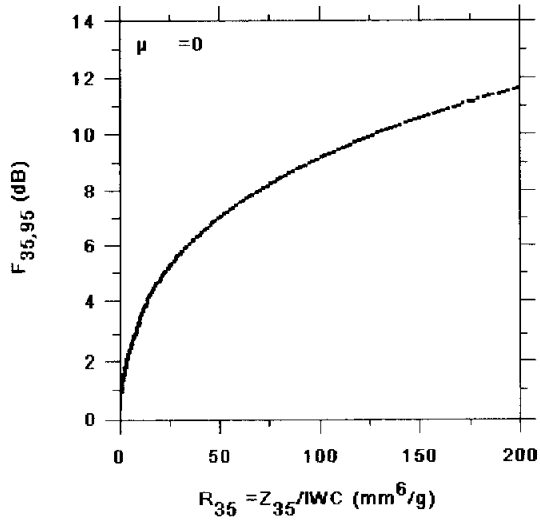

Figure 4.12 $F_{35,95}$ as a function of R_{35} for shape parameter μ=0.

4.3.2 Application of real data- 21 June 2001 case study

The technique described in section 4.3.2 is now applied to the data taken by the dual wavelength cloud radars at Tsukuba, Japan. Figure 4.13 shows 4 hours of data taken from 19 LST to 23 LST on 21 June 2001 during typical thick cirrus cloud. The panel (a) shows the measured radar reflectivity at 35 GHz and the panel (b) coincident at 95 GHz which have been averaged over 1 minute and with a range resolution of 100m. The radar reflectivity is characterized by narrow fall streaks, indicating the strongly inhomogeneous nature of the cirrus clouds.

Radars at frequencies higher than 94 GHz are generally considered to be unsuitable for ground-based observations of cirrus because of the strong water vapor and oxygen absorption in the boundary layer. The corrections of the dielectric factor and the gas attenuation are considered by the profiles of temperature, relative humidity and pressure at 1900 LST in Tateno (figure 4.7). The one-way gaseous attenuation from the space has been calculated using the line-by-line model Liebe(1985). Panel a) in figure 4.14 shows the vertical profile of the one-way attenuation by the Liebe model at 10 GHz, 35GHz and 95GHz. The attenuation at 10 GHz can be neglected, however the serious attenuation of 35 GHz and 95 GHz at low-level indicates that these effects results from the atmospheric gas concentrated in the low level.

Both radar systems have their own gas attenuation correction factor by 0.006 dB/km at 35 GHz and by 0.02 dB/km at 95 GHz with automatically correction of the attenuation. Panel b) shows the comparison of the vertically accumulated attenuation effect between the Liebe model and have their own gas attenuation correction which is too small in the low-level and is overestimated in high level. With this reason, attenuation was used in the correction by the Liebe model of line-by-line calculation.

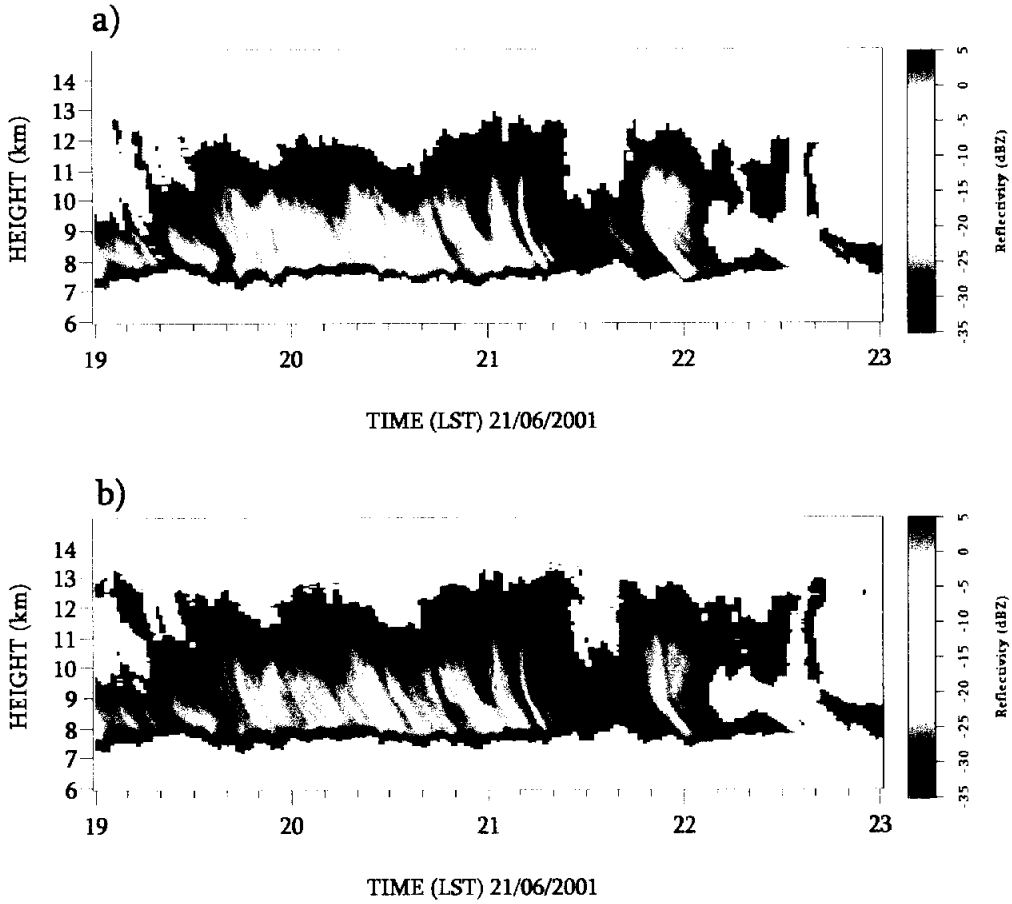

Figure 4.13 Dual wavelength radar measurement taken from 1900 LST to 2300 LST on 21 June, 2001. a) Time-height cross section of radar reflectivity factor at 35 GHz. b) Same as a), but for at 95 GHz.

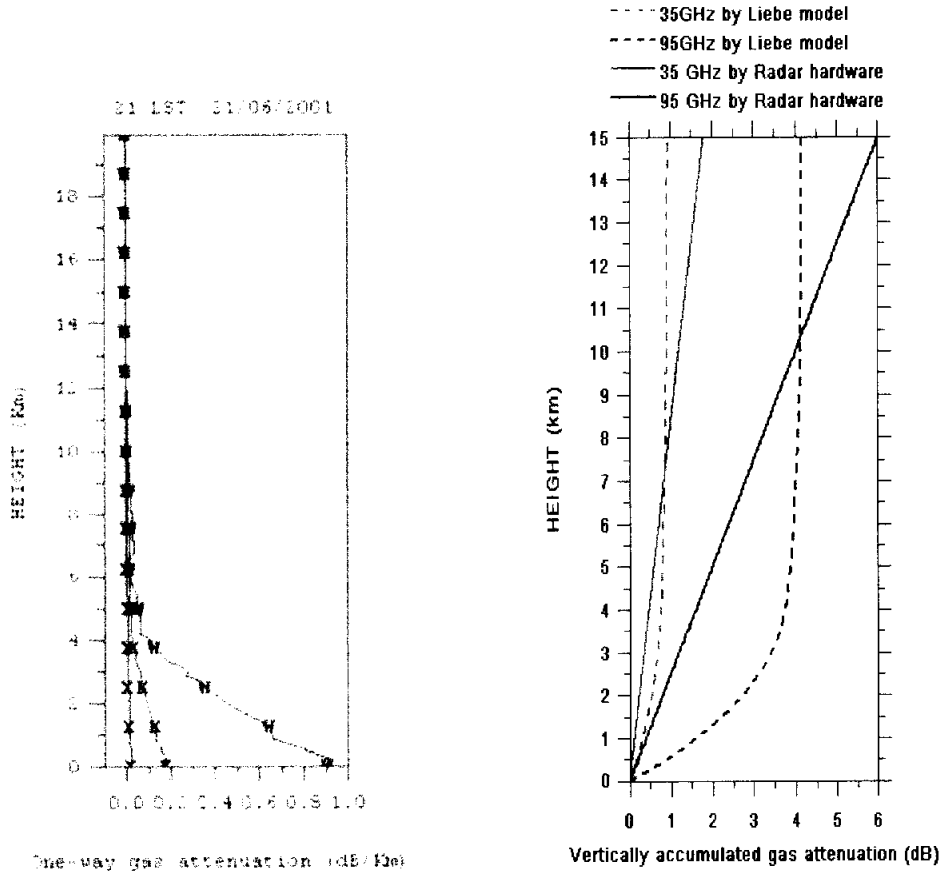

Figure 4.14 Panel a) the one-way gas attenuation by the Liebe model(1985) and b) the vertically accumulated attenuation by the attenuation constant in radar system(solid lines) and by the Liebe model(dash lines).

Figure 4.15 shows the vertical profiles of the uncorrected and corrected radar reflectivity at 35 GHz and 95 GHz in the cirrus case, 19:30 LST 21 June 2001. Figure 4.16 displays the time-height cross section of the radar reflectivity factor corrected by the dielectric constant and the atmospheric gas attenuation at 35 GHz and 95 GHz.

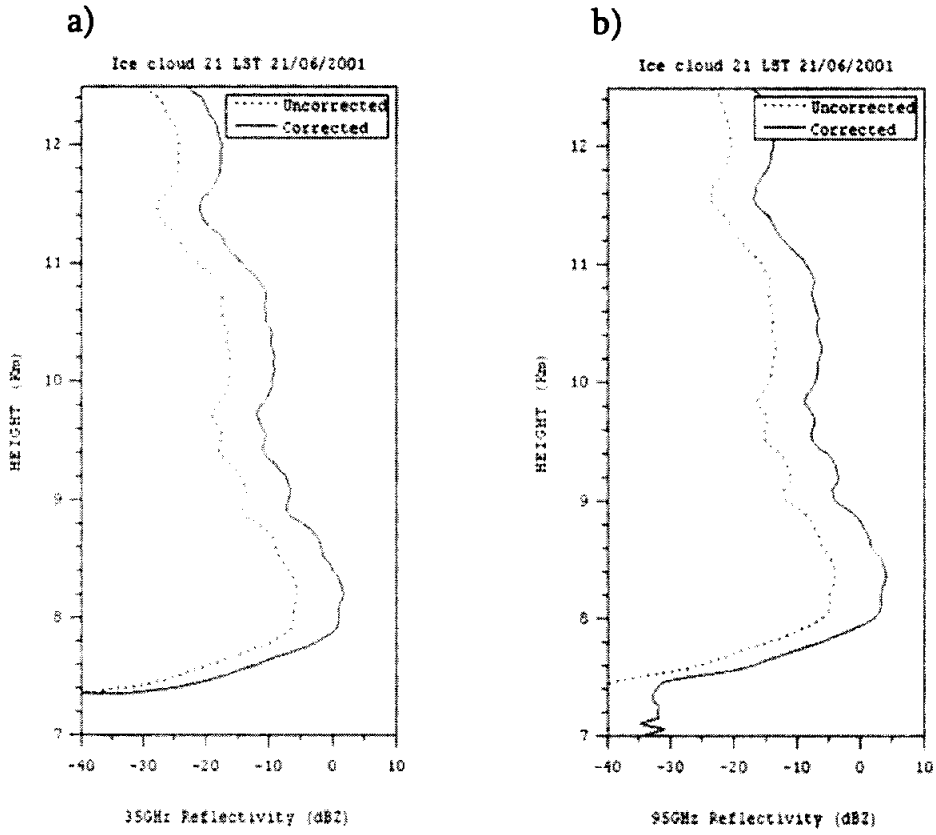

Figure 4.15 The vertical profiles of the uncorrected (dotted line) and corrected (solid line) radar reflectivity at 35 GHz and 95 GHz in cirrus case, 19:30 LST 21 June 2001. The corrections of the dielectric factor and gas attenuation are considered by the air sonde data. Gas attenuation correction was calculated by the Liebe model (1985).

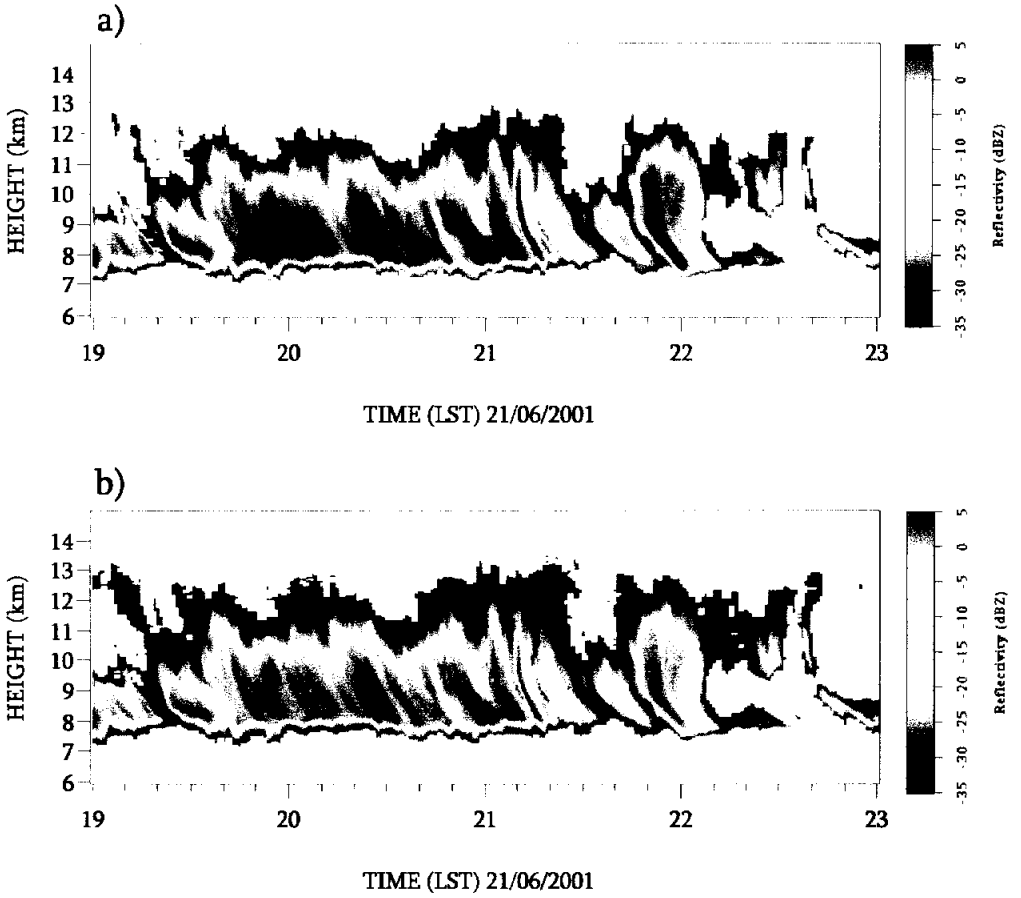

Figure 4.16 Dual wavelength measurement taken from 19 LST to 23 LST on 21 June, 2001. a) Time-height cross section of radar reflectivity factor at 35 GHz. b) Same as a), but for at 95 GHz.

The time-height cross section of dual wavelength ratio (DWR) of the ice particles derived using the previous method is shown in figure 4.17. Values of DWR range from 0 dB to 6 dB except for near the bottom of cloud base. From these DWR, relationship between (4.4) and (4.6), the D_0 and IWC can be calculated and are displayed in the panel a) and b) in figure 4.17.

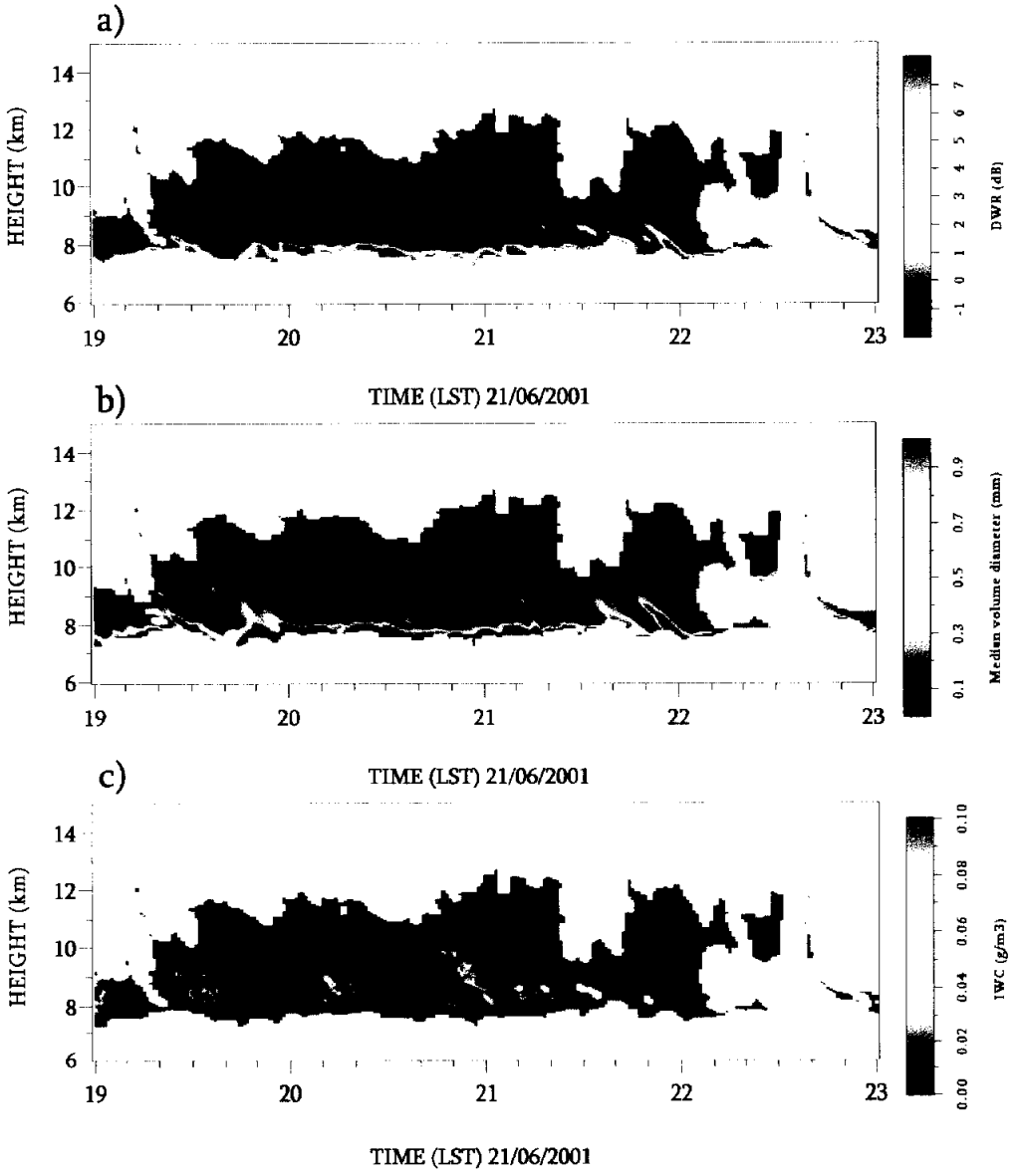

Figure 4.17 Time-height cross section of a) Dual Wavelength Ratio, DWR (dB) b) median volume diameter D_0 (mm) retrieved with dual wavelength method and c) ice water content (g/m^3) of ice crystals from 1900 LST to 2300 LST on 21 June 2001.

Values of D_0 vary from 0.1 to 0.7 mm except for the cloud base and these of IWC range from 0.001 to 0.15 g/m^3, respectively. Both have the similar range distribution to these described the reports from European Space Agency " Macrophysical and Microphysical Properties of Clouds " in 1997. It is seen that the increase of IWC toward the cloud base the decrease of IWC on the edge of cloud base demonstrate the evaporation of IWC at the cloud base in the view of cloud microphysics.

Even though the distribution of D_0 in cirrus is similar with a typical pattern, rising down from a maximum at cloud base to a minimum at the cloud top, D_0 at the cloud base intend to overestimate than typical values, reaching 1.5 mm. This over-estimating problem could be also appeared from the data which are observed from 1500 LST to 1800 LST (figure 4.18) and from 2200 LST to 2400 LST(figure 4.19) on 20 June 2001. The possible reason for the overestimation of D_0 is the preferential evaporation of the smaller ice crystal droplets at cloud base. Due to the first evaporation of the smaller droplets, the number of concentration is concentrated in the larger droplets size at the cloud base. This indicates that real cloud contains significantly larger crystals than indicated by a simple gamma distribution. And a gamma drop size distribution is not well presented in the drop size distribution near the bottom of the most cloud base.

When it is needed to assume any kind of the drop size distribution to retrieve the information within cirrus cloud in spite of this problem at cloud base, the variation of the shape parameter of the size distribution, μ, can be given as the good solution in overestimating sizes. The more the value of μ increases, the distribution is narrower and the number of the lager droplets decrease. Therefore, the decrease of the number of the small droplets due to the evaporation at cloud base can be represented with the choice of small value of μ.

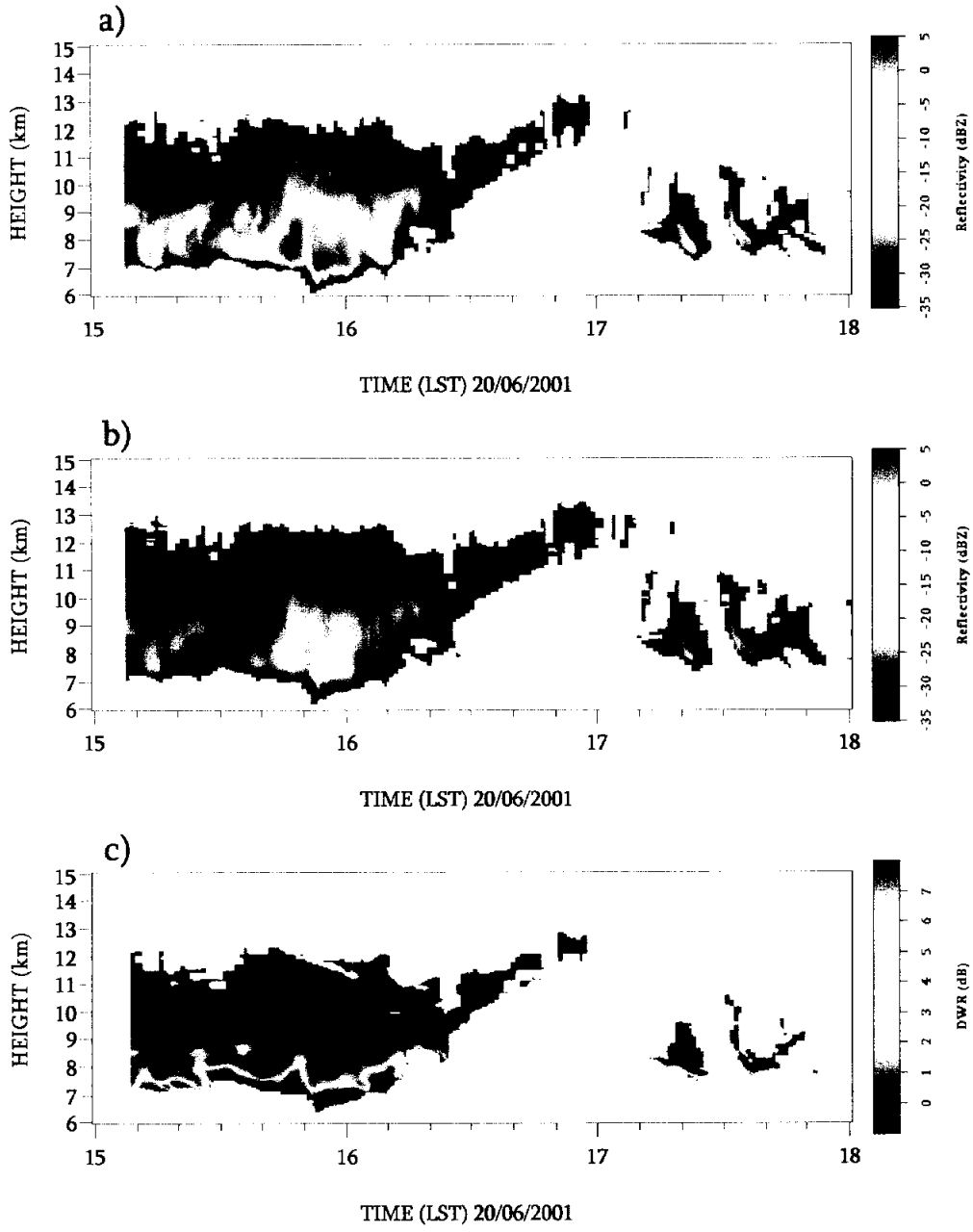

Figure 4.18 Time-height cross section of radar reflectivity factor a) at 35 GHz and b) at 95 GHz and c) DWR from 1500 LST to 1800 LST on 20 June 2001.

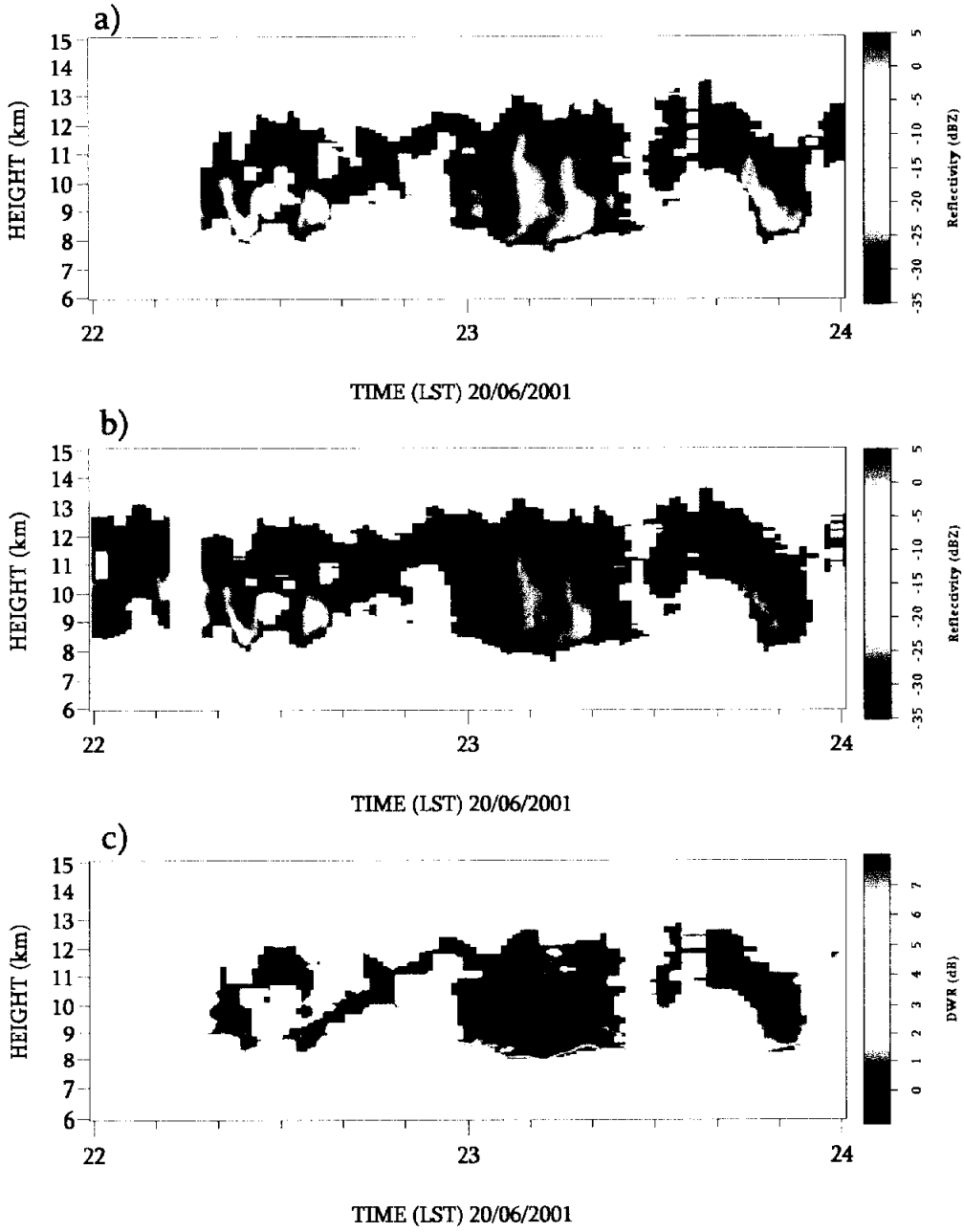

Figure 4.19 Same as figure 4.18, but for from 1500 LST to 1800 LST on 20 June 2001.

4.3.3 Sensitivity to shape parameter μ

In the previous section, it was assumed that for the scattering purposes, the shape parameter of the size distribution μ was constant (μ = 0). Hogan and Illingworth (2003) was also fixed with μ=0 for scattering simulation and Sekesky et al.(1999) used 1.0 for the μ.

To test the sensitivity of the retrieved parameters to the shape of the distribution, seven values for the shape parameter μ (-3 ~ 3) were considered. The plots in figure 4.20 show that if a gamma distribution is appropriate, then derived D_0 and IWC should be fairly insensitive to typical range (μ = -1 ~ 1) that one would expect. But, the negative μ larger than -2 is more sensitive.

It is shown that the variation of D_0 and IWC as a function of μ in figure 4.21 and 4.22, respectively. It can be seen that the more values μ increase, D_0 and R_{35} are also increasing, while IWC is decreasing. For instance, a measured DWR of 7.5 dB would be interpreted as D_0 of 1.2 mm if a gamma distribution with μ = 0 was assumed, while the change into μ = -2 indicates a value closer to 0.8 mm. It is seen that the variation of μ from 3 to -3 leads to the difference of the median volume diameter about three times in figure 4.23.

The sensitivity test suggests that the decrease of μ at cloud base has a beneficial effect on the problem abut overestimating the crystal size.

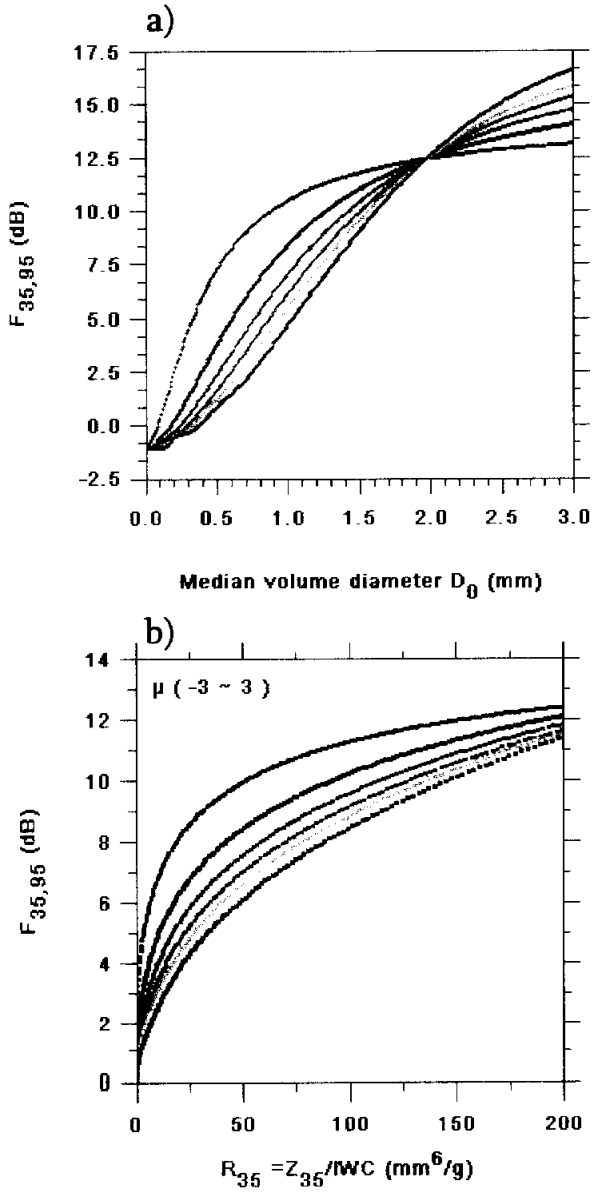

Figure 4.20 DWR as a function of D_0 and R_{35} for gamma distributions with three values of the shape parameter μ.

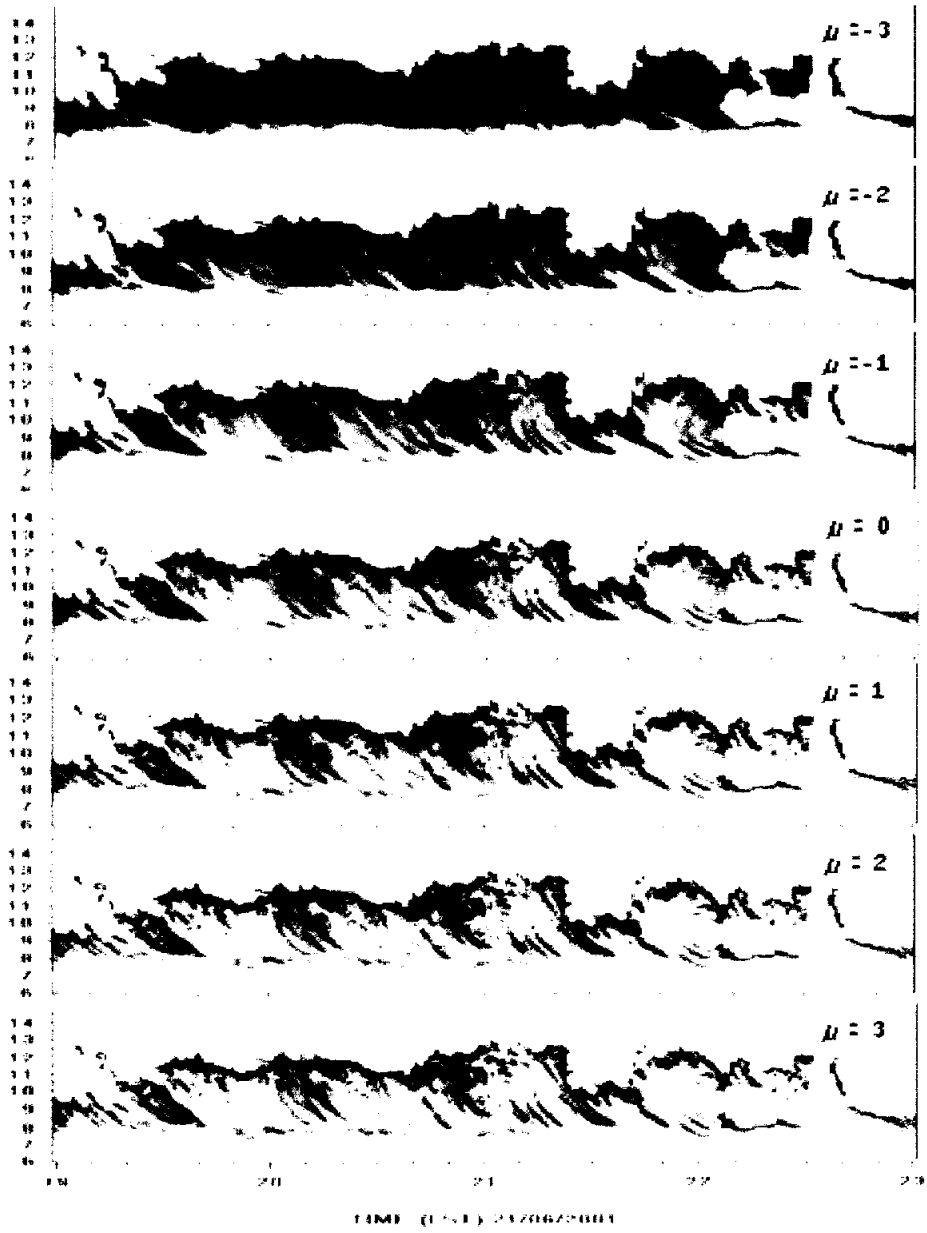

Figure 4.21 The sensitivity of median volume diameter to the shape parameter μ in cirrus cloud from 1900 to 2300 LST on 21 June 2001.

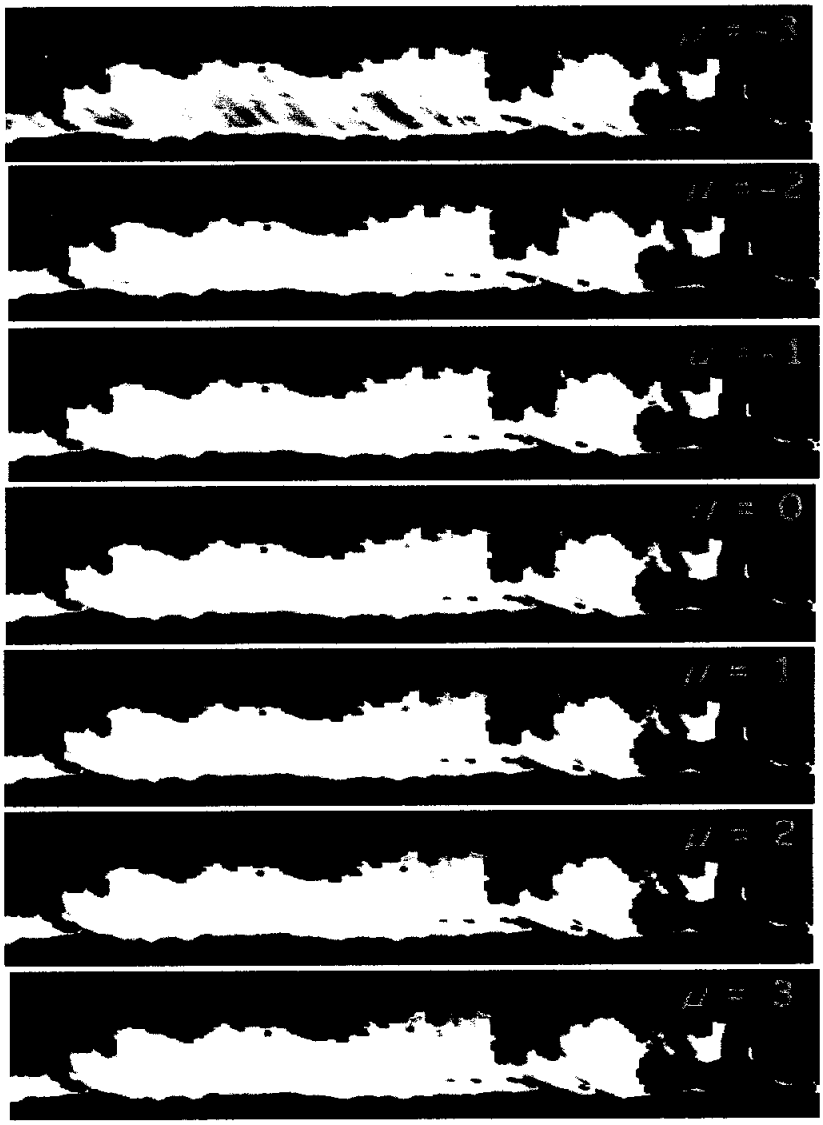

Figure 4.22 The sensitivity of ice water content(g/m^3) to the shape parameter μ.

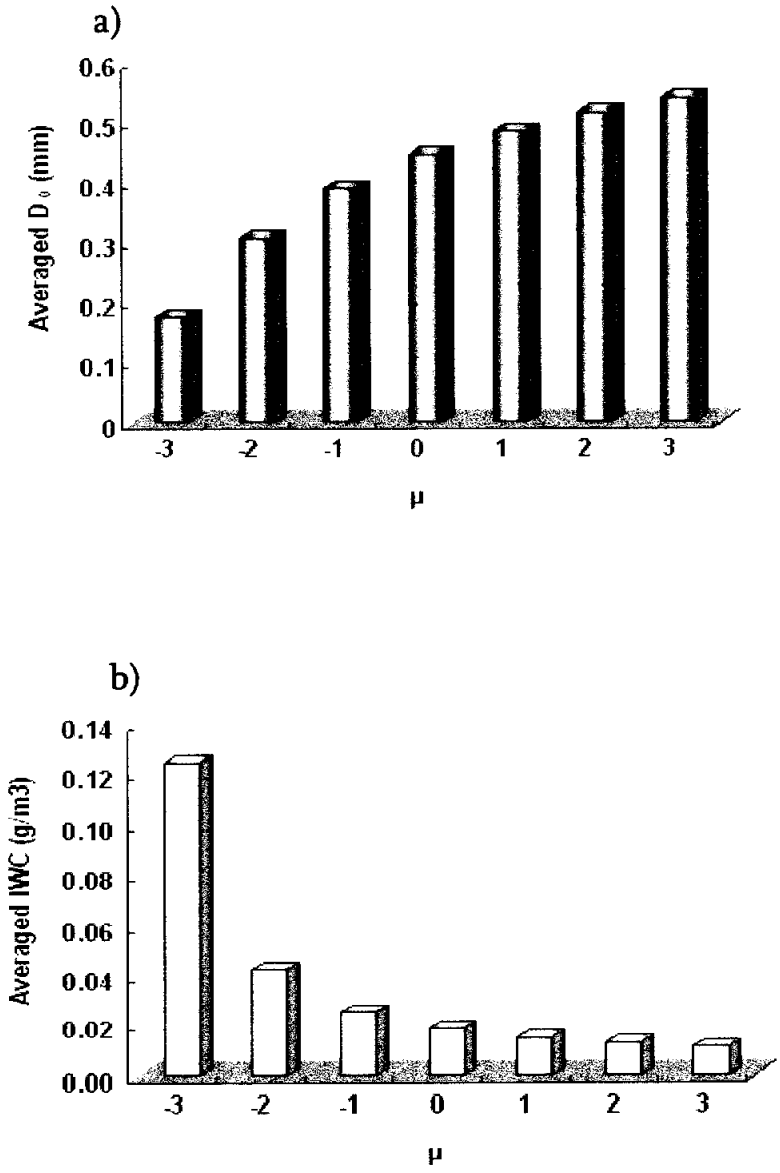

Figure 4.23 Averaged a) median volume diameter (mm) and b) IWC (g/m^3) for an hour to the shape parameter μ.

4.3.4 The comparison with other data

Ice water content (IWC) from the dual wavelength technique is compared with other methods to discern the distinct difference of each method.

Panel a) in figure 4.24 shows the derived IWC from the experimental power law relationship by Brown and Francis (1995*), IWC=0.137 Z* $^{0.643}$ and, panel b) was estimated by $Log_{10}(IWC)=0.061dBZ - 1.078$ which derived a least square fit regression between Z and $Log_{10}(IWC)$ from the aircraft datasets in the European Cloud Radiation Experiment (EUCREX) for 35 GHz. Panel c) shows IWC from the dual wavelength method of this study.

When IWC derived from the dual wavelength method is compared with that of experimental power law relationship by Brown and Francis, their patterns are different each other. Even though there are some similar pattern near 2000 LST to 2030 LST 21 June 2001, the distinct difference appears around 1940 LST to 2000 LST, having the opposition tendency of IWC. It is difficult to conclude which method is better, since there is no real data to compared.

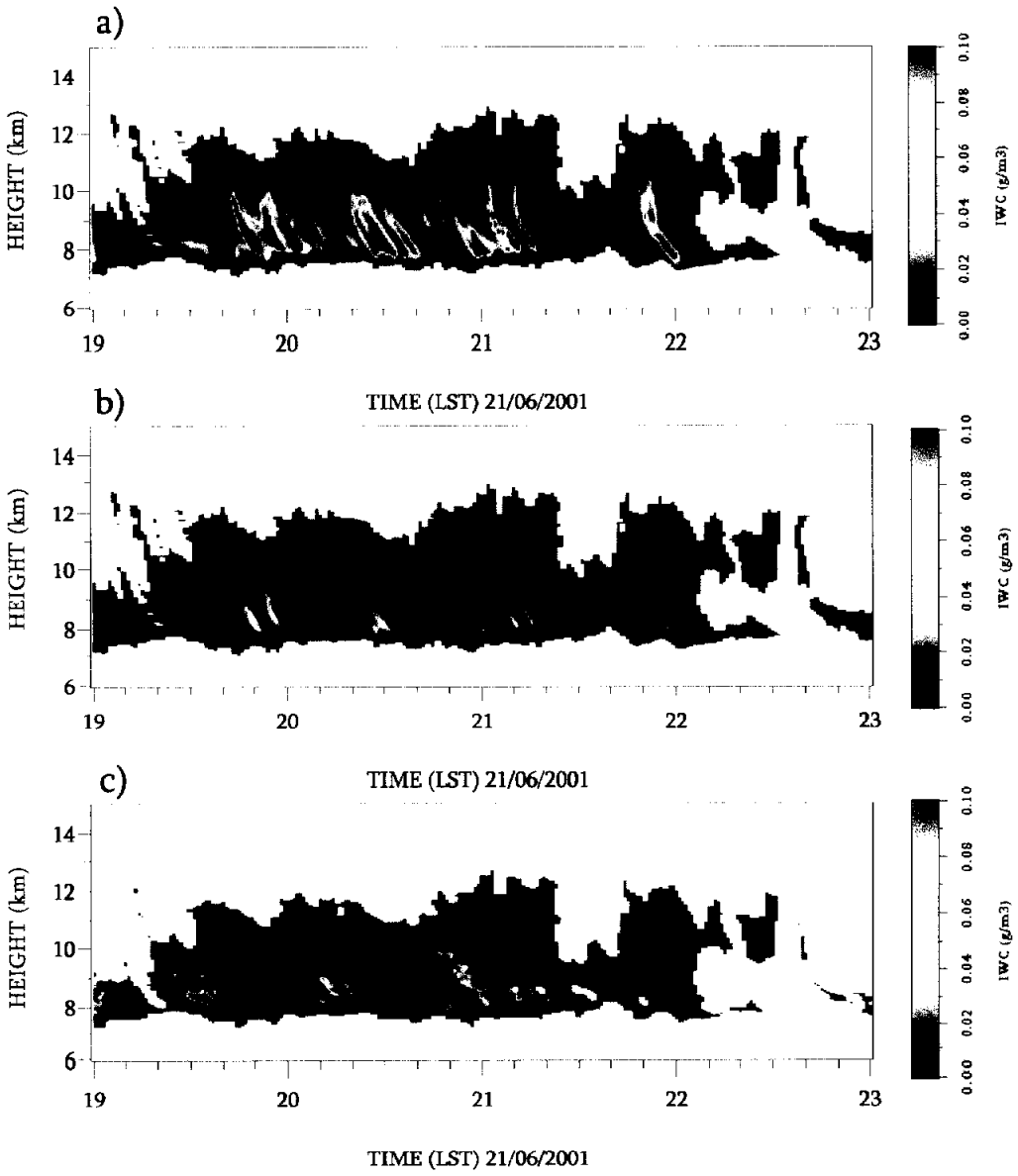

Figure 4.24 IWC a) from experimental power law relationship by Brown and Francis (1995), IWC=0.137 Z $^{0.643}$, b) the European Cloud Radiation Experiment (EUCREX), Aircraft datasets, 35GHz, Log_{10}(IWC)=0.061ZdBZ – 1.078 and from DWR method for this case.

4.4 Liquid water content in low level non precipitating cloud

The droplets which contribute the liquid water content and dominate the radiative properties of the cloud are smaller than 50 μm. The existence of two distinct components in the distribution reflects the two very different physical processes that are occurring. When a cloud first forms, droplets grow by vapor deposition for which the rate of increase in diameter D is proportional to D^{-1}. Therefore after an initial rapid increase, D tends to level out at a few tens of microns, which corresponds to a terminal fall speed of a few centimeters per second. Once the cloud is reasonably thick, a few of the largest droplets have an appreciable fall speed relative to the smaller droplets, and can grow rapidly by collision and coalescence to form drizzle.

It is invariably more difficult to make good measurements of liquid phase clouds than of cirrus using radar, principally because the small liquid droplets tend to have a much lower radar reflectivity than the much larger ice crystals found in cirrus. Furthermore, the data in the lowest few kilometers is often contaminated by birds and insects and ground clutter. Insects are not found in clouds, but their presence in the surrounding air can make cloud boundaries difficult to identify.

Early studies deduced theoretical relationships between the radar reflectivity and LWC derived from the cloud particle size distribution. Atlas(1954) proposed a relationship of the form

$$Z\ (mm^6/m^3) = 0.048\ LWC^{\ 2} \tag{4.8}$$

where Z is the radar reflectivity and the LWC is in grams per cubic meter. Later, Sauvageot and Omar(1987) used an aircraft carrying particle probes to measure the

drop size spectra of cumulus and stratocumulus over the Pyrenees and found

$$Z(mm^6/m^3) = 0.03LWC^{1.31} \tag{4.9}$$

which their claim is valid up to a reflectivity of -15dBZ. Above this level, they found that the drizzle-sized particles were present, which dominated the radar reflectivity(proportional to the sixth power of the drop diameter) and making determination of the microphysical properties from radar measurements difficult. It was shown by Fox and Illingworth (1997b) that the simple power law relationships between radar reflectivity and liquid water content (LWC), such as proposed by Atlas (1954), would be very inaccurate for estimating LWC since the ubiquitous presence of occasional drizzle drops is existed at a few hundred microns in diameter which dominate the reflectivity but contribute negligibly to LWC.

In this chapter, the attenuation method to measure LWC which circumvent the problem of drizzle is described. The method uses dual wavelength radar and exploits the fact that liquid water attenuation at millimeter wavelengths is proportional to LWC and is increased with frequency.

There is a need for the independent and quantitative observations of the precipitating clouds from ground. In this contribution, some results of the measurements were obtained with an X-band Doppler radar. The advantage of the X-band wavelength is the negligible attenuation and the possibility to use the Rayleigh approximation for the scattering calculations. The radar is calibrated and well evaluated with full Doppler spectra in use for many years. There is good hope to treat successfully the raised questions by performing simultaneous X-band and mm-wavelength radar measurements.

4.4.1 Dual wavelength method for cloud liquid water content

One of the main problems in developing radar algorithm for measuring LWC is the present of occasional drizzle drops, which contribute negligibly to LWC but dominate radar reflectivity such that the absolute value of reflectivity is essentially unrelated to LWC (Fox and Illingworth, 1997).

Here, the dual wavelength technique is used as an alternative plan to overcome this problem. Dual-wavelength measurements take advantage of the fact that small droplets dominate the attenuation and are small enough to attenuate in the Rayleigh regime. For stratoculumus cloud in the Rayleigh region, the attenuation is proportional to LWC and increase with frequency, so there is no need to resort to any empirical relationships and, furthermore, the absolute calibration of their radars is unimportant. Below will be explained the dual wavelength technique based on the differential attenuation for liquid water cloud in the low level.

The dual wavelength ratio between the longest and shortest wavelength was defined as the logarithm of the ratio of the mean powers received at each wavelength, from a volume at range r; that is,

$$\begin{aligned} DWR &= 10\log_{10}\left(\frac{Z_{m,l}}{Z_{m,s}}\right) \\ &= 10\log_{10}\left(\frac{Z_{e,l}}{Z_{e,s}}\right) + \int_0^r \left[A_s(u) - A_l(u)\right] du \end{aligned} \tag{4.9}$$

The basis of this method is the measurement of the difference ΔDWR of dual wavelength ratios between two ranges of the radar beam, separated by the range increment Δr (km):

$$\begin{aligned}\Delta DWR &= DWR(r+\Delta r) - DWR(r) \\ &= 10\log_{10}\left(\frac{Z_{e,s}(r)Z_{e,l}(r+\Delta r)}{Z_{e,l}(r)Z_{e,s}(r+\Delta r)}\right) + \int_{r}^{r+\Delta r}(A_s - A_l)\,du\end{aligned} \tag{4.10}$$

$$\Delta F_{l,s} = 10\log_{10}\left(\frac{Z_{e,s}(r)Z_{e,l}(r+\Delta r)}{Z_{e,l}(r)Z_{e,s}(r+\Delta r)}\right)$$

$$A_d = \int_{r}^{r+\Delta r}(A_s - A_l)\,du$$

Thus, ΔDWR is the sum of two terms: a term $\Delta F_{l,s}$ plus the total differential attenuation undergone along the path Δr.

Finally $\Delta F_{l,s}$ has the following expression:

$$\Delta F_{l,s} = 10\log_{10}\left(\frac{Z_s(r)Z_l(r+\Delta r)}{Z_l(r)Z_s(r+\Delta r)}\right) + 20\log\left(\frac{|K(\lambda_l,T_1)K(\lambda_s,T_2)|}{|K(\lambda_s,T_2)K(\lambda_l,T_1)|}\right) \tag{4.11}$$

Here T_1 and T_2 is air temperature at r and $r+\Delta r$, respectively. For the absent of the non-Rayleigh scatterers at both wavelength, the first term of (4.11) is very close to zero and it can be written

$$\Delta F_{l,s} = 20\log\left(\frac{|K(\lambda_l,T_1)K(\lambda_s,T_2)|}{|K(\lambda_s,T_2)K(\lambda_l,T_1)|}\right) \tag{4.12}$$

Equation (4.10) can be

$$\begin{aligned}\Delta DWR &= DWR(r+\Delta r) - DWR(r) \\ &= 20\log\left(\frac{|K(\lambda_l,T_1)K(\lambda_s,T_2)|}{|K(\lambda_s,T_2)K(\lambda_l,T_1)|}\right) + 2\int_{r}^{r+\Delta r}\left(k_{g,s} - k_{g,l}\right) + \left(k_{c,s} - k_{c,l}\right) LWC\ dr\end{aligned} \tag{4.13}$$

Therefore the mean liquid water content between r and $r+\Delta r$ is

$$\overline{LWC} = \frac{DWR(r+\Delta r) - DWR(r) - 20\log\left(\frac{|K(\lambda_l,T_1)K(\lambda_s,T_2)|}{|K(\lambda_s,T_2)K(\lambda_l,T_1)|}\right) - 2\int_r^{r+\Delta r}\left(k_{g,s} - k_{g,l}\right)dr}{2\int_r^{r+\Delta r}\left(k_{c,s} - k_{c,l}\right)dr} \tag{4.14}$$

The dielectric factor term, $20\log\left(\frac{|K(\lambda_l,T_1)K(\lambda_s,T_2)|}{|K(\lambda_s,T_2)K(\lambda_l,T_1)|}\right)$ is small but it is necessary to adjust which accounts for the difference in air temperature at the two heights. Attenuation coefficients and the dielectric factor term are the functions of temperature and the attenuation of atmospheric gases also depends on pressure and humidity, so an independent measurement of the vertical profiles of these variables over the site would be needed. In this study, these factors were calculated by the vertical profiles of the atmospheric variables by air-sonde observation.

This dual wavelength technique was introduced by Hogan *et al.* (2002) who used the two cloud radar of 35 GHz and 95 GHz for their study. In case of using the 95 GHz radar as a short wavelength radar, dual wavelength technique can be only adopted in a typical stratocumulus cloud with diameter less than 100 μm to satisfy the assumption in equation (4.11) that Mie scattering term is near to zero.

The most previous research showed that a cloud radar can be observed the drizzle particles which fall from the cloud base as well as a typical cloud particle in cloud. Hogan *et al.* is detected the cloud base from the lidar and retrieved the cloud liquid water above cloud base of stratocumulus using the cloud radar at 35 and 95 GHz. Since most of cloud particles are included the Rayleigh regime at any mm wavelength radars, it can be satisfied with the assumption of equation (4.11). There is no information of the boundary of cloud base in this study because of no vertical

observation like lidar etc. Therefore, to satisfy the assumption of equation (4.11) in which the drizzle particles below into the cloud base, the longer wave length radars at 10 GHz and 35 GHz were used than that of Hogan *et al.*(2002). The use of the long wavelength radar will be free from the limitation of previous research related to the size of cloud particle.

4.4.2 Application of real data - 21 June 2001 case study

The technique described in section 4.4.2 is applied to the data taken by the dual wavelength cloud radars owned by National Research Institute for Earth Science and Disaster in Japan. For the same day with cirrus cloud, two ground based cloud radars at 10 GHz and 35 GHz were in vertically pointing operation. The vertical resolution of the 10 GHz radar was 100 m and that of the 35 GHz radar was 50 m. The two reflectivity fields were averaged in time into 1 minute bins and interpolated on to a common 100 m height.

Figure 4.25 shows an hour data taken from 0630 LST to 0730 LST 21 June 2001 during typical low level non-precipitating clouds. Panel a) in figure 4.25 shows a radar reflectivity at 10 GHz and panel b) is coincident with radar reflectivity at 35 GHz. The reflectivities in the range between -30 dBZ and 5 dBZ at 10 GHz and 35 GHz. The relatively strong refelctivities are shown below 1.5km from the surface between 0630 and 0700 LST which are connected with the ground.

When it is considered that there is no precipitation from the surface observation at this time, the drizzle particles which are bigger than a typical cloud particle were falling from the cloud bases and evaporated before arriving to near surface.

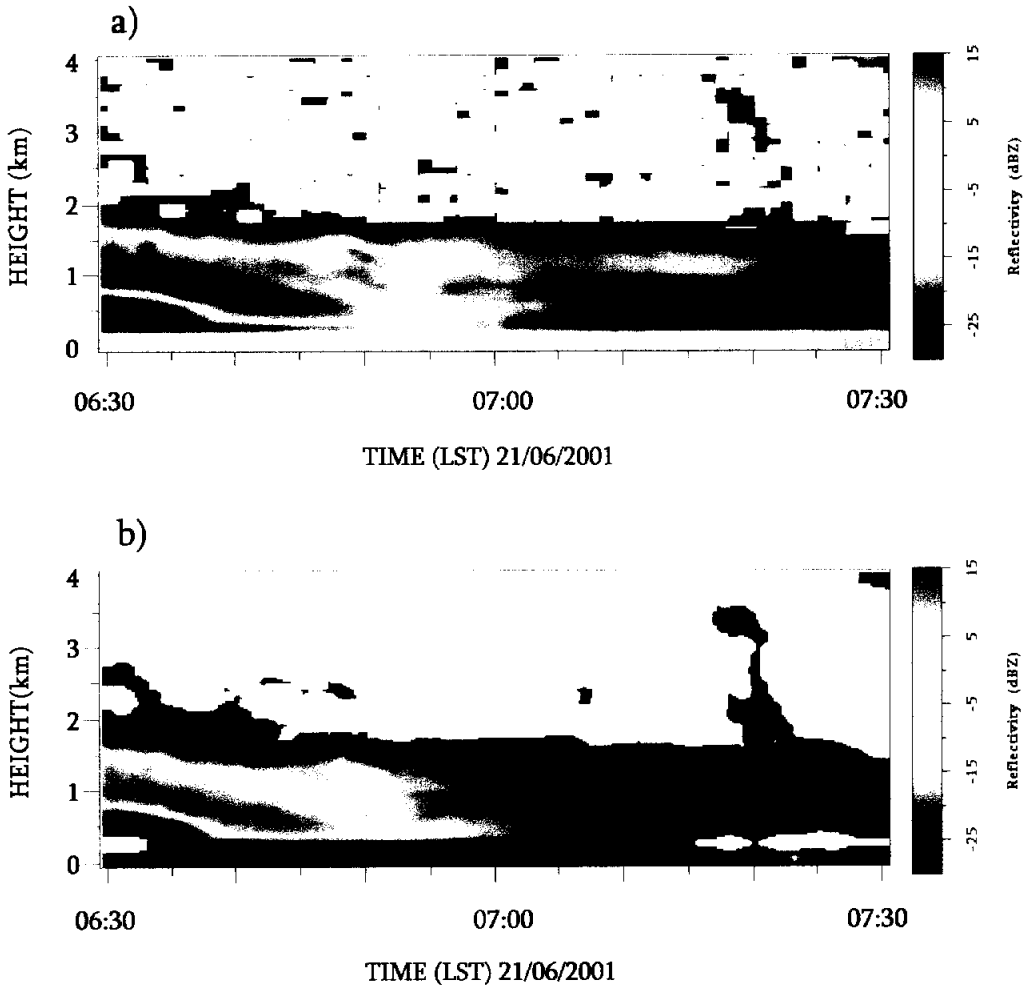

Figure 4.25 Dual wavelength radar measurement taken from 0630 LST to 0730 LST on 21 June 2001. Time-height cross section of radar reflectivity factor a) at 10 GHz and b) at 35 GHz.

Unfortunately, the evaporation couldn't be evident in this time, since both radars have the noises below about 350 m which have constant reflectivity during all the time at the same height. The existence of the large drizzle particle can be proved that the reflectitivies of cm wavelength radar at 10 GHz which have not detected well

the small cloud droplets have a clear reflectivity pattern such as shown in figure 4.25. From these two reflectivity fields, DWR was calculated and is shown the panel a) in figure 4.26. The data below the 400m height from the surface were removed because of their noises. The vertical profiles of DWR monotonously increase with height except a few times.

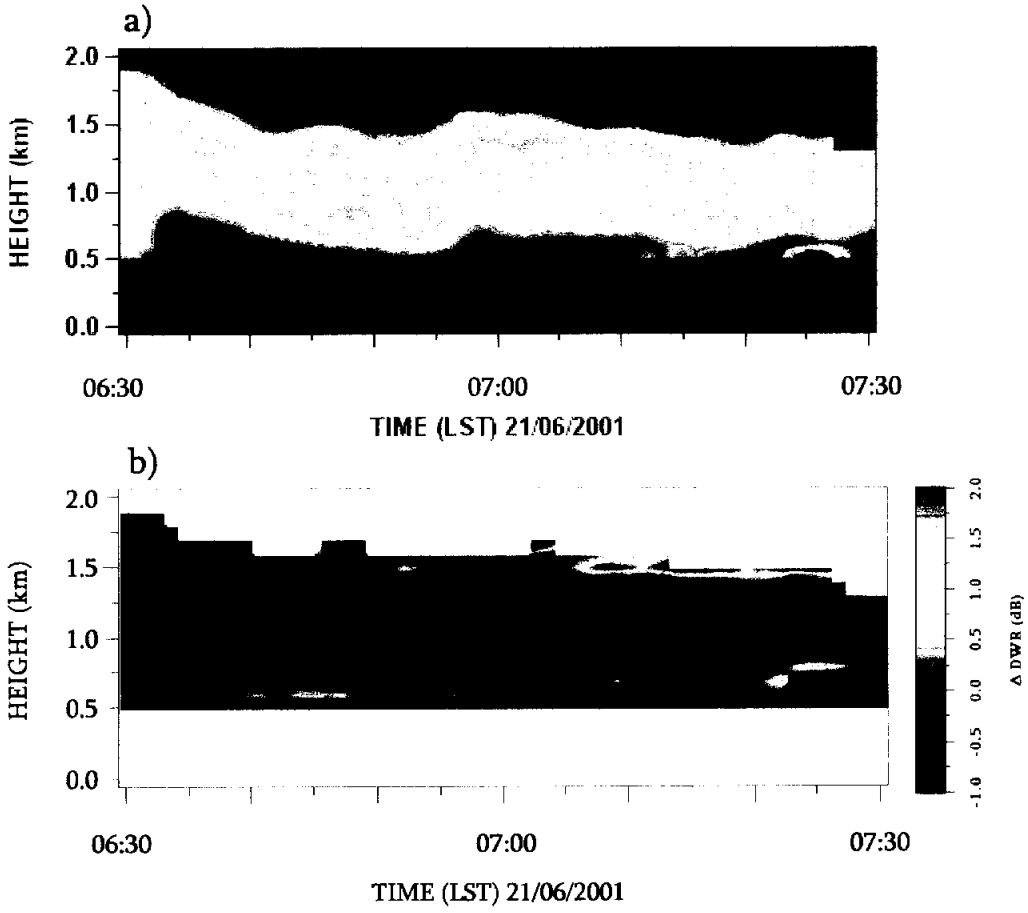

Figure 4.26 Time-height cross section of a) dual wavelength ratio(DWR) and b) Δ DWR from 0630 LST to 0730 LST on 21 June 2001.

It means that most of the liquid particles are included in Rayleigh regime at 10 GHz and 35 GHz and Mie scattering term in equation (4.11) does not contribute the value of DWR at these wavelength radar which shows the assumption is available. Consequently, because the difference of DWR between the adjacent layers with height only depends on the LWC (panel b) in figure 4.26), LWC can be calculated from the derivative of DWR and the time- height cross section of LWC is shown in figure 4.27. LWC is up to 1.0 g/m^3 and the most of values have ranged within 0.5 g/m^3 which are following the typical distribution of LWC in similar climate regime and cloud system although simultaneous aircraft measurements are required for validation.

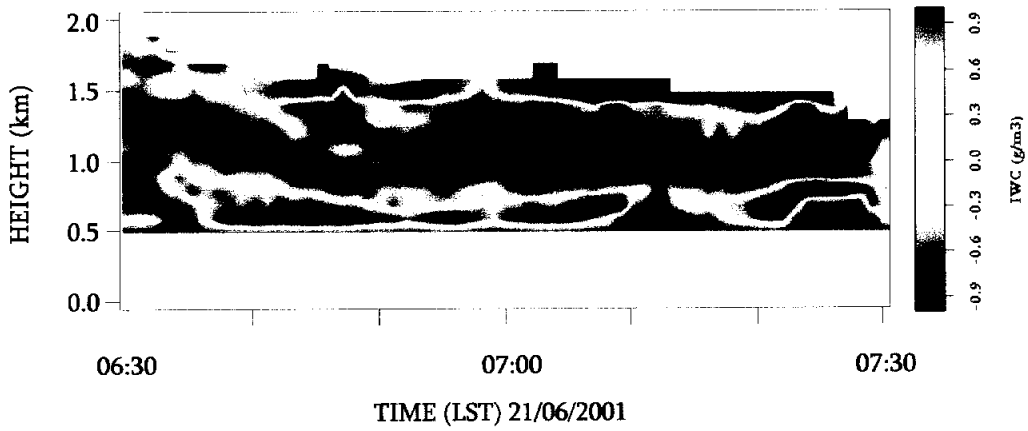

Figure 4.27 Time-height cross section of liquid water particles from 0630 LST to 0730 LST on 21 June 2001.

As shown panel a) in figure 4. 26, the vertical profiles of DWR at some points don't monotonously increase with height any more. Considering that the attenuation of LWC causes a monotonous increase of the vertical profile of DWR with height in Rayleigh regime, it can be deduced some factors contribute to DWR as a negative effect. It means that Mie scattering term in equation (4.11) can not be neglected as near zero but contribute to DWR as a negative effect because of the presence of larger drizzle in spite of using 10 GHz and 35 GHz. These effects made the negative LWC and cause to the bias of LWC as shown panel b) in figure 4.27.

Figure 4.28 shows the clear bias region which has a negative LWC. Green color means that DWR monotonously increases with height and the Mie scattering term can be neglected. On the other hand, the red color region indicates the bias error due to the Mie scatting effect which is due to the presence of the large drizzle. The existence of the larger drizzle particles than the radar wavelength causes to the improvement of bias problems.

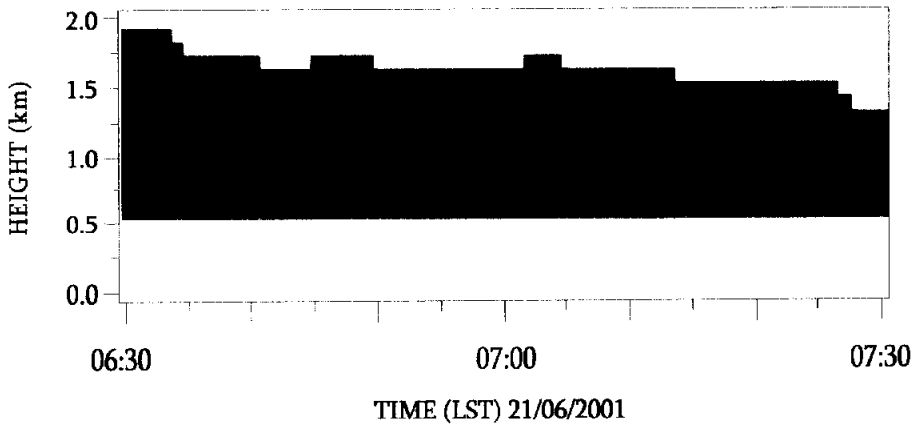

Figure 4.28 The positive ΔDWR (Green) and the negative (Red). Positive ΔDWR means Rayleigh region and Negative ΔDWR Mie region.

4.4.3 Improved technique for low level non-precipitating cloud with drizzle

Dual Observations (Miller et al., 1998; Albrecht, 1989) and modeling studies (Albrecht, 1993; Wood, 2000) have shown that drizzle is principally important, since it is involved in determining the cloud lifetime and evolution. The drizzle process may also have implications for the radiative properties of such clouds (Feingold *et al.*, 1996, 1997) through alteration of the cloud droplet spectra.

Stratocumulus which is deeper than a few 100 m, usually contains drizzle drops (Fox and Illingworth, 1997a). This implicates the presence of the aerosol particle processes, but without the subsequent rainout since most drizzle evaporates before reaching the ground.

The presence of drizzle can alter the numerous feedback mechanisms that are involved in the continual generation of stratocumulus. For instance, the evaporation of drizzle below cloud causes evaporative cooling which can cause decoupling (Nicholls, 1984; Albrecht *et al.*, 1995). The presence of drizzle droplets can change cloud droplet spectra and alter the cloud optical properties. This has an impact on the radiative fluxes and, in turn, processes in the boundary layer which generate stratocumulus, such as turbulence and vertical redistribution of heat and moisture (Driedonks and Duynkerke, 1989; Paluch and Lenschow, 1991; Feingold *et al.*, 1996).

In the previous researches, the differential attenuation method from the dual wavelength radars has a good agreement between vertically-integrated LWC and LWP by the microwave radiometer. The limitation has seen that when drizzle drops are present as Mie scatter, this method can be biased against the retrievals. A new

method to investigate the liquid water content of low level non-precipitating cloud with drizzle is introduced in this section.

Panel a) in figure 4.29 shows the vertical profile of the DWR at 0650 LST on 21 June 2001. Since DWR does not fluctuate with height, LWC can be retrieved from the differential attenuation method at these wavelengths. Panel b) in figure 4.29 shows the vertical profiles of DWR at 0647 LST. DWR is monotonously increasing until 1.1 km height and then intends to decrease between 1.2 km and 1.4 km. Above 1.4 km height, DWR is increasing again with height.

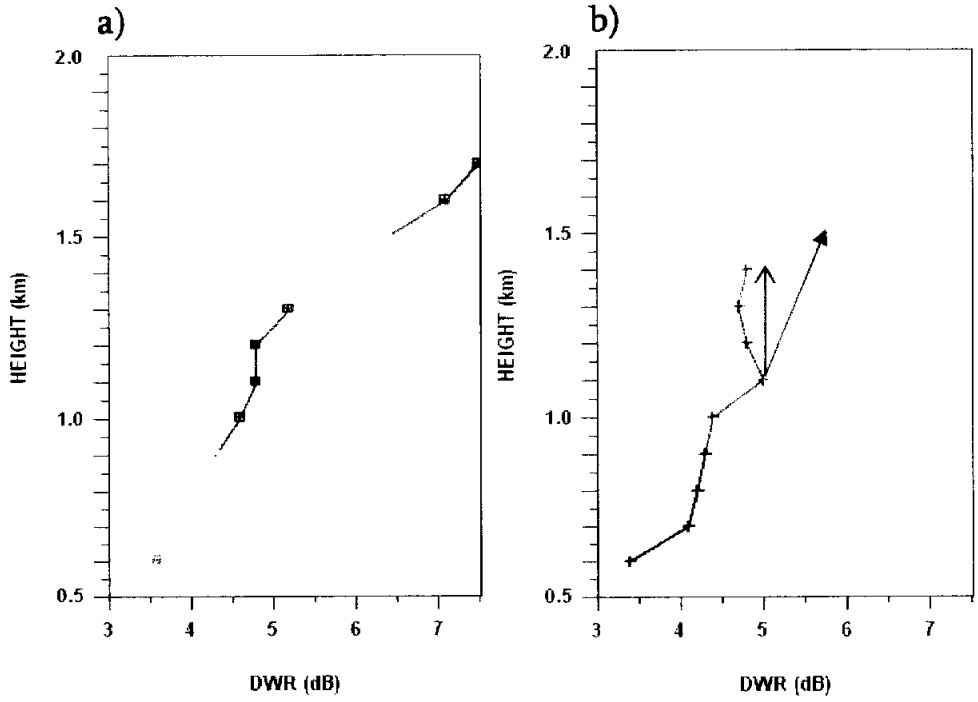

Figure 4.29 The vertical profile of the DWR in a) Rayleigh and b) Mie region. Red arrows show the contribution of LWC and Mie effect, respectively.

It was presumed that the decreasing values of DWR between 1.2 km and 1.4km is induced from the Mie scattering effect which contribute to DWR as negative values. To prove the negative contribution to DWR, it is needed to confirm this effect by simulating the relationship between the drop size and the Mie scattering term, $F_{10,35}$. Figure 4.30 shows the Mie scattering term $F_{10,35}$ as function of the median volume diameter. Mie scattering term is closer to zero on a condition that median volume diameter is smaller than about 0.25 mm. The more increase the diameter, the Mie scattering term becomes to fall with negative values and then increase again at around 0.75 mm. This can be explained as a resonance region (Van de Hulst, 1957) at higher temperature near a ≈ 0.5 where Mie scattering can exceed Rayleigh scattering.

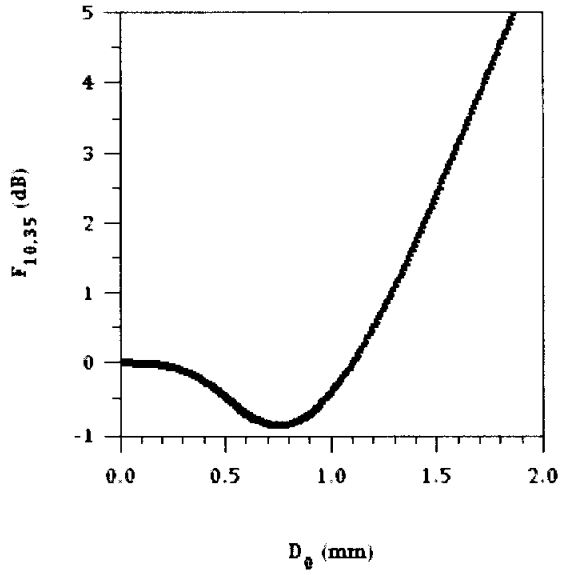

Figure 4.30 The relationship between Do and Mie scattering term at 10 GHz and 35 GHz.

As shown the panel b) figure 4.29, in the Mie region the value of the Mie scattering term can be decided by subtracting DWR at each height from DWR at 1.1 km (the last height with monotonous increase of DWR). The amount of LWC can be calculated by the difference of DWR at two height except for Mie region, 1.1 km and 1.5 km and is assumed the homogeneous distribution in Mie scattering layers(1.2, 1.3 and 1.4 km height).

If the Mie scattering term is decided, the additional median volume diameter can be calculated from the relationship of figure 4.30. Figure 4.31 shows the time-height cross section of the median volume diameter, D_0(mm) and Liquid water content, LWC derived from the method are explained above.

This method was shown to have the potential to retrieve the median volume diameter, D_0, assuming a constant liquid water content for the Mie scattering region. This study includes the retrieval of the typical drizzle droplets size distribution of which only one example. More research is necessary to improve the algorithms currently available and to provide new techniques which is capable of interpreting the vast amounts of information collected by these active instruments. It is hoped to extend this method to a large dataset to derive climatological values of liquid water content for the low level liquid water clouds. Validation of these techniques with data obtained from aircraft overpasses would be valuable and provide further information by improving the numerical climate models.

Most of all, the comparisons of the retrieved liquid water contents with aircraft measurements are seen as essential to validate the technique.

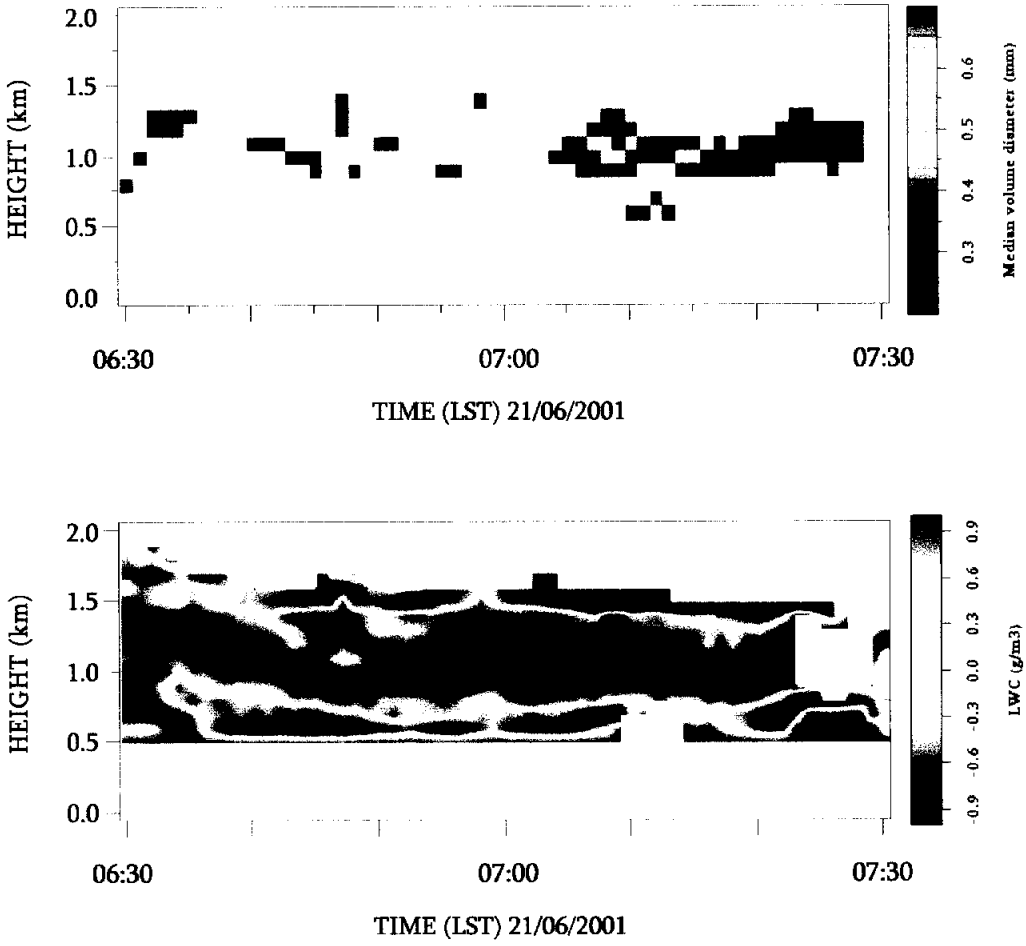

Figure 4.31 Retrieved Do by dual wavelength method in Mie region from the new approach.

4.5 Rain measurement from dual wavelength cloud radar

4.5.1 Background

Latent heat released by precipitation accounts for 75% of the heat transferred from the surface to the atmosphere (Simpson et al. 1996), and precipitation is intimately connected with both large and small scale circulations in the atmosphere and surface. Of all environmental parameters, rainfall plays one of the most significant roles in global heat and water budgets, yet a lack of accurate rainfall information persists over the vast areas of the globe. The presence of large oceanic regions, deserts, and jungle, particularly in the Tropics where two-thirds of all precipitation falls, precludes the use of rain gauges and other ground-based rainfall measurements in these regions. As a result, space-borne instruments provide the only means of obtaining global measurements of rainfall (Simpson et al. 1988).

Numerous techniques based on the satellite measurements of the microwave emission have achieved some success in mapping global rainfall (Wilheit *et al.,* 1977; Spencer et al., 1989; Kummerow and Giglio, 1994; Smith et al., 1994; Petty, 1994a and b). One draw back to these methods, however, is that few are capable of accurately determining the vertical structure of precipitation at the resolution required in global weather and climate models (Cess et al. 1993; Wang et al. 1996). In addition, such methods suffer from non-uniqueness and result from the fact that substantially different profiles of precipitating liquid and ice hydrometeors in the atmospheric column yield similar microwave radiance signatures introducing a substantial element of the uncertainty in their surface rain-rate estimates.

The profiling capabilities of space-borne radars have the potential to add vertical structure information to complement techniques based on passive measurements. As a result, the Tropical Rainfall Measuring Mission (TRMM) carried the first radar designed for precipitation measurements flown in space. Given the success of the 14-GHz precipitation radar (PR), which has been operational for more than 3 yr, future space-borne radar missions are being discussed. The potential for extensive spatial coverage offered by satellite-based radars has also been recognized by the CloudSat science team (Stephens et al. 2000, manuscript submitted to *Bull. Amer. Meteor. Soc.*), and a 94-GHz cloud profiling radar (CPR) will be adopted on that satellite, which may be capable of measuring light rainfall in addition to clouds. Recently, millimeter wavelength cloud radar has been recognized as a powerful tool for measuring the cloud properties, particularly for obtaining their vertical distributions. In the last decade a set of interrelated techniques had been developed to determine microphysical properties of clouds by combining measurements from ground-based radars with microwave radiometer measurements. Especially, 35 GHz (Ka band) and 94 GHz (W band) radar system has been proven effective for cloud imaging, and may soon become operational. One of the major questions remaining, however, is the utility of this wavelength at detecting rainfall. The energy at this frequency is highly attenuated by liquid hydrometeors at the sizes encountered during rain events, especially in the convective systems where the average size of the raindrops approaches the wavelength of the radar beam.

The Dual-frequency Precipitation Radar (DPR), which will be installed on the GPM core satellite, consists of two radars; i.e., the Ku-band (14 GHz) Precipitation Radar (KuPR) and the Ka-band (35 GHz) Precipitation Radar (KaPR). While the KaPR has high-sensitivity to detect weak rain or snow, the KuPR can detect heavy rainfall. By combining the KaPR and the KuPR, there can observe accurate rainfall rate in the

range from weak rain or snow in the high-latitude regions to strong rainfall in the tropics. The high-frequency microwaves used by the DPR are affected by the rain attenuation in general. The amount of the attenuation depends on the frequency and the size of the raindrops. Therefore, the drop size distribution (DSD) of rain can be estimated using the difference of attenuation between two frequencies in the KuPR and KaPR. To obtain the difference of attenuations, the simultaneous observation of precipitation at the same location is required. The DSD information, which cannot be obtained by TRMM PR, is useful to improve the accuracy of the rainfall estimation. Also, the difference of attenuation may be used for the distinction between rain and snow.

Many ground-based radar retrieval algorithms are based on the Rayleigh approximation that the rain drops are small with respect to the radar wavelength. It also assumes the drop size distribution (DSD) to derive a simple relationship between radar reflectivity and rain rate. From an operational standpoint, these algorithms are computationally efficient, relatively simple to implement, and productive for the useful results but they can incur uncertainties that are difficult to estimate as a result. Errors associated with the assumption of an idealized size distribution were pointed out by Wexler (1948); Gunn and East (1954) showed that the Rayleigh approximation is not valid for wavelengths less than 3 cm (or frequencies greater than 10 GHz), emphasizing the need for an algorithm that is not restricted by such assumptions in space borne applications. This has been recognized by the designers of the TRMM PR rainfall profile algorithm which selects a DSD based on rain type and the presence or absence of a bright band and correct the DSD based on a PIA estimate (Iguchi *et al.,* 2000).

4.5.2 The feasibility of cloud radars for rain measurement

The mm wavelength cloud radars have been developed to measure the non-precipitating cloud and to gether the information the of rain drop size distribution for light rain, which have relatively small attenuation. Since the radar signal is highly attenuated by the rainfall in case of cloud radar at 95 GHz, it is not easy to use the rainfall estimation with the 95 GHz radar. The preliminary studies use the cloud radar at the 35 GHz and the 95 GHz for the rain measurement. To get the vertical profile of rain as a function of rain intensity, it is also necessary to evaluate the intensity of the attenuation and the location of the maximum height. Figure 4.32 shows where the maximum height can be observed as a function of rain intensity with the 35 GHz and 95 GHz cloud radars owned in NIED, Japan. The drop size distribution to calculate the rain intensity was assumed by Marshall and Palmer. To get the perfect vertical profile of the rain drop size within 5 km height, the limitation of rain intensity is about 20 mm/hr. At higher intensity, the radar signal would be disappeared by the attenuation. For cloud radar at 95 GHz, the limitation corresponds to less than 6 mm/hr as shown in figure 4.32.

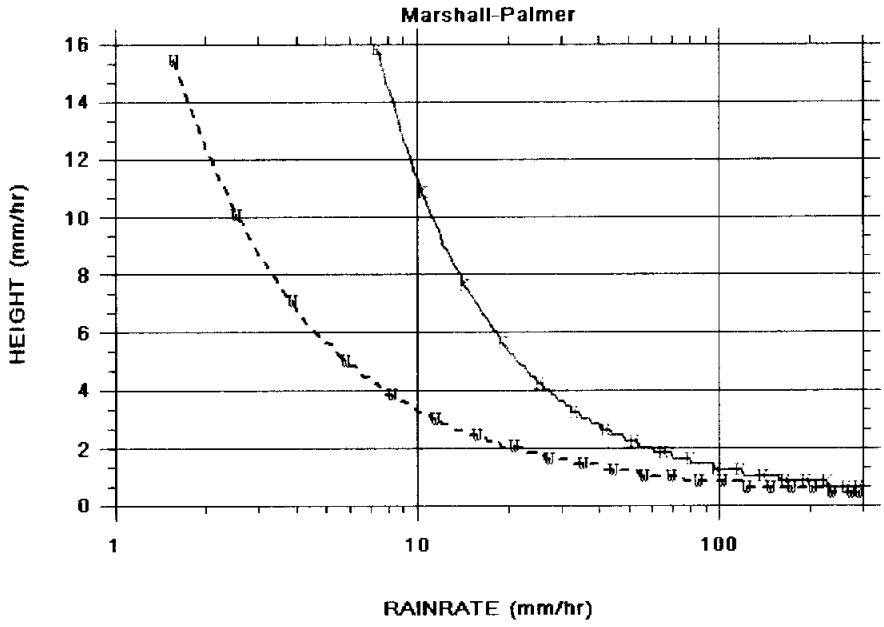

Figure 4.32 The relationships of rainrate vs. height at 35 GHz (solid line) and 95 GHz(dash line). Assumed vertically homogeneous rain distribution, 35 GHz radar can be observed the vertical profiles of rain information by the 3.5 km height and 95 GHz radar by 10 km height in the rain intensity with 10mm/hr.

4.5.3 Dual wavelength method for weak rain

The Equivalent reflectivity factor measured at 35 GHz and 95 GHz frequency is invalid until the attenuation between radar and scattering rain cell is removed. Attenuation is induced through oxygen and water vapor absorption and attenuation from rain or liquid water drops. Therefore, measured reflectivity at each bin of mm-wave radars showed in equation (3.14) and dual wavelength ratio between 35 GHz and 95 GHz also can be also rewritten from equation (4.3)

$$10 \log Z_m = 10 \log Z_e + 2 \int_0^r \alpha_{ext}(s)\, ds$$

$$DWR = F_{35,95}(D_0) + R_{35,95} + A_d$$

$$F_{35,95}(D_0) = \left[\frac{\lambda_{35}^4 \int_0^\infty \xi_b D^{\mu+2} \exp[-(3.67+\mu)D/D_0]\, dD}{\lambda_{95}^4 \int_0^\infty \xi_b D^{\mu+2} \exp[-(3.67+\mu)D/D_0]\, dD} \right]$$

$$R_{35,95} = 20 \log \frac{|K_{95}|}{|K_{35}|}$$

$$A_d = 2 \int_0^r (A_{95} - A_{35})\, du$$

Under the Rayleigh approximation, $F_{35,95}(D_0)$ term is equal to zero for cloud liquid water (less than 100 μm) and DWR is just induced from the differential attenuation (A_d) and the dielectric factor ($R_{35,95}$). But $F_{35,95}(D_0)$ for the rain drops is no longer equal to zero, since Mie resonances affect the scattering cross sections of the drops (Firda *et al.*, 1999). Therefore, the contribution of $F_{35,95}(D_0)$ and A_d to the dual wavelength ratio should be known.

Figure 4.33 shows the simulated parameters as a function of median volume diameter for 35 and 95GHz assuming the Marshall-Palmer exponential drop size distribution and the spherical water droplets. Liquid water content can be determined by this theoretical relationships and the procedure as described below.

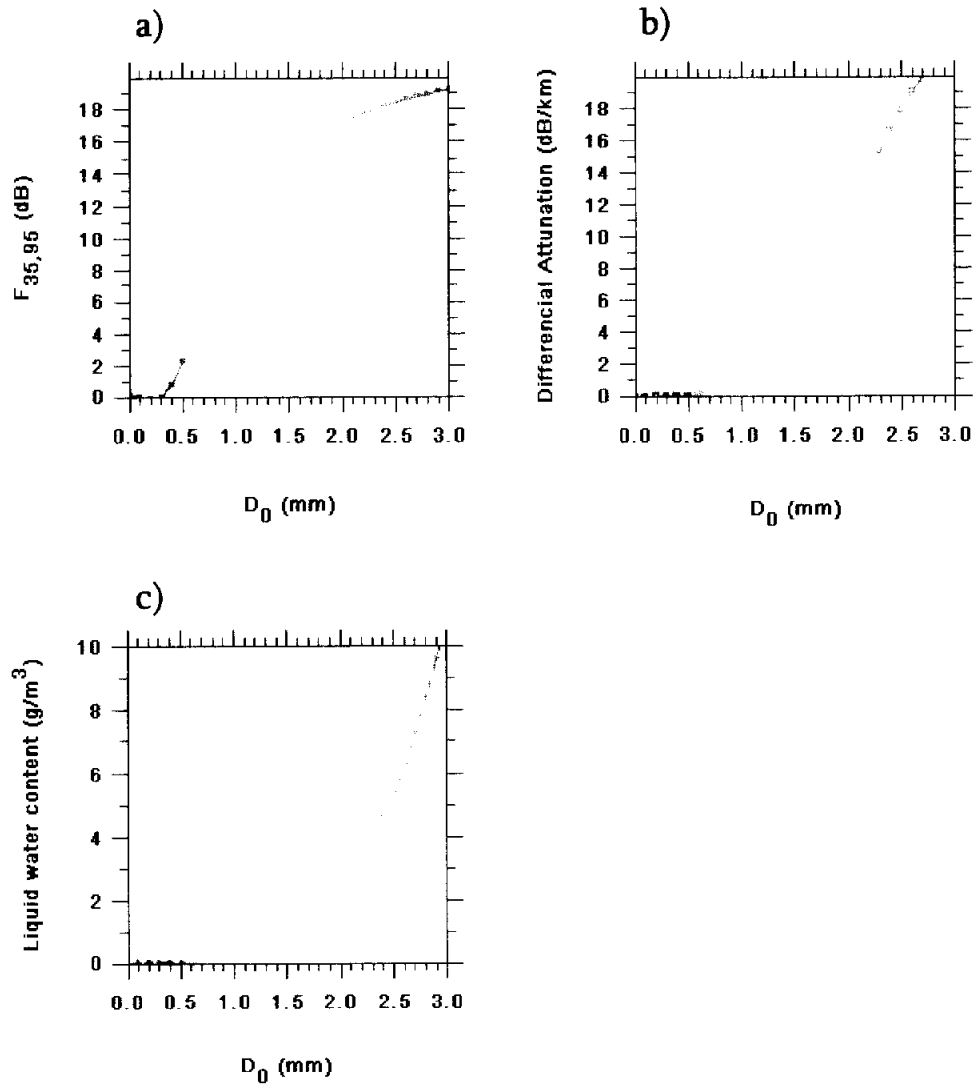

Figure 4.33 Panel a) Mie scattering term, $F_{35,95}$, b) differential attenuation and c) liquid water content are numerically calculated by T-matrix method also considering the Mie scattering for the 35 and 95GHz radar assuming the exponential drop size distribution.

1) The Reflectivity factors of Z_{35} and Z_{95} were calibrated by co-located disdrometer data observed at the same time with the radar data.
2) Next, DWR is calculated from the radar reflectivities between 95 and 35GHz.
3) Assuming that first gate has no attenuation by liquid water contents effect, the median volume diameter (D_0) derived from the observed DWR can be estimated, and furthermore the liquid water contents are retrieved by theoretical relationships between D_0 and LWC at first gate (height of the first gate is 400m in this study because of the noisy data below the height).
4) Because LWC at the first range bin brings the attenuation effect at the next range bin, the two-way differential attenuation (dB/km) between 95 and 35GHz radar by LWC in the first range bin was calculated, then subtracted it from observed DWR at the second range bin.
5) LWC and D_0 at the second range bin are retrieved from the attenuation-corrected DWR.
6) Attenuation-corrected DWR of the third range bin is calculated by subtracting vertically accumulated differential attenuation (the sum of differential attenuation at the first and second range bin) from the observed DWR.
7) As the above procedures were carried out at every range bin repeatedly, it can be retrieved D_0 and LWC at every range bin.

4.5.4 Application of real data

The data obtained by cloud radar at 35 GHz and 95 GHz and disdrometer from between 0800 and 1100 LST on 21 June 2001 are calculated using the algorithm described in the previous section. Panel (a) in figure 4.34 shows the radar reflectivity measured at 35 GHz and panel (b) coincident at 95 GHz which have been averaged over 1 minute with a range resolution of 50m during the weak rain.

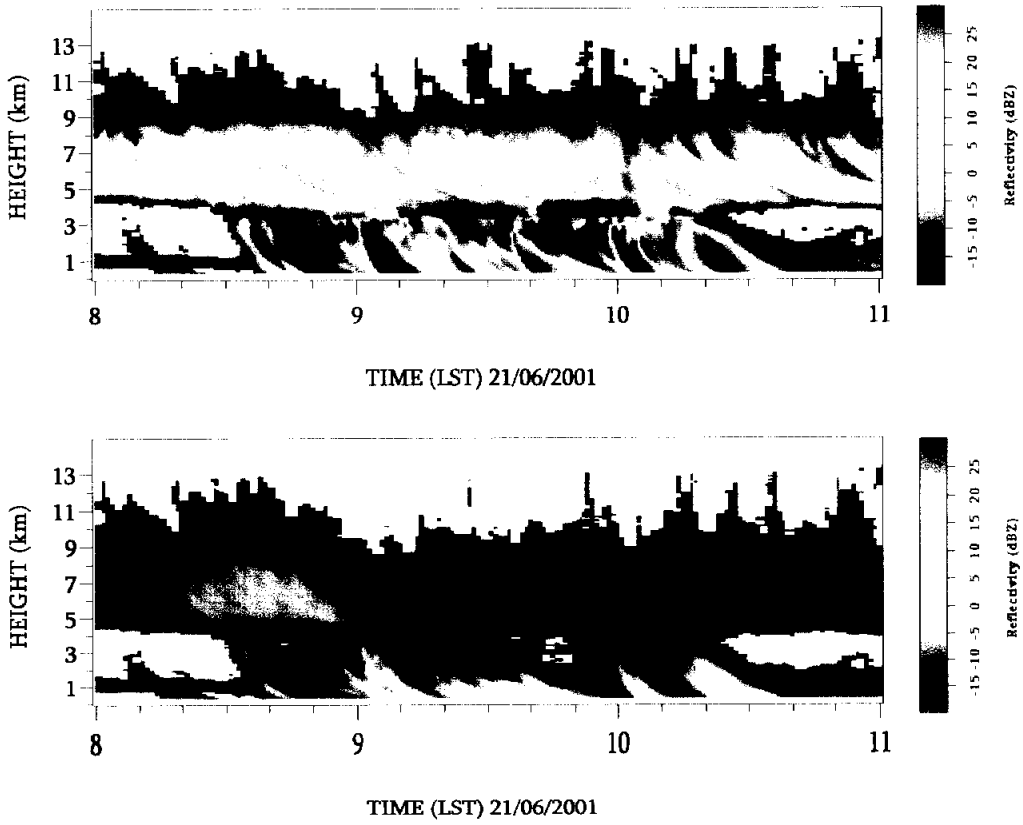

Figure 4.34. Time-height cross-section of the radar reflectivity Z_{35} , Z_{95} (dBZ) and DWR(dB) observed with the dual wavelength cloud radar from 0800 to 1100 LST on 21 June 2001.

The corrections of the dielectric factor and the gas attenuation are made with the profiles of temperature, relative humidity and pressure at 0900 LST in Tateno in figure 4.6. The one-way gaseous attenuation from the space has been calculated using the line-by-line model by Liebe(1985). Figure 4.35 shows the vertical profile of one-way attenuation by the Liebe model at 10 GHz, 35GHz and 95GHz.

Figure 4.36 shows the time-height cross-section of DWR from the dual wavelength cloud radar at 35 GHz and 95 GHz from 0800 to 1100 LST on 21 June 2001. The larger DWR is appeared due to the vertically accumulated attenuation in the rain. And the DWR results from the Mie scattering effect and attenuation effect by the rain. The attenuation effect was removed from DWR by using the dual wavelength technique explained in section 4.5.3 and the median volume diameter and the rain water content were also retrieved. Figure 4.37 shows the time-height cross-section of the Mie scattering term, $F_{35,95}$(dB) derived from the dual wavelength cloud radar from 0800 to 1100 LST on 21 June 2001, and figure 4.38 is coincident with the median volume diameter D_0 and rain water content(g/m^3) .

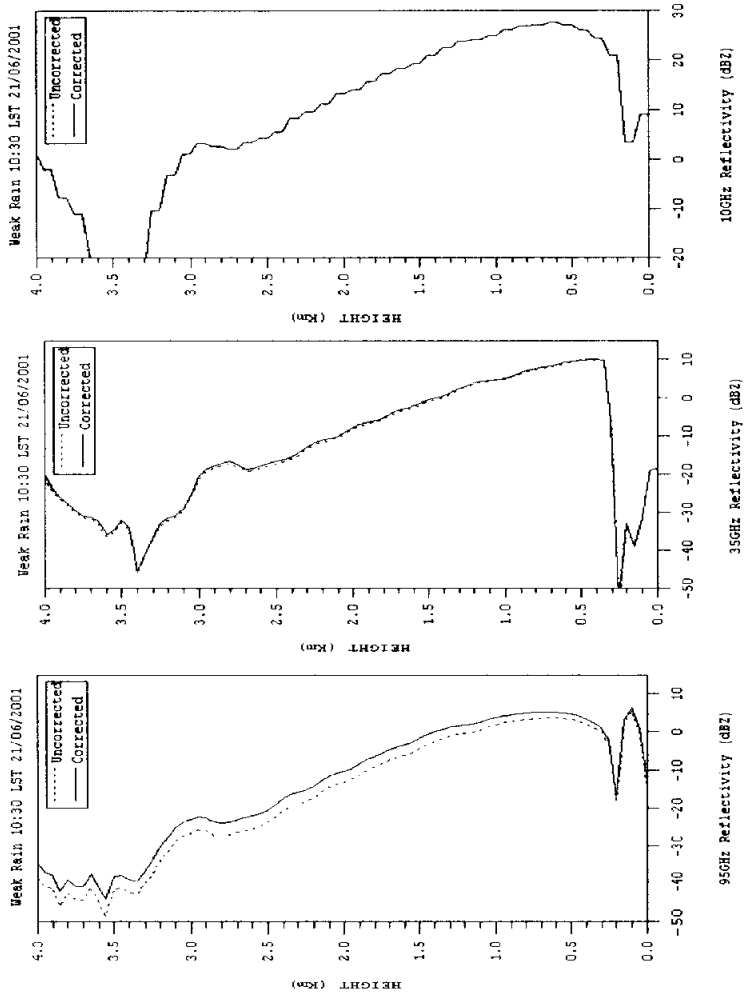

Figure 4.35 The vertical profiles of uncorrected (dotted line) and corrected (solid line) radar reflectivity at 10 GHz, (b) 35 GHz and (95 GHz) for precipitation case, 1010 LST 21 June 2001. The corrections of dielectric factor and gas attenuation are considered by sonde data. Gas attenuation correction was calculated by Liebe model(1995).

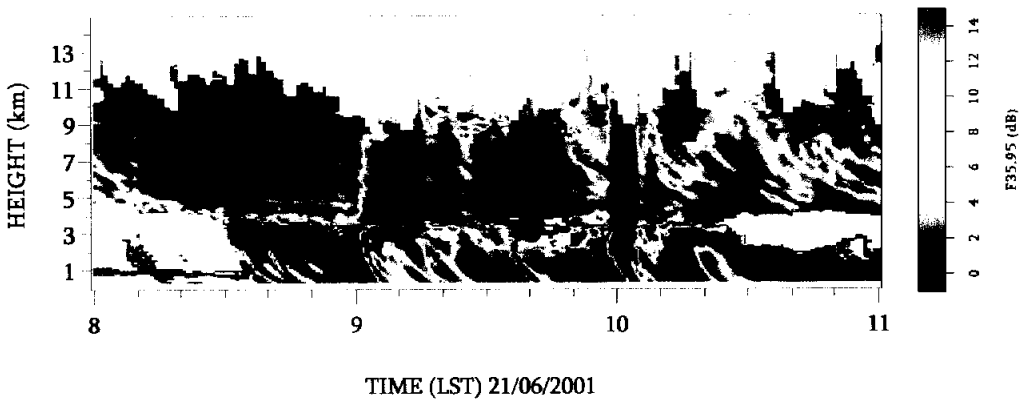

Figure 4.36 Time-height cross-section of DWR observed with the dual wavelength cloud radar from 0800 to 1100 LST on 21 June 2001.

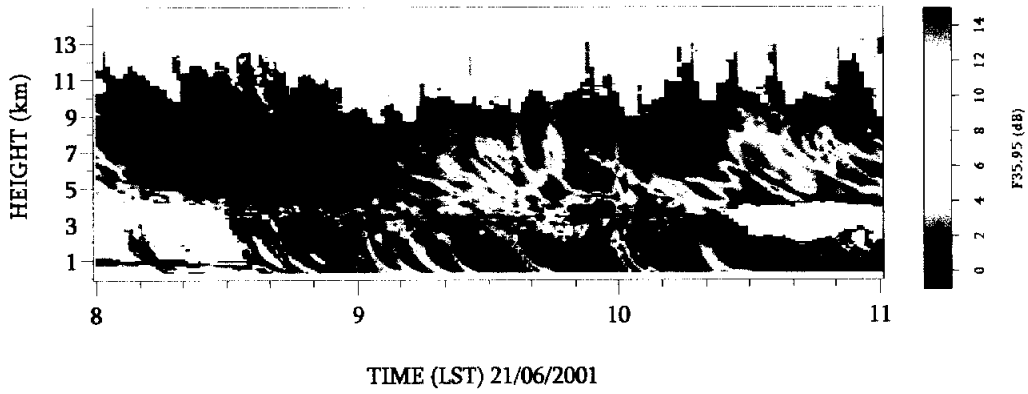

Figure 4.37 Time-height cross-section of Mie scattering term, $F_{35.95}$ (dB) observed with the dual wavelength cloud radar from 0800 to 1100 LST on 21 June 2001.

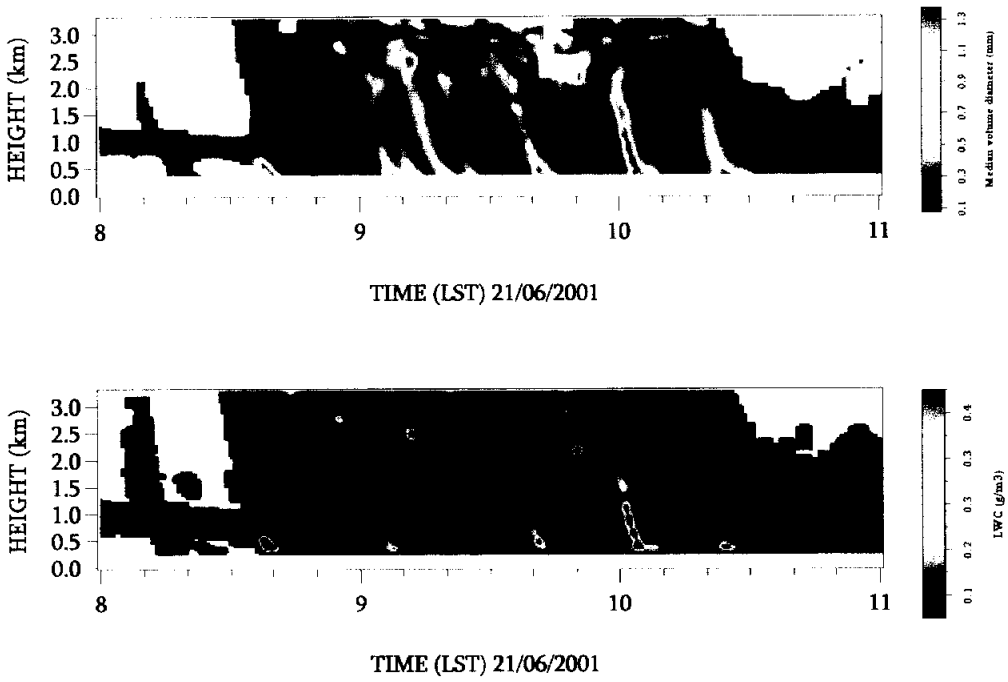

Figure 4.38 Time-height cross-section of retrieved (a) median volume diameter D_0 and (b) liquid water content LWC(g/m^3) with the dual wavelength radar from 0830 to 1100 LST on 21 June 2001.

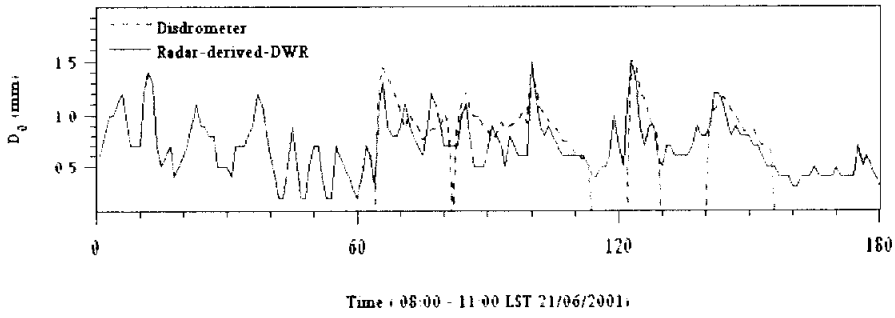

Figure 4.39 The comparison of the median volume diameter (mm) between disdrometer and radar derived from dual wavelength technique from 0800 to 1100 LST on 21 June 2001.

4.5.5 Rain measurement from weather and cloud radar

To evaluate the ability of mm wavelength cloud radar for rain measurement it was compared the rain drop size derived from cloud radar with that from weather radar at 10 GHz. Figure 4.40 showed the time-height cross-section of the weather radar reflectivity at the 10 GHz co-located dual wavelength cloud radar from 0800 to 1100 LST on 21 June 2001. Figure 4.41 displayed the median volume diameter D_0 derived from 10 GHz weather radar. To estimate the median volume diameters from weather radar it was assumed the Marshall-Palmer drop size distribution (N_0=8000 and μ=0) which is a same assumption as the case of dual wavelength cloud radar. Figure 4.42 showed the comparison of the median volume diameter between the disdrometer and derived from the 10 GHz weather radar from 0800 to 1100 LST on 21 June 2001. The median volume diameters between disdrometer and weather radar both have a range distribution between 0.5 and 1.5 mm for rain.

When it was compared the median volume diameter derived from the cloud radar (figure 4.39) with that from weather radar (figure 4.42), both have a good agreement with the median volume diameter from disdrometer. Figure 4.39 and 4.42 showed that median volume diameters from cloud radar have better agreement than the weather radar at peak point. At peak point the median volume diameters derived from weather radar underestimated as compared with disdrometer. In this study the methodology was different between cloud radar and weather radar each other to retrieve the median volume diameter. The better agreement of cloud radar at peak point might imply that the dual wavelength technique is better than single radar method.

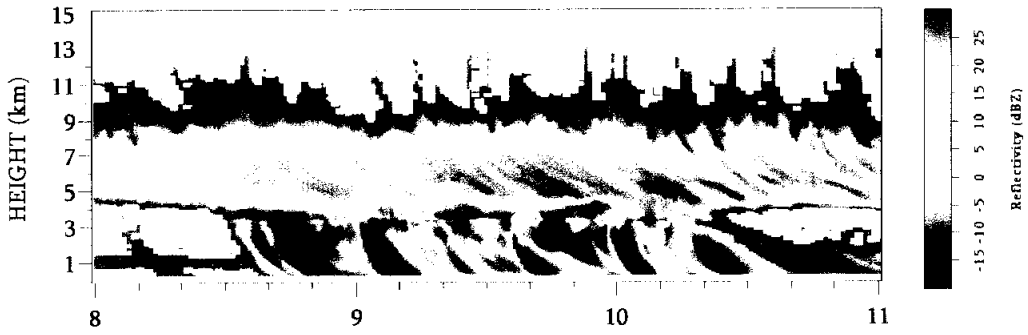

Figure 4.40 Time-height cross-section of the radar reflectivity Z_{10} (dBZ) at the 10 GHz co-located dual wavelength cloud radar from 0800 to 1100 LST on 21 June 2001.

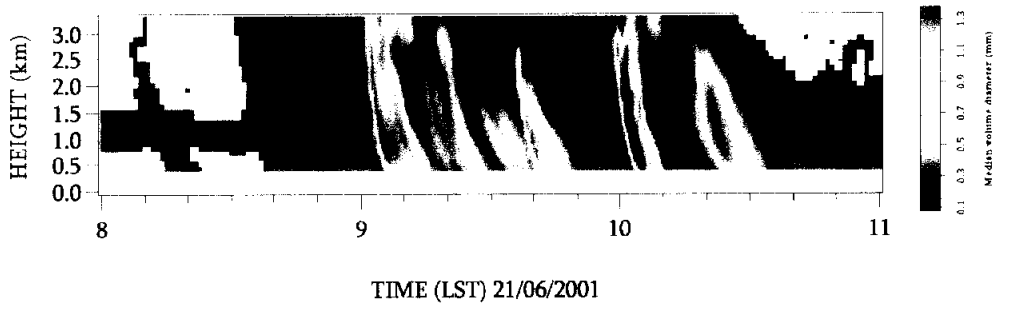

Figure 4.41 Same as panel a) in figure 4.38, but D_0 derived from 10 GHz radar .

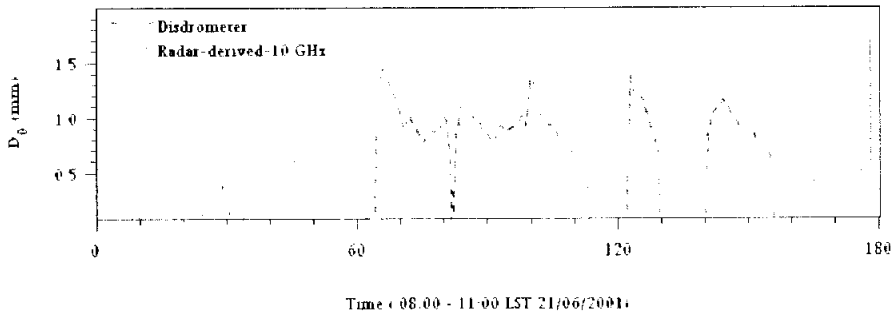

Figure 4.42 The comparison of the median volume diameter (mm) between the disdrometer and derived from the 10 GHz weather radar from 0800 to 1100 LST on 21 June 2001.

Chapter 5

SUMMARY AND CONCLUSIONS

Clouds play a fundamental role in the earth's radiation budget, and in order to determine their effects on the climate system, there is an urgent need for the vertically-resolved remote sensing measurements of cloud radiative properties.

The purpose of this thesis is to retrieve drop size and to quantify ice and liquid phase hydrometeors in non-precipitation clouds using mm wavelength cloud radar, which is a powerful tool for monitoring clouds. Especially, the study was focused on the analysis of dual wavelength cloud radars. In addition to the research of cloud, the potential of the dual wavelength radar to measure precipitation has been investigated. Liquid phase water contents were retrieved from the low level non-precipitating clouds that have the most profound impact on the earth radiation budget because of their high large global coverage. However, ice water content and its drop size distribution in cirrus clouds are not understood well. The vertical profiles of cloud water and its drop size distribution were retrieved from the mm wavelength cloud radars (35 / 95 GHz) and the 10 GHz radar which are operated by National research Institute for Earth science and Disaster (NIED) in Japan for the day on 21 June 2001.

- Estimating microphysical properties in General Circulation Models (GCMs) which is used for the prediction of climate change and earth's radiation budget, accurate hydrometeors of cirrus clouds are essential.

5.1 Ice water content in cirrus clouds

To validate ice cloud parameterizations, an active measurement of Ice Water Content(IWC), crystal sizes and shapes are needed. Unfortunately, in the Rayleigh scattering regime, radar reflectivity Z is proportional to the sixth power of droplet diameter, so it is not directly related to either IWC or crystal size. However, if a cirrus cloud consist of ice crystals is observed by two different wavelength cloud radars, the reflectivity would be different by scattering regimes each other. The difference of reflectivity, the Dual Wavelength Ratio(DWR), is defined as the ratio of measured Z at the longer wavelength to the shorter wavelength and is equal to the sum of two terms: one term is the differences of scattering properties and the other is the total differential attenuation undergone along the beam path at two wavelengths. The simulation showed that the attenuation by ice crystal is generally so small to be detected for all mm wavelength radars. And the differential attenuation term does not contribute to DWR. It means that DWR for ice crystals depends on the scattering term which is directly related to ice crystal size, however the vertical profiles of drop size can be calculated from it.

To test dual wavelength method, a case study is conducted on 21 June 2001 when typical thick cirrus in mid-latitude was observed by the 35 GHz and 94 GHz radars. The simulation of gas attenuation at mm wavelength radar showed that the reflectivity attenuation by atmospheric gas is not a negligible factor but comes to around 1 dB at 35 GHz and 4 dB at 95 GHz at the height of typical cirrus clouds. This implies that corrections of attenuation is needed in advance for estimating the exact drop size. By assuming a gamma distribution (μ=0) for crystal sizes and spherical shape, the density of crystal decreases as its size increases. Mie scattering calculations have been carried out to find out how DWR varies with median volume

diameter, Do and IWC. From these relationships, the retrieved median volume diameters in cirrus clouds reach up to 0.8 mm except for the cloud base with 100 m thick. The IWC is in a range distribution between 0.001 and 0.15 g/m^3.

Due to the absence of the real aircraft data, the vertical distribution of the retrieved values between cloud base and top are compared to the previous researches. It is interesting to note that Do is highly overestimated up to 1.5 mm at the most cloud bases although IWC is similar at cloud top and base. For the given IWC, a distinct difference of crystal size between the cloud base and the cloud top supports the idea that the small crystals evaporate first at cloud base. It implies that cirrus size distributions are not well represented by gamma distributions, since they tend to underestimate the number of larger size crystals. As a result, if a gamma distribution is inevitably assumed for the retrieval ice crystal size at the cloud base, the sensitivity test of the shape parameter μ will indicate that the overestimated Do can be adjusted by choosing a smaller μ at the cloud base. However, it seems cloud top is better for the both size and ice water content measurements.

Compared with the IWC by the experimental power law relationship, it is found that the pattern of the derived IWC from dual wavelength method is so different as compared with IWC by $IWC=0.137\ Z^{0.643}$. Therefore, it can be inferred the reason for the typical problems in a single wavelength radar which is the ubiquitous presence of occasional drizzle drops with a few hundred microns in diameter and dominates the reflectivity, but contribute negligible to IWC in this study.

5.2 Liquid water content in low-level clouds

One of the main problems in using radar to make quantitative measurements of stratocumulus is that the occasional large drizzle droplets (around 100 microns in diameter) can produce a large signal for the radar, but their contribution is negligible compared to liquid water content (LWC). However, the attenuation is proportional to LWC and increases with frequency, so two radars at different frequencies should be able to measure LWC by taking the derivative with height of the Dual Wavelength Ratio (DWR). In previous studies, the differential attenuation method from dual wavelength radars has a good agreement between a vertically-integrated LWC and a LWP obtained by microwave radiometer. The limitation is that when drizzle drops are present in Mie scatter regime, this method can bias the retrieval values.

To test dual wavelength method for the non-precipitating liquid phase clouds, - low-level clouds were observed by the 10 GHz and 35 GHz radars on 21 June 2001. The 10 GHz and 35 GHz are selected rather than 35 GHz and 95 GHz. The reason is that DWR from 35 GHz and 95 GHz is too noisy to attempt taking a vertical derivative due to relatively larger droplets than at the typical stratocumulus. The existence of larger droplets was possible to be detected the reflectivity of 10 GHz radar which is insensitive in the low level weak clouds. The reflectivities have a range between -30 dBZ and 5 dBZ at both 10 GHz and 35 GHz and the vertical profiles of DWR did not monotonously increase with height in this study. This implies that large particles included in the cloud negatively contribute to the Mie scattering term in DWR.

As a result, if it were assumed the vertically homogenous attenuation by LWC in Mie region, the Mie scattering effect term contributed in DWR would be calculated

by subtracting the assumed attenuation by LWC from DWR. Median volume diameter Do can be retrieved from derived Mie scattering term and DWR. In this study, new approach method was developed and could be obtained Do as well as LWC in Mie scattering region and could also be adopted in the presence of the drizzle. Since the limitation of this method, it can not be used with the drizzle drops larger than 0.7mm even if the coupled 10 GHz and 35 GHz radars are used simultaneously.

5.3 Rain measurement

A 94 GHz radar system has been proposed for the optically thin cloud systems studies. In addition to clouds properties, a question has been raised whether this system can measure a reasonable amount of the precipitation events. The main obstacle to rainfall parameterization at this frequency experiences severe attenuation due to the liquid hydrometeors.

This work showed that cloud radars of 35 GHz and 95 GHz radars are reliable tool to retrieve vertical profiles of rain drop size distribution and rain water content in weak rain. Near the surface, median volume diameter derived from radar and disdrometer have a good agreement each other. Assumed vertically homogeneous rain distribution, 35 GHz radar was able to observe the vertical profiles of rain information by the 3.5 km height and 95 GHz radar by 10 km height with the rainfall intensity of 10mm/hr. In the heavier rain falls, the available height is intended to exponentially decrease in this study.

Finally, the potential of dual wavelength radar was examined to measure the drop size and the amount of hydrometeor in clouds and precipitation and retrieved from the real radar data. It was found that dual wavelength radar is very useful instrument for the retrieval of hydrometeors contents detection at high level cloud as well as precipitation at low level. These new developed algorithms for the more accurate hydrometeors retrieval by using dual wavelength technique would improve the understanding of cloud processes and a global climatologiy of cloud parameters.

REFERENES

Albrecht, B. A., M. A. Miller, and R. M. Peters, 1990: The development of a surface-based system for observing boundary layer clouds. Preprints, *Ninth Symp. on Turbulence and Diffusion,* Roskilde, Denmark, Amer. Meteor. Soc., 70–73.

Atlas, D., 1954: The estimation of cloud parameters by radar. *J. Meteor.*, **11** , 309-317.

Atlas, D., and F. H. Ludlam, 1961: Multi-wavelength radar reflectivity of hailstorms. *Quart. J. Roy. Meteor. Soc.,* **87**, 523–534.

Atlas, D., S.Y. Matrosov, A.J. Heymsfield, M.-D. Chou, and D.B. Wolff (1995): Radar and Radiation Properties of Ice Clouds. *J. Appl. Meteor.*, **34**, 2329-2345.

Babb D.M., J. Verlinde, and B.A. Albrecht, 1999: Retrieval of cloud microphysical parameters from 94 GHz radar Doppler power spectra. Submitted to *J. Atmos. Sci.*

Baran, A, P. Watts, and J. Foot, 1998: Potential retrieval of dominating crystal habit and size using radiance data from a dual-view and multiwavelength instrument: A tropical cirrus anvil case, *J. Geophys. Res., 103*(D6), 6075-6082.

Barber, P. and C. Yeh, 1975: Scattering of electromagnetic waves by arbitrarily shape dielectric body. *Appl. Opt.,* 14, 2864-2872.

Bringi, V. N., V. Chandrasekar, N. Balakrishnan and D. S. Zrnic, 1990: An examination of propagation effect in rainfall on radar measurements at microwave frequencies. *J. Atmos. Oceanic Technol.,* 7, 829-840.

Brown, P. R. A., A. J. Illingworth, A. J. Heymsfield, G. M. McFarquhar, K. A. Browning and M. Gosset, 1995: The role of spaceborne millimeter-wave radar in the global monitoring of ice-cloud. *J. Appl. Meteor.*, **34**(11), 2346–2366.

Cess, R. D., and Coauthors, 1993: Uncertainties in carbon dioxideradiative forcing in atmospheric general circulation models. *Science*,**262**, 1252–1255.

Cess, R.D., et al., 1996: Cloud feedback in atmospheric general circulation models: an update. *J. Geophys. Res.*, **101**, 12761-12795.

Clothiaux, E. E., M. A. Miller, B. A. Albrecht, T. P. Ackerman, J. Verlinde, D. M. Babb, R. M. Peters, and W. J. Syrett, 1995: An evaluation of a 94-GHz radar for remote sensing of cloud properties. *J. Atmos. Oceanic Technol.*, **12**, 201–228.

Ecklund, W. L., P. E. Johnston, J. M. Warnock, W. L. Clark, and K. S. Gage, 1995: An S-band profiler for tropical precipitatingcloud studies. Preprints, *27th Conf. on Radar Meteorology*,Vail, CO, Amer. Meteor. Soc., 335–336.

Firda J.M., S.M. Sekelsky, and R.E. McIntosh, 1999: Application of dual-frequency millimeter wave Doppler spectra for the retrieval of drop size distributions and vertical air motion in rain. *J. Atmos. Oceanic Tech.*, **16**, 216-236.

Fox, N.I., and A.J. Illingworth, 1997: The retrieval of stratocumulus cloud properties by ground-based cloud radar. *J. Appl. Meteor.*, **36**, 485-492.

Frisch, A.S., C.W. Fairall, and J.B. Snider, 1995: Measurement of stratus cloud and drizzle parameters in ASTEX with a Kα —band Doppler radar and microwave radiometer. *J. Atmos. Sci.*, **52**, 2788-2799

Goddard, JWF, Eastment, JD, and Thurai, M., 1994: The Chilbolton Advanced Meteorological Radar: a tool for multidisciplinary atmospheric research. J. IEE Electronics and Communication Eng., **6**, 77-86

Gossard E.E., J.B. Snider, E.E. Clothiaux, B. Martner, J.S. Gibson, R.A. Kropfli, and A.S. Frisch, 1997: The potential of 8-mm radars for remotely sensing cloud drop-size distributions. *J. Atmos. Oceanic Technol.*, 13, 76-87.

Gossard E.E., 1994: Measurements of cloud droplet size spectra by Doppler radar. *J. Atmos. Oceanic Tech.*, 11, 712-726.

Gossard E.E., 1988: Measuring drop size distributions in cloud with a clear-air sensing Doppler radar. *J. Atmos. Oceanic Technol.*, 5, 640-649.

Greenwald, TJ, GL Stephens, TH Vonder Haar, and DL Jackson, 1993: A physical retrieval of cloud liquid water over the global oceans using Special Sensor Microwave/Imager (SSM/I) observations, J. Geophysical Research, 98, 18471-18488.

Gunn, K. L. S., and T. W. R. East, 1954: The microwave properties of precipitation particles. *Quart. J. Roy. Meteor. Soc.*, 80, 522– 545.

Han, Q-Y., W.B. Rossow and A.A. Lacis, 1994: Near-global survey of effective cloud droplet radii in liquid water clouds using ISCCP data. J. Climate, 7, 465-497.

Herman, G. F., and J. A. Curry, 1984: Observational and theoretical studies of solar radiation in arctic stratus clouds. *J. Climate Appl. Meteor.*, 23, 5–24.

Heymsfield, A. J., L. M. Miloshevich, A. Slingo, K. Sassen and D. O'C. Starr, 1991: An observational and theoretical study of highly supercooled altocumulus. *J. Atmos. Sci.*, 48(7), 923–945.

Hobbs, P. V., N. T. Funk, R. R. Weiss, and J. D. Locatelli, 1985: Evaluation of a 35-GHz radar for cloud physics research. *J. Atmos. Oceanic Technol.*, 2, 35–48.

Hogan, R. J., and A. J. Illingworth, 1999: The potential of spaceborne dual-wavelength radar to make global measurements of cirrus clouds. *J. Atmos. Oceanic Technol.,* 16(5), 518–531.

Iguchi, T., T. Kozu, R. Meneghini, J. Awaka, and K. Okamoto, 2000: Rain-profiling algorithm for the TRMM Precipitation Radar. *J.Appl. Meteor.,* **39,** 2038–2052.

Intrieri, J. M., G. L. Stephens, W. L. Eberhart and T. Uttal, 1993: A method for determining cirrus cloud particle sizes using lidar and radar backscatter techniques. *J. Appl. Meteor.,* 32(6), 1074–1082.

Iwanami, K., R. Misumi, M. Maki, T. Wakayama, K. Hata, and S. Watanabe, 2001: Development of a multiparameter radar system on mobile platform, *Preprints 30th Inter. Conf. Radar Meteor.,* 104-106.

Knight, C. A., and L. J. Miller, 1993: First radar echoes from cumulus clouds. *Bull. Amer. Meteor. Soc.,* **74,** 179–188.

Kosarev, A. L., and I. P. Mazin, 1989: Empirical model of physical structure of the upper level clouds of the middle latitudes. *Radiation Properties of Cirrus Clouds.* Nauka, 29–52.

Kropfli, B. W. Bartram, and S. Y. Matrosov, 1990: The upgraded WPL dual-polarization 8-mm-wavelength Doppler radar for microphysical and climate research. Preprints, *Conf. on Cloud Physics,* San Francisco, CA, Amer. Meteor. Soc., 341–345.

Kropfli, RA, SY Matrosov, T. Uttal, BW Orr, AS Frisch, KA Clark, BW Bartram, RF Reinking, JB Snider,and BE Martner, 1995: Cloud physics studies with 8 mm wavelength radar. Atmos. Res. , **35** , 299-313.

Kropfli, R. A., and R. D. Kelly, 1996: Meteorological research applications of mm-wave radar. *Meteor. Atmos. Phys.,* **59**, 105–121.

Kummerow, C., and L. Giglio, 1994: A passive microwave technique for estimating rainfall and vertical structure information from space. Part I: Algorithm description. *J. Appl. Meteor.,* **33**, 3–18.

Lhermitte R., 1987: A 94 GHz Doppler radar for clouds observations. *J. Atmos. Oceanic Technol.,* **4**, 36-48.

Lhermitte R. and C. R. Frush, 1984: Millimeter wave radar for meteorological observations. Preprints 22nd Conf. on Radar Meteor., Zurich, *Amec. Meteor. Soc.,* 228-231.

Lhermitte R., 1981: Millimeter wave Doppler radars. Preprints 20th Conf. on Radar Meteor., Boston, *Amec. Meteor. Soc.,* 744-748.

Liebe, H. J., 1985: An updated model for millimeter-wave propagation in moist air. *Radio Science,* 20(5), 1069–1089.

Liao, L., and K. Sassen, 1994: Investigation of relationships between Ka-band radar reflectivity and ice and liquid water content. *Atmos. Res.,* **34**, 231–248.

London, J. (1957): A Study of the Atmospheric Heat Balance. Final Rep., Contract AF19(122)--165. Dept. of Meteorology and Oceanography, New York University, 99 pp.

Martner, B. E., and R. A. Kropfli, 1993: Observations of multilayered clouds using Ka-band radar. Paper 93-394, *Proc. 31st Aerospace Science Meeting,* Reno, NV, Amer. Institute of Aeronautics and Astronautics, 1–8.

Matrosov, S. Y., 1993: Possibilities of cirrus particle sizing from dualfrequency radar measurements. *J. Geophys. Res.*, **98**(D11), 20 675–20 683.

Miller, M., J. Verlinde, C. Gilbert, J. Tongue, and G. Lehenbauer, 1997: Cloud detection using the WSR-88D: An initial evaluation. Preprints, *28th Conf. on Radar Meteorology,* Austin, TX, Amer. Meteor. Soc., 442–443.

Orr, B. W., and B. E. Martner, 1996: Detection of weakly precipitating winter clouds by a NOAA 404-MHz wind profiler. *J. Atmos. Oceanic Technol.*, **13**, 570–580.

Pasqualucci, F., B. W. Bartram, R. A. Kropfli, and W. R. Moninger, 1983: A millimeter-wavelength dual-polarization Doppler radar for cloud and precipitation studies. *J. Climate Appl. Meteor.*, 22, 758–765.

Paulsen, W. H., P. J. Petrocchi, and G. McLean, 1970: Operational utilization of the AN/TPQ-11 cloud detection radar. Air Force Cambridge Labs Instrumentation Papers, Vol. 166, 37 pp.

Pazmany, A. L., R. E. McIntosh, R. Kelly, and G. Vali, 1994: An airborne 95-GHz dual-polarized radar for cloud studies. *IEEE Trans. Geosci. Remote Sens.*, **32**, 731–739.

Petty, G. W., 1994a: Physical retrievals of over-ocean rain rate from multichannel microwave imagery. Part I: Theoretical characteristics of normalized polarization and scattering indices. *Meteor. Atmos. Phys.*, **54**, 79–99.

——, 1994b: Physical retrievals of over-ocean rain rate from multichannel microwave imagery. Part II: Algorithm implementation. *Meteor. Atmos. Phys.*, **54**, 101–121.

Ralph, F. M., P. J. Nieman, D. W. van de Kamp, and D. C. Law, 1995: Using spectra moment data from NOAA's 404-MHz radar wind profilers to observe precipitation. *Bull. Amer. Meteor. Soc.*, **76**, 1717–1739.

Ray, P. S., 1972: Broadband complex refractive indices of ice and water. *Appl. Opt.*, **11**, 1836–1844.

Rinehart RE and Tuttle JD, 1982: Antenna beam patterns and dual wavelength processing, J. Appl. Meteor., vol.21, pp.1865-1880.

Rossow, W. B., and R. A. Schiffer, 1991. ISCCP cloud data products, *Bull. Amer. Meteor. Soc.*, 72:2-20.

Sassen, K., and L. Liao, 1996: Estimation of cloud content by W-band radar. *J. Appl. Meteor.*, **35** (6), 932-938.

Sassen, K., J. M. Comstock, Z. Wang, and G. G. Mace, 2001: Cloud and aerosol research capabilities at FARS: The Facility for Atmospheric Remote Sensing. Bull. Amer. Meteor. Soc., **82**, 1119-1138.

Sekelsky S. M., W. L. Ecklund, J. M. Firda, K. S. Gage and R. E. McIntosh, 1999: Particle size estimation in ice-phase clouds using multifrequency radar reflectivity measurements at 95, 33 and 2.8 GHz. *J. Appl. Meteor.*, **38**(1), 5–28.

Simpson, J., R. F. Adler, and G. R. North, 1988: A proposed Tropical Rainfall Measuring Mission (TRMM) satellite. *Bull. Amer. Meteor. Soc.*, **69**, 278–295.

——, C. Kummerow, W.-K. Tao, and R. F. Adler, 1996: On the Tropical Rainfall Measuring Mission (TRMM). *Meteor. Atmos. Phys.*, **60**, 19–36.

Smith, E. A., X. Xiang, A. Mugnai, and G. J. Tripoli, 1994: Design of an inversion-based precipitation profile retrieval algorithm using an explicit cloud model for initial guess microphysics. *Meteor. Atmos. Phys.*, **54**, 53–78.

Smith, R. N. B. 1990: A scheme for predicting layer clouds and their water content in a general circulation model. *Q. J. R. Meteorol. Soc.*, **116**, 435–460.

Spencer, R. W., H. M. Goodman, and R. E. Hood, 1989: Precipitation retrieval over land and ocean with the SSM/I: Identification and characteristics of the scattering signal. *J. Atmos. Oceanic Technol.*, **6**, 254–273.

Stephens, G. L., S. C. Tsay, P. W. Stackhouse Jr. and P. J. Flatau, 1990: The relevance of the microphysical and radiative properties of cirrus clouds to climate and climatic feedback. *J. Atmos. Sci.*, **47**, 1742–1752.

Tiedtke, M., 1993: Representation of Clouds in Large-Scale Models, *Mon. Wea. Rev.*, 121,3040-3061.

Tuttle, J. D., and R. E. Rinehart, 1983: Attenuation correction in dualwavelength analyses. *J. Climate Appl. Meteor.*, **22**, 1914–1921.

Sauvageot, H., and J. Omar, 1987: Radar reflectivity of cumulus clouds. *J. Atmos. Oceanic Technol.*, **4**, 264-272.

Vali, G., R. D. Kelly, J. French, S. Haimov, D. Leon, R. E. McIntosh, and A. Pazmany, 1998: Finescale structure and microphysics of coastal stratus. *J. Atmos. Sci.*, **55**, 3550–3564.

Vivekanandan, J., W.M. Adams and V.N. Bringi, 1991: Rigorous approach to polarimetric radar modeling of hydrometeor orientation distributions. *J. Appl. Meteor.*, **30**, 1053-1063.

Wang, Y., and Coauthors, 1996: Mesoscale model simulations of TRACE A and preliminary regional experiment for storm-scale operational and research meteorology convective systems and associated tracer transport. *J. Geophys. Res.*, 101, 24 013–24 027.

Wexler, R., 1948: Rain intensities by radar. *J. Meteor.*, **5**, 171–173.

Wilheit, T. T., A. T. C. Chang, M. S. V. Rao, E. B. Rodgers, and J. S. Theon, 1977: A satellite technique for quantitatively mapping rainfall rates over the oceans. *J. Appl. Meteor.*, **16**, 551–560.

White, A. B., C. W. Fairall, A. S. Frisch, B. W. Orr, and J. B. Snider, 1996: Recent radar measurements of turbulence and microphysical parameters in marine boundary layer clouds. *Atmos. Res.*, **40**, 177–221.

APPENDIX

MIE FORMULA FOR MM WAVELENGTH RADAR

The theory of the scattering of electromagnetic waves by particles has been the subject of a large number of studies since the end of the last century, when the optical properties of colloidal suspensions were discovered. A general solution has been given by Mie (1908) from previous results and then reformulated by several authors, in particular Stratton (1941), Van de Hulst (1957), and Deirmendjian (1969). It is based on the application of Maxwell's equations to the scattering of a planar wave by a homogeneous sphere in a non-absorbing medium.

The basic parameters used for formulating the problem are

1. The dimensionless product of the radius a of the sphere and the propagation constant in vacuum of the incident wave $2\pi/\lambda$, namely $\alpha = 2\pi a / \lambda$ (α is sometimes called the *radio-electric size* of the sphere);
2. The complex refractive index m with respect to vacuum of the material of the sphere with $m = n - ik$ where n is the ordinary refractive index ($n = \varepsilon_r^{1/2}$, where ε_r is the permittivity dielectric, also called *the constant dielectric*) and k the absorption coefficient of the material of the sphere;
3. A scattering angle θ formed by the vectors of the incident and scattered waves.

When an electromagnetic wave meets a stationary and inert body (i.e., not charged, not excited, and with its own emission negligible) with dielectric properties different from those of the surrounding medium, an interaction develops so that some of the energy of the incident field is absorbed by the body and appears in the form of heat whereas another part is scattered in all directions in the form of an electromagnetic field with the same wavelength as the exciting energy. The scattering results from the combination of the oscillating electric and magnetic multi-poles induced by the electromagnetic wave in the body.

Under these conditions, the scattered electric field at a great distance from the sphere can be described by a vector A whose two scalar components A_1 and A_2 are perpendicular and parallel, respectively, to the scattering plane defined by the vectors of the incident and scattered waves. The Mie solution gives the complex amplitude of these components in the form of convergent series that can be written

$$A_1 = \frac{\lambda}{2\pi} \sum_{n=1}^{\infty} \frac{2n+1}{n(n+1)} (a_n \pi_n + b_n \tau_n)$$
$$A_2 = \frac{\lambda}{2\pi} \sum_{n=1}^{\infty} \frac{2n+1}{n(n+1)} (b_n \pi_n + a_n \tau_n) \qquad (A.1)$$

where n is a positive integer, a_n and b_n are the " Mie coefficients " obtained from Bessel and Hankel functions with arguments α and m. These coefficients correspond to scattering by the induced magnetic and electric modes of order n, respectively.

The quantities π_n and τ_n only depend on θ and can be defined with the

help of the Legendre polynomials. The amplitudes A_1 and A_2 make it possible to express the differential scattering cross section $d\sigma_d$ as a function of m , α , and θ . The term σ_d is defined by the ratio of the incident flux to the scattered flux. We can show that for unit solid angle and a unit incident flux

$$d\sigma_d(\theta,\alpha,m)=\frac{1}{2}AA^*d\Omega \qquad (A.2)$$

where A^* is the conjugate vector to A and $d\Omega$ is the solid angle element.

From this expression, we can define the following specific cross sections. The total scattering cross section, Q_s , is the surface intercepting the amount P_s of incident power effectively scattered by the sphere. It is obtained by integrating (A.2) for the solid angle $\Omega=4\pi$. If S_i is the incident power density,

$$P_s=Q_sS_i$$

The radar backscattering cross section (already defined in Section 1.3), σ , is the equivalent surface of an isotropic scattered, that is, scattering in all directions with an intensity equal to that scattered to the radar. It is obtained by multiplying the value of σ_d taken from (A.2) for $\theta=\pi$, by 4π (in the particular case of isotropic scattering, $\sigma=Q_s$). The term σ is specific to radar backscattering and different from cross sections usually used in physics because it is applied to a privileged scattering direction.

The total attenuation cross section, Q_t , is obtained from (A.2) when $\theta=0$ and defined as the surface intercepting an amount P_a of power equal to that taken in total by the sphere from the incident wave by absorption and scattering:

$$P_a = Q_t S_t \qquad (A.3)$$

The absorption cross section Q_a, is the surface intercepting an amount of incident power equal to that absorbed in the form of heat by the sphere. It is equal to the difference $Q_t - Q_s$.

The Mie formulas are

$$Q_s = \frac{\lambda^2}{2\pi}\sum_{n=1}^{\infty}(2n+1)(|a_n|^2 + |b_n|^2) \qquad (A.4)$$

$$\sigma = \frac{\lambda^2}{4\pi}\left|\sum_{n=1}^{\infty}((-1)^n(2n+1)(a_n - b_n)\right|^2 \qquad (A.5)$$

$$Q_t = \frac{\lambda^2}{2\pi}(-\mathrm{Re})\left[\sum_{n=1}^{\infty}(2n+1)(a_n + b_n)\right] \qquad (A.6)$$

where n is a positive integer.

Deirmendjian (1969) adapted the Mie expressions to machine computation. The proposed computational form involves no approximation and is simpler to use for machine processing than the expressions involving Bessel function of the complex argument. Using the recurring function

$$W_n = \left(\frac{2n-1}{\alpha}\right)W_{n-1} - W_{n-2} \qquad (A.7)$$

with

$$W_o = \sin\alpha + i\cos\alpha$$
$$W_{-1} = \cos\alpha - i\sin\alpha \qquad (A.8)$$

the Mie coefficients are written in the form

$$a_n = \frac{\left(\frac{A_n}{m} + \frac{n}{\alpha}\right)\mathrm{Re}(Wn) - \mathrm{Re}(W_{n-1})}{\left(\frac{A_n}{m} + \frac{n}{\alpha}\right)W_n - W_{n-1}} \qquad (A.9)$$

$$b_n = \frac{\left(mA_n + \frac{n}{\alpha}\right)\mathrm{Re}(Wn) - \mathrm{Re}(W_{n-1})}{\left(mA_n + \frac{n}{\alpha}\right)W_n - W_{n-1}} \qquad (A.10)$$

where

$$A_n = -\frac{n}{y} + \left(\frac{n}{y} - A_{n-1}\right)^{-1} \qquad (A.11)$$

$$A_0 = \cot y \qquad (A.12)$$

$$y = m\alpha \qquad (A.13)$$

For $y = p - iq$, where $p = n\alpha$ and $q = k\alpha$, we have

$$A_0 = \frac{\sin p \cos p + i \sinh q \cosh q}{\sin^2 p + \sinh^2 q} \qquad (A.14)$$

In general, the radio-electric size of the spheres considered $\alpha = \pi D / \lambda$ is small because the meteorological scatterers are small compared to the wavelengths used. Under these conditions, the multi-polar moments can be neglected and the effective reflectivity of a spherical particle is obtained approximately by replacing the sphere with an equivalent dipole as long as the diameter of the sphere. The time average of the intensity of radiation scattered by an oscillating dipole with moment μ in the

direction of the source is

$$S_r = \frac{2\pi^3 \mu^2 c}{\lambda^4 r^2} \qquad (A.15)$$

where c is the velocity of propagation in vacuum, and r is the distance of the radar from the target. The dipole moment of a particle of diameter D and dielectric constant ε is

$$\mu = \frac{\varepsilon - 1}{\varepsilon + 2} \frac{D^3}{8} E \qquad (A.16)$$

where E is the electric field acting on the dipole.

Substituting (A.16) in (A.15),

$$S_r = \frac{\pi^3}{32}\left(\frac{\varepsilon - 1}{\varepsilon + 2}\right)^2 \frac{c E^2 D^6}{\lambda^4 r^2} = \frac{\pi^4}{4}\left(\frac{\varepsilon - 1}{\varepsilon + 2}\right)^2 \frac{S_i D^6}{\lambda^4 r^2} \qquad (A.17)$$

where $S_i = cE^2/8\pi$ is the intensity of the incident radiation. The backscattering cross section σ is obtained by writing that $\sigma = 4\pi r^2 S_r / S_i$.

The same result is obtained by starting from the "exact" Mie expression, assuming that for $\alpha \langle\langle \lambda$, the terms of an order higher than 5 in the expansion of a_n and b_n can be neglected as a power series in α. Substituting the coefficients by their expansion in eqs. (A.4) to (A.6) then leads to the following simple expressions:

$$Q_s = \frac{2}{3}\frac{\pi^5}{\lambda^4}|K|^2 D^6 \qquad (A.18)$$

$$\sigma = \frac{\pi^5}{\lambda^4} |K|^2 D^6 \qquad (A.19)$$

$$Q_a = \frac{\pi^2}{\lambda} D^3 \, \mathrm{Im}(-K) \qquad (A.20)$$

$$Q_t = Q_a + Q_s \qquad (A.21)$$

where $K = (m^2 + 2)$; *Im* means that the imaginary part is taken.

Expression (A.19) is the Rayleigh law, according to which the scattered power is proportional to the reciprocal of the fourth power of the wavelength and to the sixth power of the diameter. It is analogous to the expression giving the effective scattering cross section of atmospheric molecules at optical wavelengths, which Rayleigh used to explain the color of the sky by increasing scattering for decreasing wavelengths.

In the Rayleigh region, the energy scattered by the particle is radiated almost isotropically. In the Mie region, the diffusion diagram is more complex and the maximum radiation direction is not backward. Relations (A.18) to (A.21) are very important. They are at the basis of any discussion on the use of microwaves to observe clouds and precipitation.